University of Alberta

The Function of the Electron Transfer Chain of *Escherichia coli*
Succinate Dehydrogenase

by

Quang Minh Tran

A thesis submitted to the Faculty of Graduate Studies and Research
in partial fulfillment of the requirements for the degree of

Doctor of Philosophy

Department of Biochemistry

©Quang Minh Tran
Fall 2011
Edmonton, Alberta

Abstract

Complex II, or succinate dehydrogenase, is a vital component of aerobic life. Its function is critical for both the tricarboxylic acid cycle and the mitochondrial respiratory chain since it catalyzes the oxidation of succinate to fumarate, liberating two electrons that feed into the lipid-soluble quinone pool. Despite over 50 years of research, and the fact that it is the simplest of all the mitochondrial respiratory chain complexes, there is still much to learn regarding the catalytic mechanism of complex II. In recent years, there has been a renewed interest in this enzyme, due to its central role in a subset of human cancers, hereditary paraganglioma and pheochromocytoma. For my research, I chose *Escherichia coli* succinate dehydrogenase as the model system due to its innumerable similarities to mitochondrial complex II. In chapter two, I examine key residues that enable succinate dehydrogenase to interact with its quinone substrate. Chapters three and four focus on the function of the single *b*-type heme in the enzyme, and its potential role, or lack thereof, in enzyme catalysis and suppression of reactive oxygen species production. In chapter five, microsecond freeze-hyperquench experiments are utiilized to empirically quantify electron transfer rates through the succinate dehydrogenase iron-sulfur cluster relay, and examine the control that endergonic electron tunneling steps exert on those rates.

Acknowledgement

It was an absolute pleasure to be involved in the graduate research described in this thesis and a huge reason for that is all the amazing people that worked alongside me in the lab. Thank you all for all your support and stimulating conversations. I love you all.

I would like to thank my supervisor, Dr. Joel H. Weiner, for his mentorship during my PhD research. He first took me into his lab for my undergraduate Honors research project and encouraged me to pursue a graduate degree. The depth of his knowledge and his passion for science were truly inspiring.

I would also like to thank those in the lab that taught me the critical techniques required to do the science. I would especially like to thank Dr. Richard A. Rothery for all his guidance throughout my degree and for teaching me everything I know about EPR. Thank you to Dr. Zhongwei Zhao for all his help on the Sdh project and introducing me to the stopped flow machine. I would also like to acknowledge Dr. Steve Brokx for taking me under his wing when I first came into the lab and showing me the ropes.

Thank you to the technicians in the lab that made sure we had everything we needed to make sure our experiments ran smoothly: Gillian McCuaig, Glen Zhang, Nasim Boroumand, and Francesca Sebastian.

I would like to give a big shoutout to all the fellow graduate students that grew their scientific careers alongside me in the Weiner lab. Much thanks to my scientific big brother Dr. Victor Cheng, who I first met in undergrad, for all the good times we've had working on Sdh. I can think of no one else who I would have rather had with me during all our adventures around the globe. Thanks to Greg Workun, Huipo Tang, Justin Fedor, Matt Solomonson, and Yanfei Zhang for being great

colleagues and sharing in the many trials and tribulations of grad school. Thank you to all the other graduate students in the Department of Biochemistry for all the fun times. Much thanks goes out to Carmen Fong and Scott Meyer, two summer students that poured much of their sweat into the Sdh project.

Thank you to my supervisory committee, Dr. Bernard Lemire and Dr. Mark Glover, for their guidance over the years. I would also like to thank Dr. Frank Nargang and Dr. Tina Iverson for serving on my examining committee.

This work would not have been possible without the help of numerous collaborators. Thanks to Dr. Elena Maklashina and Dr. Gary Cecchini for providing many Sdh mutants and for their invaluable Sdh-related insights. Thank you to Marc Strampraad and Dr. Simon de Vries for being great hosts in the Netherlands and letting us visit multiple times to use their state of the art MHQ machine. Thanks to Dr. Sarah Chobot and Dr. Leslie Dutton for providing their electron tunneling expertise.

Thank you to the agencies that provided me with financial support during my degree: Alberta Heritage Foundation for Medical Research (now called Alberta Innovates) and the Canadian Institutes for Health Research.

I would to finish by thanking all those outside my life in academia. Thank you to my parents for their lifelong support and encouragement. I reserve a ginormous amount of gratitude for my wife Annie, who was my rock for the entirety of my graduate career. Her patience with me was truly superhuman and nothing seemed too overwhelming with her by my side. Thank you to all my family and friends for all their support.

Table of Contents

List of Tables

List of Figures

Abbreviations used in this thesis

[Fe-S]	iron-sulfur
5-ALA	5-amino-levulinate
ADP	adenosine 5'-diphosphate
ATP	adenosine 5'-triphosphate
DCPIP	2,6-dichlorophenolindophenol
DMQ	demethylmenaquinone
DMSO	dimethylsulfoxide
DNP	dinitrophenol
e^-	electron
EDTA	ethylenediaminetetraacetic acid
E_m	midpoint potential
EPR	electron paramagnetic resonance
$FAD/FADH_2$	flavin adenine dinucleotide (oxidized/reduced)
FMN	flavin mononucleotide
Fnr	fumarate nitrate reductase regulator
Frd	fumarate reductase
FSQ	flavosemiquinone
GAPDH	glyceraldehyde-3-phosphate dehydrogenase
HEPES	4-(2-hydroxyethyl)-1-piperazineethanesulfonic acid
HIF-1α	hypoxia-inducible factor-1α
HOQNO	2-n-heptyl 4-hydroxyquinoline
MOPS	3-(N-morpholino)propanesulfonic acid
MQ	menaquinone
mtDNA	mitochondrial DNA
MTT	3-(4,5-dimethylthiazol-2-yl)-2,5-diphenyltetrazolium bromide
$NAD^+/NADH$	nicotinamide adenine dinucleotide (oxidized/reduced)
PCP	pentachlorophenol
PDB	Protein Data Bank
P_i	phosphate
pmf	proton motive force
PMS	phenazine methosulfate
PMSF	phenylmethylsulfonyl fluoride
Q	quinone
Q-pool	quinone-pool
Q-site	quinone-binding site
QFR	quinol:fumarate oxidoreductase

rmsd	root-mean-square-deviation
ROS	reactive oxygen species
Sdh	succinate dehydrogenase
SDHAF	succinate dehydrogenase assembly factor
SQ	semiquinone
SQR	succinate:quinone oxidoreductase
SRP	signal recognition particle
TCA	tricarboxylic acid
TMAO	trimethylamine N-oxide
TTFA	thenoyltrifluoroacetone
UQ/UQH$_2$	ubiquinone(oxidized)/ubiquinol(reduced)
USQ	ubisemiquinone
UV-VIS	ultraviolet-visible

Chapter 1: General Introduction

"Life is beautiful. Life is a struggle. Life is a beautiful struggle." – Dante Terrell Smith (a.k.a. Mos Def)

1.1 Introduction to Bioenergetics

The resiliency of life on this planet is awe-inspiring. From the bitter cold of the Antarctic ice sheets to the blistering heat of the deep-sea hydrothermal vents, life has developed to fill every ecological niche. It isn't easy: life requires work, and work is energy. No matter the ecosystem, for life to continue there must exist a constant supply of harvestable energy from which organisms can power the multitude of chemical reactions that make survival possible. The key here is the ubiquitous molecule ATP, adenosine 5'-triphosphate, which powers many of the useful metabolic reactions within the cell via its coupled hydrolysis to adenosine 5'-diphosphate (ADP). Whatever the primary energy source available to an organism is, that energy must ultimately be converted to the currency of ATP. This is the problem that all life characterized thus far has solved and it forms the basis for the study of bioenergetics.

In this thesis, I examine a tiny piece of that system: complex II (succinate:quinone oxidoreductase, SQR; succinate dehydrogenase, Sdh). Complex II oxidizes succinate to fumarate while also reducing ubiquinone (UQ) to ubiquinol (UQH$_2$). Using the *Escherichia coli* enzyme as the model system, structure-function relationships are studied in order to gain insight into the sophisticated catalytic mechanisms of complex II. Particular focus is given to the examination of electron transfer and quinone chemistry within the membrane-spanning domain of SQR.

1.1.1 Mitochondria

In order for most eukaryotic cells to meet their constant energy demands, they have developed specialized organelles called mitochondria. The mitochondria are ATP "factories" and in humans, these organelles can turn over the equivalent of a full body weight's worth of ATP in a single day (*1*). In addition to their role in energy conservation, mitochondria function in a variety of other cellular processes such as regulation of the cell cycle, cell signaling, embryonic development, and apoptosis (*2*).

According to the theory of endosymbiosis, mitochondria originated when a primitive single-celled organism, ancestral to modern eukaryotes, enveloped a *Rickettsia*-like bacterial cell, eventually developing a mutual dependence (*3*). Accordingly, mitochondria also have their own genomic DNA (mtDNA), located in the matrix and distinct from nuclear DNA, with its own transcriptional/translational machinery. The mtDNA is believed to be a remnant of the original endosymbiont genome; although mtDNA codes for a handful of genes, over 95% of the mitochondrial proteome is nuclear encoded (*4*).

The architecture of a typical mitochondrion is unlike that of any other cellular organelle and they are similar to modern gram-negative bacteria, such as *E. coli*. Mitochondria are organelles with dual membrane architecture: an inner and an outer membrane, which creates two distinct compartments within the organelle. The central compartment is the mitochondrial matrix, which is enveloped by the inner membrane. The space between the inner and outer membranes is called the

intermembrane space. Likewise, *E. coli* cells also have both an inner and outer membrane. The bacterial cytoplasm and periplasm are structurally equivalent to the mitochondrial matrix and intermembrane space, respectively. As far as ATP production is concerned, the inner membranes are the most important as it is here where the energy transducing enzymes are located.

1.1.2 Aerobic Metabolism – the Tricarboxylic Acid Cycle

During aerobic metabolism, numerous cellular catabolic processes eventually converge on the tricarboxylic acid (TCA) cycle, which occurs within the mitochondrial matrix. The main entry point into the TCA cycle is at the level of acetyl-CoA, which is ultimately oxidized to two molecules of CO_2 (*5*). The full oxidation of acetyl-CoA proceeds through eight chemical reactions (**Figure 1.1**), and the completion of one full cycle results in the reduction of three molecules of nicotinamide adenine dinucleotide (NAD^+) to NADH, which will eventually feed electrons directly into the mitochondrial respiratory chain when NADH is reoxidized. In addition, as intermediates in the TCA cycle, the oxidation of succinate to fumarate by complex II also introduces reducing equivalents into the respiratory chain.

The TCA cycle is essential not just for its role in the production of substrates for aerobic respiration, but also because several of the cycle intermediates serve as precursors for key biosynthetic pathways (*6*). The genes for all the enzymes involved in the TCA cycle have been identified in the *E. coli* genome (*7*) so this particular bacterium is capable of completing the full cycle when grown under fully

aerobic conditions. However, there exist a number of prokaryotic and eukaryotic species that do not express a full complement of TCA cycle enzymes suggesting that some variability in the cycle can exist (*8*).

1.1.3 The Chemiosmotic Theory and Oxidative Phosphorylation

The usefulness of ATP stems directly from the ability of the cell to maintain a high ATP:ADP ratio, far away from equilibrium concentrations (*9*). Yet, how the energy in reducing substrates like NADH could be harnessed for use in the synthesis of ATP was unclear until the seminal work by Peter Mitchell, who first proposed his chemiosmotic theory in 1961 (*10*), for which he eventually won the Nobel Prize.

According to the chemiosmotic theory, the intermediate that links the high-energy products of cellular metabolism with ATP synthesis is the proton motive force (pmf, Δp), an electrochemical potential across the membrane. As electrons pass through the mitochondrial respiratory chain, the redox potential of the electron decreases, and some of that energy is coupled to the translocation of protons against their concentration gradient. This maintains a proton electrochemical gradient across the highly impermeable membrane, with protons extruded into the positive P-side of the membrane (the intermembrane space in mitochondria) and negative on the N-side of the membrane (mitochondrial matrix). In turn, the pmf is a potential energy well that is used to drive the oxidative phosphorylation of ADP to ATP by the ATP synthase, the major source of ATP production within the cell. In addition to its usefulness in oxidative phosphorylation, the pmf is also consumed in the transportation of some molecules across the

membrane and the powering of bacterial flagella. At 25 °C, the following equation is used to calculate the magnitude of the Δp:

$$\Delta p(mV) = \Delta\psi + 59\Delta pH \quad (9)$$

From this equation, it is useful to recognize that the pmf arises from two components: a transmembrane electric potential, $\Delta\psi$, and a proton gradient, ΔpH. In most mitochondrial and bacterial membranes, the major component of the pmf derives from $\Delta\psi$, whereas in plant thylakoid membranes, which harvest solar energy, ΔpH is the major contributing factor (*9*).

1.2 The Mitochondrial Respiratory Chain

The canonical mitochondrial respiratory chain is comprised of five protein complexes, denoted complex I-V (**Figure 1.2**). Complex I (NADH:ubiquinone oxidoreductase) harnesses the reducing power of NADH and funnels those electrons into the membrane-soluble quinone(Q)-pool. Complex II oxidizes succinate and transfers those electrons into the Q-pool. In mitochondria, the predominant quinone species is ubiquinone. Reduced UQH_2 diffuses into complex III (*bc$_1$* complex) whereupon it gets oxidized, passing its electrons onto soluble cytochrome *c*. Cytochrome c diffuses through the intermembrane space and donates electrons to complex IV (cytochrome *c* oxidase). Assuming a lack of short circuits in the electron transport chain, the final fate of all electrons is the terminal reduction of O_2 to H_2O by Complex IV. The activities of complex I, III, and IV are coupled to proton translocation from the N-side to the P-side of the inner membrane, while complex II activity is non-electrogenic. Once-extruded protons are returned into the

mitochondrial matrix, down their electrochemical and concentration gradients through complex V (ATP synthase), thus driving the synthesis of ATP from ADP and inorganic phosphate. A review of the mitochondrial respiratory complexes follows in this section while an in-depth review of complex II is presented later in this chapter.

1.2.1 Redox Cofactors in the Respiratory Chain

The electron transport chain depends on the ability of the electron to travel across large distances, on the atomic scale, in order to couple the multiple active-sites within each respiratory protein. Nature has solved this dilemma by evolving electron transfer relays, which allow for efficient electron transfer through proteins. As long as each node along the relay is within 14Å of the next, electrons are capable of tunneling through proteins on a physiologically-relevant timescale (*11*). Bridging the length of the mitochondrial respiratory chain, redox-active prosthetic groups include flavin cofactors, iron-sulfur [Fe-S] clusters, hemes, and copper atoms (*9*). Importantly, when 2e$^-$ acceptors such as flavin cofactors and UQ must interact with 1e$^-$ acceptors, the reaction proceeds via a semiquinone radical intermediate, unless a mechanism allows otherwise.

Flavin cofactors, which act as 2e$^-$ acceptors, are found in proteins as either flavin mononucleotide (FMN) or flavin adenine dinucleotide (FAD) (**Figure 1.3**). In mammals, flavin cofactors are synthesized directly from dietary riboflavin within the mitochondrial matrix (*12, 13*). The biosynthesis of FMN from riboflavin is a one step process, catalyzed by riboflavin kinase. FMN can be further converted to FAD

by the catalytic action of FAD synthetase. The mitochondrial localization of the FAD biosynthesis enzymes suggests that a system must exist for the import and export of flavins. In yeast, the Flx1p protein is an inner membrane transporter that has been implicated in flavin homeostasis (*14*). The specific function of Flx1p is still controversial, but evidence suggests that it may only operate as a FAD exporter (*15, 16*); if so, the mechanism for riboflavin import is still unknown. Many prokaryotes, including *E. coli*, do not require an external source of riboflavin, since they are capable of *de novo* synthesis of riboflavin from guanosine 5'-triphosphate and D-ribulose-5-phosphate (*17*).

Although certain rare forms can exist (*18*), [Fe-S] clusters in the mitochondrial respiratory chain are only present as [2Fe-2S], [3Fe-4S], and [4Fe-4S] forms; and all are $1e^-$ acceptors. Bacteria contain three [Fe-S] cluster biosynthesis pathways – the Nif, Isc, and Suf systems (*19*) – that are homologous to the systems utilized by mitochondria. These systems consist of two components: a cysteine desulfurase, which uses cysteine as the sulfur source, and a protein scaffold, which facilitates the assembly of sulfur with iron, to form the [Fe-S] clusters before delivering them to the appropriate apoproteins (*19*).

Of all the redox cofactors, hemes, which act as $1e^-$ acceptors, have the most structural diversity. Heme biosynthesis is a very complex and energy intensive process. In mammals, the biosynthetic pathway begins with the condensation of succinyl-CoA and glycine (*20*), while in *E. coli* the building blocks are glutamate molecules (*21*). The eukaryotic and prokaryotic pathways converge at the level of 5-amino-levulinate (5-ALA), whereupon the rest of the biosynthetic pathway is

conserved. Through a series of six enzymatic reactions, eight molecules of 5-ALA are utilized to generate the porphyrin ring system wherein ferrochelatase inserts the iron atom to form protoheme IX (*22*). In eukaryotic cells, the synthesis of 5-ALA and the last three steps of protoheme IX biosynthesis are catalyzed in the mitochondria, while the other intermediate steps occur in the cytosol (*20*). Different types of heme can be synthesized directly from protoheme IX, or in some cases from intermediates from the biosynthesis pathway (*23*).

The major types of heme found in respiratory enzymes are shown in **Figure 1.4**. The simplest form of heme is the *b*-type heme, which is simply protoheme IX. Heme *c* is similar in structure to heme *b*, but the porphyrin ring is covalently attached to the protein backbone through two conserved cysteine residues. Other types of hemes are classified based on additional modifications to the porphyrin ring. Mitochondrial respiratory chains contain only *b*-type, *c*-type, and *a*-type hemes while prokaryotic respiratory chains are more diverse and may also contain *o*-type or *d*-type hemes. The reason for all the different modifications to the heme is unclear, but may involve control of redox potential, as electron-donating and electron-withdrawing groups conjugated to the porphyrin ring can have substantial effects on heme potential (*24*).

Protein-bound Cu can exist as either a single Cu ion, or as a dimeric Cu-Cu cofactor, but both are 1e⁻ acceptors. Molybdenum-containing cofactors can also be incorporated into redox enzymes; molybdoenzymes are more common in prokaryotic respiratory chains where the ion is typically coordinated by a complex molybdopterin ring system (*25*).

1.2.2 Complex I

Mitochondrial complex I, or NADH dehydrogenase, is a massive protein complex comprising at least 40 individual subunits (*26, 27*), of which 14 are considered essential core subunits; the core subunits are sufficient for the redox and proton pumping activity and homologs can be found in many bacterial species (*28*). Until recently, the only structural data available were generated by electron microscopy, which revealed the overall architecture of complex I as L-shaped (*29-32*). The protein has a long membrane domain to which at one end is attached a soluble peripheral stalk that projects into the mitochondrial matrix. Of the 14 core subunits, seven are located in the peripheral arm while the remaining seven are found in the membrane arm. A number of X-ray crystal structures are now available for complex I (*33-35*), although most are incomplete. Amazingly, the most recent structure available reveals the full, intact complex I from *Thermus thermophilus*, which contains the 14 core subunits and one additional subunit (*34*).

It is at complex I where reducing equivalents from NADH are fed directly into the electron transport chain. A representation of the catalytic mechanism of complex I is shown in **Figure 1.5**. The oxidation of NADH occurs at the tip of the peripheral stalk at an active-site FMN cofactor, which liberates two electrons onto the FMN. These electrons must then sequentially tunnel through eight conserved [Fe-S] clusters: two [2Fe-2S] clusters and six [4Fe-4S] clusters, located in the peripheral arm. Finally, two electrons are used to reduce UQ at a quinol-binding site (Q-site) near the membrane interface. The low midpoint potential of the

NAD$^+$/NADH couple ($E_{m,7}$ = -320 mV) combined with the relatively high potential of the UQ/UQH$_2$ couple ($E_{m,7}$ = +90 mV) means that electrons span a 410 mV drop in potential energy as they pass through the enzyme. The redox energy is coupled to proton-pumping activity in the membrane domain that pumps protons with a stoichiometry of 4H$^+$ /2e$^-$ (*36*). Despite the large ΔE_m between NADH and UQ, complex I activity is fully reversible under the right conditions, where the pmf is utilized to produce NADH (known as reverse electron transport) (*37, 38*).

The high-resolution crystal structures reveal interesting details about electron transfer through complex I. Firstly, of the eight conserved [Fe-S] clusters, only seven of them lie in the main path from FMN to UQ. One of the [2Fe-2S] clusters, N1a, sits off of the direct circuit, but adjacent to the FMN. Its location suggests that it may accept an electron from the reduced FMN and transfer it to the first of the other seven [Fe-S] clusters in the chain. The function of cluster N1a is unclear, but its presence may allow the reduced FMN to transfer both of its electrons into the [Fe-S] chain in a single, concerted reaction (*39*). This should reduce the occupancy of electrons at the FMN, thus preventing the undesirable short-circuit reduction of molecular oxygen to superoxide (*40*).

The second curiosity that arose from the structure is the position of the last [Fe-S] cluster in the chain, denoted cluster N2, approximately 20-25Å above the membrane interface (*34*). This suggests that the UQ must come out of the membrane somewhat, since 14 Å is the upper limit for physiologically-relevant electron transfer (*11*). Residues around cluster N2 have been implicated in UQ binding (*41*),

and a large hydrophobic patch between the membrane domain and the putative Q-site may facilitate the diffusion of UQ up to cluster N2 (*34*).

Given the most recent structural data (*34*), the mechanism of how the redox activity of the enzyme is coupled to its proton-pumping activity is just now reaching clarity. Three of the core membrane subunits are homologous to a family of antiporters (*42*). These antiporter-like subunits are linked to the Q-site and to each other by a 60 Å-long amphipathic helix. It is possible that conformational changes associated with the binding and reduction of UQ may be communicated via the amphipathic helix to helices within the antiporter-like subunits, resulting in the translocation of three protons (*34, 43*). The fourth proton is likely translocated directly at the Q-site (*44*).

1.2.3 Complex III

Complex III, also known as the cytochrome bc_1 complex, accepts electrons from the reduced Q-pool and transfers them to the soluble cytochrome *c* protein. Complex III may contain up to 11 subunits (*45*), of which three are essential catalytic subunits that are found conserved in bacteria: cyt *b*, cyt c_1, and the Rieske iron-sulfur protein (*46*). Numerous high-resolution structures exist for bc_1 complexes from both mitochondrial and bacterial origins (*45, 47-49*). In many structures, the complex appears as a dimer, which is believed to be the functional unit (*45, 48, 50, 51*).

The catalytic mechanism, known as the Q-cycle (*52-54*), describes an electron transfer pathway that is bifurcated into a high-potential chain, which includes the

[2Fe-2S] cluster within the Rieske iron-sulfur protein and a heme c_1 within the cyt c_1 subunit, and a low potential-chain comprised of two hemes, heme b_L and heme b_H, coordinated by the cyt b subunit (**Figure 1.6**). UQH_2 binds to the enzymes at the Q_o-site, located on the P-side of the membrane. The two electrons liberated by the oxidation of UQH_2 are separated into the two branches: one e^- is transferred to the [2Fe-2S] cluster in the high-potential chain and the other e^- to heme b_L in the low-potential chain, although whether this occurs sequentially, or through a concerted reaction is still controversial (*55-57*). Thermodynamically, electron transfer to the high-potential chain is energetically favorable while electron transfer to the low-potential chain is not; thus, electron transfer to the [2Fe-2S] cluster provides the driving force for electron transfer to heme b_L (*50*).

Through a significant conformational change of the Rieske protein (*47*), electrons at the [2Fe-2S] cluster are passed to heme c_1 and ultimately reduce the soluble electron carrier, cytochrome c, which dissociates from the complex upon reduction. The domain movement of the Rieske protein may serve to inhibit undesirable short-circuit reactions; the physical separation between the [2Fe-2S] cluster and the ubisemiquinone (USQ) at the Q_o-site prevents the unwanted scenario where two electrons enter the high-potential chain (*57*). Electrons in the low-potential chain tunnel from heme b_L to heme b_H and finally to the Q_i-site on the N-side of the membrane, where a UQ gets reduced to a stable USQ intermediate (hence the term, Q-cycle) (*58*). Since two electrons are required to reduce the UQ at the Q_i-site, and only a single electron is entered into the low-potential chain with each UQH_2 oxidation at the Q_o-site, two molecules of UQH_2 must be oxidized at the

Q_o-site for every UQ reduced at the Q_i-site. This is the basis for the translocation of protons in complex III, as the two Q-sites are on opposing sides of the membrane; the reaction at the Q_o-site releases protons to the P-side, while the reaction at the Q_i-site consumes protons from the N-side, constituting a typical Mitchellian redox loop (*59*). The net reaction is

QH_2 + 2 cyt *c* (oxidized) + $2H^+$ (N-side) $\rightarrow$ Q + 2 cyt *c* (reduced) + $4H^+$ (P-side)
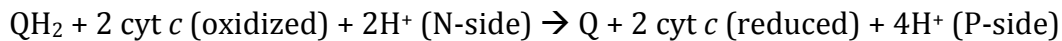
and the proton pumping stoichiometry is $1H^+/e^-$ (*9*).

1.2.4 Complex IV

Complex IV, or cytochrome *c* oxidase (C*c*O), is the last enzyme in the electron transport chain and it catalyzes the terminal reduction of O_2. Mammalian C*c*O comprises 13 subunits (*60*) of which only two are essential for enzyme catalysis; denoted subunit I and subunit II; these catalytic subunits are very well conserved in bacterial C*c*Os (*61, 62*). As with complex III, X-ray structures are available for C*c*Os from both eukaryotic and prokaryotic sources (*60, 63, 64*).

A schematic of complex IV function is shown in **Figure 1.7**. Electrons are introduced into complex IV by the soluble cytochrome *c* reduced by complex III; cytochrome *c* transiently docks to the P-side of the enzyme while it donates its electron into complex IV (*65*). The first entry point for electrons into C*c*O is a dimeric copper center, Cu_A, located in subunit II. The electrons are then transferred to subunit I, to a heme *a* cofactor, and eventually to the binuclear center, the catalytic site comprised of a heme a_3 and a single Cu_B. O_2 binds to the heme a_3 and through a complicated, but well-described reaction sequence (*66*) is reduced to

water, in the process consuming four electrons and four protons (from the N-side of the membrane). Since four electrons are required for the full reduction of O_2, four molecules of cytochrome c must sequentially bind and donate electrons into CcO during each reaction cycle.

Certain steps in the reaction cycle are coupled to the pumping of protons, such that the complete reduction of O_2 results in four protons pumped to the P-side of the membrane (*67*). The net reaction catalyzed by complex IV is thus:

4 cyt c (reduced) + 8H$^+$ (N-side) + O2 $\rightarrow$ 4 cyt c (oxidized) + 4H$^+$ (P-side) + 2H$_2$O
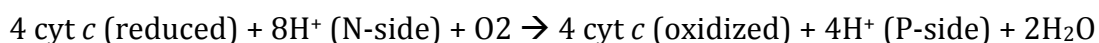
for a proton pumping stoichiometry of 1 H$^+$/e$^-$. Overall, the net H$^+$/e$^-$ ratio is 2, as the electrons and the protons used for the reduction of O_2 originate from opposing sides of the membrane (*9*). Note that the imbalance in protons here (eight in, four out) cancels out the perceived imbalance in the complex III reaction described in the previous section (two in, four out).

Two main channels consisting of water molecules and protonatable amino acid side chains, termed the D-pathway and the K-pathway, are proposed to play a role in the transfer of protons from the N-side of the membrane to the binuclear center for both proton pumping and the reduction of O_2 (*68*). The pathway for proton extrusion to the P-side of the membrane is more ambiguous, but is thought to follow a path above the propionates of hemes a and a_3 (*69-71*).

1.2.5 Complex V

Complex V, or the F$_0$F$_1$-ATP synthase, is a remarkable nano-motor that is well conserved throughout all kingdoms of life (*9*). Using an elegant rotary mechanism

(**Figure 1.8**), this large enzyme is able to synthesize ATP by utilizing the pmf generated by the other respiratory complexes. Alternatively, in the absence of pmf and the abundance of ATP, the ATP synthase can work in reverse, hydrolysing the ATP to generate a proton gradient (*72*). Although an X-ray structure of the complete enzyme is unavailable, crystallographic and electron microscopic information for many of the individual parts are available (*73-80*). The simplest form of the enzyme is the bacterial model; for example, the *E. coli* homolog consists of eight distinct subunits in varying stoichiometries. In contrast, in bovine mitochondria, up to 13 different subunits have been identified (*81*), however, the overall architecture is similar. We will restrict discussion to the core subunits found in the *E. coli* enzyme, which are all conserved in the mitochondrial enzyme.

The F_0F_1-ATP synthase is arranged as two domains: the soluble F_1 domain and the membrane-intrinsic F_0 domain. The F_1 domain is the site of ATP synthesis/hydrolysis and is comprised of five distinct subunits in the stoichiometry $(\alpha\beta)_3\gamma\delta\epsilon$. The F_0 domain contains the proton translocation machinery and is assembled from the three remaining subunits, with a preferred stoichiometry of ab_2c_{10}, although the exact number of c-subunits may vary (*82*). The α- and β-subunits are arranged in an alternating, hexameric ring where each $\alpha\beta$ dimer lies within a three-fold axis of symmetry. Each $\alpha\beta$ dimer contains an active-site for ATP synthesis. The δ-subunit associates with the $\alpha\beta$ ring and along with the b-subunits, forms the stator, which links the ring in F_1 to the stationary a-subunit in the F_0 domain. The ϵ-subunit binds to the δ-subunit and acts as a natural inhibitor to rotation. The c-subunits circularize and also form a rotary motor, but one that spans

the membrane. Together, the a- and c-subunits form the unit that translocates protons across the membrane. The γ-subunit lies in the middle of the F_1 ring and forms the spinning rotor that is driven by rotation of the c-ring (*81*).

A "Brownian ratchet" model has been offered to explain how the translocation of protons can drive rotation of the c-ring (*83, 84*). The model proposes a pair of "half-channels" in subunit a, which juxtapose against the c-ring. Protons must enter one half-channel on the P-side of the membrane, and bind to a protonation site on one of the c subunits. That proton can only access the other exit channel on the N-side of the membrane through a complete 360° rotation of the c-ring, thus generating the required torque to drive the γ-rotor.

ATP synthesis at the catalytic site in F_1 occurs through an "alternating binding sites mechanism" (*85*). Each αβ dimer in the F_1 ring contains a non-equivalent catalytic site, due to the asymmetry of the γ-rotor in the center. Each catalytic site has a different affinity for the substrates and products at any one time, such that when one site is open and able to bind ADP and inorganic phosphate, another has closed around the bound substrates, while the third has just released the newly formed ATP molecule. Thus, rotation of the c-ring drives rotation of the γ-rotor within the F_1 ring. A 360° rotation of the rotor forces each active-site to cycle through the three different conformations, resulting in the production of three ATP molecules (*86*). When working in reverse, it is ATP hydrolysis by the F_1 catalytic sites that drives rotation of the γ subunit (*87*), which causes the c-ring to turn in reverse, driving proton translocation.

While the *E. coli* ATP synthase optimally assembles with 10 c-subunits, that number can vary depending on the species (*79, 82, 88, 89*). As each c-subunit binds a single proton, the number of c-subunits will determine the H^+/ATP ratio. For example, since three ATP molecules are synthesized per complete rotation of the c-ring, in *E. coli,* the H^+/ATP ratio is 3.3.

1.3 Respiration in *E. coli*

1.3.1 Diversity of the *E. coli* Respiratory Chain

Compared to the mitochondrial respiratory chain, cellular respiration in *E. coli* is simple. Under certain aerobic growth conditions, the *E. coli* respiratory chain can resemble a truncated form of the mitochondrial respiratory chain, consisting of NADH dehydrogenase, SQR, quinol *bo$_3$*-oxidase, and a F_0F_1-ATP synthase, which are homologous to complexes I, II, IV, and V, respectively (*9*). *E. coli* lack protein homologs of complex III or soluble cytochrome *c*.

As a facultative anaerobe, *E. coli* can grow via fermentation pathways in the absence of a suitable terminal electron acceptor (*90*); however, that pathway will not be discussed further. *E. coli* can respire on a multitude of substrates in addition to oxygen, such as nitrate, nitrite, fumarate, trimethylamine N-oxide (TMAO), and dimethylsulfoxide (DMSO). Its respiratory chain has a modular design, consisting of a primary dehydrogenase and a terminal reductase, linked together by the lipid-soluble Q-pool (**Figure 1.9**). The diversity in the respiratory chain derives from the large number of dehydrogenases (15) and reductases (10) encoded by the *E. coli* genome (*91*).

The energy available under anoxic conditions is considerably less than during aerobic growth. Thus, while aerobic growth can sustain the pmf through the proton pumping activities of NADH dehydrogenase and quinol bo_3-oxidase, the oxidoreductases expressed during anaerobic growth can only translocate protons using Mitchellian redox loops (*91*) (**Figure 1.10**).

Additional diversity is present at the level of the Q-pool. Whereas mitochondria only utilize ubiquinone, *E. coli* is capable of synthesizing three types of quinones: UQ ($E_{m,7}$ = +110 mV), menaquinone (MQ, $E_{m,7}$ = -80 mV), and demethylmenaquinone (DMQ, $E_{m,7}$ = +40 mV) (*92*). UQ, a benzoquinone, is the major component of the Q-pool under aerobic conditions while the latter two napthoquinones are synthesized under anaerobic growth conditions. However, the method by which the composition of the Q-pool is controlled is unknown (*93*).

1.3.2 Regulation of Gene Expression during Aerobic and Anaerobic Growth

The exact composition of the respiratory chain is under the control of gene expression, based on the availability of terminal electron acceptors (*94*). The expression of the terminal reductase is selected for the substrate with the highest redox potential; thus, respiration on O_2 ($E_{m,7}$ = +820 mV) is the most preferred, while in anoxic conditions, respiration on nitrate ($E_{m,7}$ = +420 mV) is optimal. The presence of O_2 and nitrate will suppress the expression of all other terminal reductases (*94*). While the expression of the dehydrogenases can also be responsive to the presence of O_2 and nitrate, other factors such as metabolic needs of the cell appear to be more determinant (*95*). The regulation of gene expression in the

respiratory chain is under the control of several global regulators, which act in concert to optimize the constituents of the respiratory chain for the environmental conditions.

The fumarate nitrate reductase regulator (Fnr) protein is a constitutively-expressed transcriptional regulator of anaerobic gene expression (*96, 97*). Depending on the gene loci, Fnr can act as either a transcriptional activator or repressor (*98, 99*). Generally, genes associated with anaerobic respiration are activated by Fnr, while genes linked with aerobic respiration are repressed (*94*). The active form that is able to bind to DNA is dimeric, with each monomer containing a single [4Fe-4S] cluster (*100*). The presence of O_2 causes spontaneous collapse of the [4Fe-4S] cluster to a [2Fe-2S] cluster and dissociation of the dimer into inactive Fnr monomers (*97*). If O_2 persists in the environment, the [2Fe-2S] cluster is eventually lost, forming apo-Fnr (*100*), which given time can re-acquire a [4Fe-4S] cluster (*100*). Thus, the three forms of the enzyme are in a constant state of equilibrium, while the concentrations of each form are a function of the intracellular O_2 concentration (*101*).

Another level of gene expression arises from the ArcAB two-component regulatory system. The ArcB sensor recognizes the aeration state of the cell, and in response regulates the phosphorylation state of ArcA. Like Fnr, ArcA-P induces expression of genes linked with anaerobic respiration and represses those linked with aerobic respiration (*94*). In contrast to Fnr, ArcB does not respond to O_2 concentrations. Instead, the regulation of the ArcB appears to be at the level of the Q-pool, and specifically, its redox state. Both MQH_2 and UQ levels have been shown

to affect the stability of a disulfide bond within ArcB that is critical for its kinase activity (*102, 103*).

The nitrate-responsive regulatory mechanism stems from two homologous two-component systems, NarXL and NarQP. NarL/NarP are the response regulators that once phosphorylated, bind DNA to activate expression of genes associated with nitrate respiration and suppress the genes of the other terminal reductases (*104*). As opposed to ArcB, NarX/NarQ responds directly to nitrate concentrations through direct binding of the molecule, which stimulates their kinase activities (*105*).

Another important two-component regulatory system is the DcuRS system. Similar to the two-component systems discussed above, DcuS in the membrane responds to C_4-dicarboxylates in the environment, such as succinate and fumarate, and phosphorylates the response regulator, DcuR (*106, 107*). DcuR-P is mostly responsible for inducing transcription of genes related to fumarate metabolism.

1.4 Complex II

Mitochondrial complex II (succinate:quinone oxidoreductase, SQR; succinate dehydrogenase, Sdh) directly links the TCA cycle with the mitochondrial respiratory chain through the oxidation of succinate to fumarate in the mitochondrial matrix, liberating two electrons that are transferred directly into the lipid-soluble Q-pool. Since the redox potential of the succinate/fumarate couple ($E_{m,7}$ = +30 mV) and the UQ/UQH$_2$ couple ($E_{m,7}$ = +110 mV) are relatively close, the transfer of electrons from succinate to UQ is not energetic enough to support the translocation of protons across the membrane (*91*). As predicted from the thermodynamics, the redox

activity of complex II is non-electrogenic; the oxidation of succinate, which releases two protons, and the reduction of UQ, which consumes two protons, both occur on the matrix side of the membrane (or in the case of bacteria, on the cytoplasmic side).

Mitochondrial complex II is a heterotetrameric protein: SdhA, which refers to the large, soluble catalytic subunit, SdhB, the electron transfer subunit, containing three distinct [Fe-S] clusters; and SdhC and SdhD, which together form a membrane anchor subunit that binds a single b heme (**Figure 1.11**). Due to the high overall sequence and structure similarities, the ease of genetic manipulation, and the ability to overexpress very large quantities of enzyme (*108*), *E. coli* SQR is an excellent model system to study structure-function relationships in mitochondrial complex II. The following sections examine the function of complex II, with particular emphasis on *E. coli* SQR.

1.4.1 Complex II Genetics

The *E. coli* genome contains two operons, both around 3.2kb in length – *sdhCDAB* and *frdABCD* – that encode the distinct complex II paralogs SQR and quinol:fumarate oxidoreductase (QFR; fumarate reductase, Frd), respectively*.* The *sdhCDAB* operon is centered at 16.29 min on the chromosome while the *frdABCD* operon is centered at 94.37 min (*7*).

While the function of *E. coli* SQR is the aerobic conversion of succinate to fumarate*, E. coli* QFR catalyzes the anaerobic, terminal reduction of fumarate to succinate, using reduced MQH_2 as the electron donor. Interestingly, the two paralogs are similar enough that their catalytic profiles are identical. In other words, SQR can

function as a MQH_2-dependent fumarate reductase and QFR can catalyze the succinate-dependent reduction of UQ (*109, 110*). Moreover, given the proper enzyme expression, either enzyme can complement an *E. coli* strain deleted in the other (*108*).

The control of SQR expression is regulated by Fnr and the ArcAB system, which suppresses gene expression at the *sdh* promoter during anaerobiosis (*111, 112*). Expression of QFR at the *frd* promoter is induced by the anaerobic regulator Fnr and is suppressed by the presence of nitrate (*113*). Thus, in wild-type *E. coli*, the regulatory systems ensure that SQR and QFR expression do not overlap.

The *E. coli* DcuRS two-component regulatory system is important in both aerobic and anaerobic growth. During aerobic growth on succinate, DcuR up-regulates expression of DctA (*114*), a C_4-dicarboxylate symporter that utilizes the H^+ gradient to import succinate into the cell (*115*). During anaerobic growth on fumarate, DcuR enhances expression of QFR (*107*); the expression of other C_4-dicarboxylate transporters is also increased. DcuA and DcuB are succinate:fumarate antiporters, while DcuC operates as a succinate efflux pump (*116, 117*). DcuA is constitutively expressed (*118*) while DcuB expression is induced by both Fnr and DcuR (*107, 118*). DcuC is only expressed anaerobically, under the control of Fnr (*117, 119*).

In humans, the genes that encode the four structural subunits of complex II, *SDHA, SDHB, SDHC, and SDHD* are all nuclearly encoded (on chromosomes 5p15, 1p36.1-p35, 1q23.3, and 11q23, respectively), in contrast to the other mitochondrial respiratory complexes, which all have at least one subunit encoded by the

mitochondrial genome. The promoter regions of the *SDH* genes have been found to contain binding sequences for the nuclear respiratory factors, NRF-1 and NRF-2 (*120-122*).

1.4.2 Structural Similarity Between Complex II and the *E. coli* Homologs

Sequence identity between mitochondrial complex II and *E. coli* SQR is roughly 50% identity between the hydrophilic SdhAB dimers, but is slightly less than 20% identity in the SdhCD membrane domains (*123*). High-resolution X-ray crystal structures are available for *E. coli* SQR, as well as porcine and avian complex II (*123-125*). A comparison of the *E. coli* and pig enzymes reveals a root-mean-square-deviation (rmsd) of 1.0Å over 541 of 613 C_α atoms in SdhA and an rmsd of 0.8Å over 214 of 249 C_α atoms in SdhB (*123*). As may be expected from the low sequence identity, structural similarity within the membrane domains is also much lower. In SdhC, an rmsd of 1.3Å over 76 of 138 C_α atoms is observed and an rmsd of 1.7Å over 79 of 102 C_α atoms in SdhD (*123*). A representative alignment of porcine complex II and *E. coli* SQR is shown in **Figure 1.12**.

The crystal structure of *E. coli* QFR was the first one published for a complex II homolog (*126*). The overall architecture of QFR is very similar to SQR. In comparison with the structure of *E. coli* SQR, the FrdAB and SdhAB catalytic dimers share considerable structural similarity. In contrast, the membrane domains are very different: two striking differences are immediately noticeable. First, the Q-sites are not conserved, and QFR does not bind a heme within its transmembrane domain (*125, 126*).

1.4.3 Classification of complex II homologs

Among different complex II homologs, the subunit and cofactor compositions can be highly variable. While the catalytic dimer, SdhAB, is very well conserved across the three kingdoms of life, the same cannot be said about the membrane domains. Based on these differences, a classification scheme was developed to encompass all the complex II variants (*127, 128*):

1) Type A: two membrane anchor subunits; two hemes

2) Type B: one membrane anchor subunit; two hemes

3) Type C: two membrane anchor subunits; a single heme

4) Type D: two membrane anchor subunits; no heme

5) Type E: two radically different membrane anchor subunits, denoted SdhE and SdhF; no heme

Mitochondrial complex II and *E. coli* SQR fall into the Type C class of enzymes while *E. coli* QFR is a Type D enzyme. Type A enzymes include 'classical' SQRs in archaeal organisms (*129*) and the crystal structure of a Type A SQR, from *Thermus thermophilus,* was recently published (*130*). Type B SQRs are more extensive and are typically found in gram-positive bacteria and ε-proteobacteria (*128*). Examples here are the SQR from *Bacillus subtilis* (*131*) and the QFR from *Wolinella succinogenes*; the X-ray structure is available for the latter (*132*). Examples of Type E enzymes are the 'non-classical' SQRs found in archaea (*129*).

1.4.4 Assembly of Complex II

In *E. coli*, newly translated SQR must be targeted to the bacterial inner membrane. Although not essential, the insertion of SQR is enhanced by the signal recognition particle (SRP) (*133*). SRP binds to the hydrophobic targeting sequences in transmembrane proteins, co-translationally, and directs them to the inner membrane for insertion either by the SecYEG translocon, or by the insertase YidC, in a Sec-independent manner (*134*). In eukaryotes, since the four complex II structural genes are all nuclear encoded, newly-translated polypeptides must contain a leader signal peptide that ensures proper targeting to the mitochondria (*135*).

Unlike for many of the *E. coli* molyboenzymes, such as nitrate reductase, TMAO reductase, DMSO reductase, and formate dehydrogenase, a dedicated chaperone has never been identified for SQR (*136-139*). This is not the case for mitochondrial complex II, where two specific maturation proteins have been identified.

A *SDHAF1* (succinate dehydrogenase assembly factor 1) gene mutation was identified in a patient with reduced complex II activity, but normal activity in the rest of the respiratory chain. A deletion of the homologous gene in *Saccharomyces cerevisiae* confirmed aberrant expression of complex II, exclusively (*140*). The exact function of SDHAF1 is still unknown, but the protein contains a LYR-motif that is common in other proteins associated with [Fe-S] metabolism (*141-143*). Therefore, it is postulated that SDHAF1 aids in the insertion of the [Fe-S] clusters into SdhB (*140*).

SDHAF2 mutants in yeast are also complex II deficient, and show decreased levels of all four SDH subunits (*144*). The active site in SdhA contains a FAD cofactor that is covalently linked to a conserved histidine. The covalent bond is critical for enzyme function (*145, 146*). It was shown that the absence of SDHAF2 activity resulted in the complete loss of covalently-bound FAD in SdhA; however, other flavoproteins were not affected in a similar manner (*144*). This suggests that SDHAF2 has a direct role in the flavination of complex II.

Neither SDHAF1 nor SDHAF2 are conserved in *E. coli*. Prior to the discovery of SDHAF2, it was believed that the formation of the covalent bond to the FAD was autocatalyzed (*147, 148*). As no chaperone has yet been identified, this may still be the case for *E. coli* SQR.

In general, little is known about the mechanism of heme insertion into proteins, except for the c-type cytochromes, which have their own well-characterized maturation machinery (*149, 150*). How the heme is inserted into *E. coli* SQR, whether co-translationally or post-translationally, and how *b*-type hemes are selected for, is unknown. Free heme is toxic to the cell, as it can generate harmful reactive oxygen species (ROS) (*151*). Therefore, newly synthesized heme molecules must be sequestered prior to insertion into apoproteins. While numerous heme carrier proteins have been identified, the role, if any, that these proteins play in the insertion process is unclear (*152*).

Nevertheless, our understanding of the cytochrome maturation process is slowly advancing. The assembly of cytochrome *c* oxidase is dependent on the Surf1 protein (*153*), which has the capability to bind *a*-type hemes (*154*). Surf1 homologs

have been identified in humans, yeast, and some bacteria (*153, 155, 156*). In addition, the CbaX protein in *T. thermophilus* was associated with heme *a* insertion into the *ba₃*-oxidase in this organism, although it does not show any sequence similarity to Surf1 (*157*) Recently, it was proposed that in the eukaryotic cytosol, glyceraldehyde-3-phosphate dehydrogenase (GAPDH) could mediate the insertion of heme *b* into inducible nitric oxide synthase (*158*). The mechanism by which these three proteins are able to promote heme insertion has yet to be established, but as evidence mounts for protein-mediated heme insertion into proteins, it is increasingly unlikely that the insertion of the heme *b* into *E. coli* SQR occurs spontaneously.

1.4.5 SdhA – the Large Catalytic Subunit

The sequence and structure of SdhA are well conserved within the complex II family of proteins, including *E. coli* SQR and QFR (*127*). The two major domains in SdhA are a FAD-binding domain and a capping domain. In *E. coli* SQR, substrate binding occurs at the interface of the two domains at a highly conserved dicarboxylate-binding site comprised of SdhA[H242], SdhA[T254], SdhA[E255], SdhA[H354], and SdhA[R399] (*159, 160*). In addition to succinate and fumarate, a number of other dicarboxylates are able to bind here, such as oxaloacetate, malonate, and malate, which act as competitive inhibitors of the enzyme (*161-163*). SQR isolated from *E. coli* is typically found tightly associated with oxaloacetate, and must first be "activated" (the oxaloacetate must be removed) in order to achieve optimal catalytic efficiency (*164*).

Adjacent to the dicarboxylate-binding site is the covalently-bound 8α-N3-hystidyl-FAD (*165*) that accepts the two electrons derived by the oxidation of succinate. During catalysis, a fairly stable flavosemiquinone (FSQ) intermediate is formed (K_{stab} = 1) (*166*). The covalent linkage (to SdhA[H45]) is believed to raise the midpoint potential of the FAD cofactor which is -138mV at pH 8.0 ($E_{m,7}$ = -90mV in E. coli QFR, $E_{m,7}$ = -79mV in bovine complex II) (*166-168*), as non-covalently linked FAD in *Shewanella frigidimarina* QFR has a much lower potential ($E_{m,7}$ = -156mV). Mutation of the residue equivalent to SdhA[H45] in other complex II homologs abolishes the covalent linkage; this results in a drop in FAD redox potential and a corresponding loss of succinate oxidation catalytic activity (but retained some fumarate reductase activity) (*145, 146*). Still, the redox potential of the FAD does not seem to be the only variable that affects directionality of the reaction at the FAD, as long range coloumbic effects from residues near the FAD are also thought to contribute (*166*). Interestingly, protein film voltammetry experiments have found that the rate of fumarate reduction at the FAD is inhibited when the driving force is very high (about -85 mV at pH 7.5) – a so-called 'tunnel diode effect' – but only in *E. coli* SQR and not QFR (*169-171*). The cause of this effect has yet to be elucidated.

The interconversion of succinate and fumarate is believed to proceed through a twisted transition-state intermediate. Crystal structures in which SdhA have fumarate bound to the active-site indicate the molecule is held in a non-planar orientation (*159, 172*). This is a result of steric constraints within the active-site and may be induced by closure of the capping domain, which shifts the conformation of the carboxylate-binding site, notably SdhA[T254], which is believed to drive much of

the twisting (*173*). As well, closing of the capping domain may also prevent undesirable side reactions at the active-site, such as the genesis of superoxide. In addition to steric considerations, catalysis is aided by polarization of the double bond in the fumarate molecule due to the vast hydrogen-bonding network provided by the enzyme around the C4-carboxylate (*159*). Succinate oxidation proceeds through hydride transfer from the C2 carbon to the N5 position of the FAD. The second proton is transferred to a conserved SdhA[R286] adjacent, possibly via a water molecule (*159, 160*). 3-nitropropionate, which binds near the FAD, can irreversibly inhibit SdhA activity, likely due to the formation of a cyclic adduct with the conserved SdhA[R286] (*123, 174*).

In mitochondrial complex II, SdhA is subject to post-translational modification. Sites for acetylation (*175*) as well as phosphorylation (*176*) have been identified, both of which can modulate the physiological activity of the enzyme. Acetylation of SdhA reduces the activity of the enzyme, possibly by restricting substrate access (*175*). Interestingly, the phosphorylation state of SdhA could affect whether the enzyme worked better as a succinate dehydrogenase or a fumarate reductase (*176*). Phosphorylation of complex II decreased its SQR activity while increasing its QFR activity, while the reverse was true in the dephosphorylated enzyme (*176*).

1.4.6 SdhB – the Electron Transfer Subunit

The SdhB polypeptide coordinates a chain of three [Fe-S] clusters that serve to shuttle the electrons from the active-site FAD to the Q-site located within the

transmembrane domain. As each [Fe-S] cluster is a single electron acceptor, the two electrons from the FAD must tunnel individually along each node in the relay. Each [Fe-S] is structurally and spectroscopically distinct. Nearest to SdhA is a [2Fe-2S] cluster (FS1, $E_{m,7}$ = +10 mV), followed by a [4Fe-4S] cluster (FS2, $E_{m,7}$ = -175 mV) and finally a [3Fe-4S] cluster (FS3, $E_{m,7}$ = +65 mV) (*177*). While the structure and cofactor composition of SdhB is well conserved among complex II homologs, the midpoint potentials of the [Fe-S] clusters can be quite variable (*178*).

In *E. coli* SQR, FS1 is coordinated by three cysteines and an aspartate: SdhB[C55], SdhB[C60], SdhB[C75], and SdhB[D63] (*125*). The three Cys residues are conserved within all SdhB homologs, but the residue in the Asp position shows much more variability, as in human complex II and *E. coli* QFR, that ligand is a Cys (*127*). FS2 is coordinated by a ferredoxin-like domain, characterized by three Cys ligands within a CysXXCyxXXCys motif and the fourth Cys ligand at another position within the polypeptide. The four ligands to FS2 are SdhB[C149], SdhB[C152], SdhB[C155], and SdhB[C216] (*125*). A similar cysteine motif is observed with the ligands to FS3, although only three Cys ligands are required for the [3Fe-4S] cluster: these are SdhB[C159], SdhB[C206], and SdhB[C212] (*125*). Presumably, when FS3 evolved, the fourth Cys ligand was lost and in *E. coli*, an isoleucine (SdhB[I209]) is present at that position. In *E. coli* QFR, the [3Fe-4S] cluster can be converted to a [4Fe-4S] cluster by introducing a Cys ligand in the appropriate position (*179*). However, attempts at a similar cluster conversion in SQR were unsuccessful, as an *E. coli* SdhB[I209C] mutant retains the [3Fe-4S] cluster (our data, unpublished), and likewise in *B. subtilis* SQR containing a SdhB[S215C]

mutation (*180*). Coincidentally, some type E SQRs in archaea contain a second [4Fe-4S] cluster instead of the [3Fe-4S] (*181*).

Of particular interest is the [4Fe-4S] cluster, which to date, is always found with a significantly lower midpoint potential relative to the other two centers (*178*). In SQR, the surrounding polypeptide can exert considerable influence on the redox potential of the iron sulfur clusters (*182, 183*). The presence of a low potential center in the middle of an electron transfer relay is quite common in other oxidoreductases and is found in, for example, *E. coli* nitrate reductase, QFR, and DMSO reductase (*184-186*).

It seems that highly endergonic electron tunneling steps within the electron transfer relay are permitted as long as the overall reaction catalyzed by the protein is exergonic. The function of such a low potential cluster is unclear, since according to Page *et al.*, even the most endergonic electron transfer steps occur on a faster timescale than most catalytic reactions, so long as the distances between cofactors are kept below 14Å (*11*). Nature may have evolved these low potential [Fe-S] clusters as rate-limiters, ensuring that electrons don't build up at the ends of the electron transfer relays. However, the experimental evidence on whether the midpoint potentials are important in determining catalytic turnover rates is inconsistent (*167, 182, 187, 188*). Protein film voltammetry studies by Hudson *et al.* have suggested that varying the potential of FS2 in *E. coli* QFR does not have an effect on the reduction of fumarate at the FAD (*167*). In contrast, Cheng *et al.* showed that when the potential of FS2 is decreased in *E. coli* SQR, by mutating the nearby residue SdhB[I150], significant decreases in physiological activity can be

observed (*182*). The effect of reducing the potential of the [4Fe-4S] cluster in *E. coli* SQR on empirically measured electron transfer rates is the subject of Chapter 5.

1.4.7 SdhCD – the Hydrophobic Membrane Anchor Subunits

As mentioned earlier, the transmembrane domains of complex II homologs can be very diverse; they may contain one or two subunits and coordinate zero, one, or two hemes. The transmembrane domains of *E. coli* SQR and QFR, as well as mammalian complex II, have the same overall architecture consisting of two hydrophobic subunits, a total of six transmembrane helices, and a core four-helix bundle (*123-126*).

The most significant difference between *E. coli* SQR and QFR is the presence of a *b* heme (b_{556}) sandwiched between the two membrane subunits in SQR, which is lacking in QFR. In *E. coli* SQR, the heme is bis-His coordinated ($E_{m,7}$ = +36 mV) (*189*); one histidine from each membrane subunit provides the fifth and sixth ligands to the heme iron – SdhC^{H84} and SdhD^{H71}. The heme is also found in mitochondrial complex II, however, its redox potential is much lower ($E_{m,7}$ = -185 mV) (*190*), rendering it resistant to succinate-dependent reduction (*191*). The two heme ligands are conserved across all type D SQRs, except in the yeast *S. cerevisiae* SQR where a cysteine replaces one of the histidines as a heme ligand (*192*). The lack of bis-His coordination of the heme in yeast SQR suggests that it may be an outlier amongst the mitochondrial complex II family of enzymes. In fact, it has been recently submitted that *S. cerevisiae* SQR does not really bind any heme at all (*193*), in spite of previous reports to the contrary (*194*).

Also associated with the heme in *E. coli* SQR is a cardiolipin molecule that associates between the two membrane subunits, just beneath the heme pocket (*125*). The presence of a lipid group here may stabilize the membrane domain as the acyl chains are in close contact with both membrane subunits. However, the cardiolipin here may not be necessary, and could likely be replaced by any lipid, as later structures of the enzyme did not show clear electron density in that region (*195*). As well, in the structure of porcine complex II, cardiolipin was not identified and a phosphatidylethanolamine was modeled in that site instead (*124*).

The quinone-binding site in *E. coli* SQR is located at the junction between SdhB, SdhC, and SdhD, just below the cytoplasmic face of the membrane. Despite the low sequence identity in the membrane domains of mitochondrial complex II and *E. coli* SQR, all the key residues that form the Q-site are very well conserved. The Q-site is fairly polar and many of the residues surrounding the Q-site are able to hydrogen bond to the head of the UQ: SdhB[W164], SdhB[H207], SdhC[S27], SdhC[R31], SdhD[D82], and SdhD[D83] (*196*). In Chapter 2, I examine the role that some of these residues have in the binding and protonation of the UQ. The Q-site in *E. coli* SQR is not conserved in the QFR enzyme; although in QFR, the Q-site also consists of residues from FrdB, FrdC, and FrdD, its spatial orientation lies in a slightly different area of the protein, compared to the Q-site in SQR (*126*). Despite the differences, Q-sites in both SQR and QFR are able to catalyze the reduction of UQ or the oxidation of MQH_2 (*109*).

A number of inhibitors are able to competitively inhibit Q-binding to varying degrees in *E. coli* SQR and QFR. These include carboxin, 2-thenoyltrifluoroacetone (TTFA), pentachlorophenol (PCP), dinitrophenol (DNP) derivatives, atpenin A5,

carboxanilides, and 2-n-heptyl 4-hydroxyquinoline (HOQNO) (*197-201*). Many of these have different affinities for SQR and QFR, reflecting the preferential binding for either UQ or MQ in these enzymes, respectively (*109*). Due to the varied shapes of the UQ and MQ head groups, it is highly likely that each type of quinone binds to the Q-site in a slightly different orientation; structural evidence suggests that the Q-site can support quinone binding at various depths (*195, 197*).

Another difference between the Q-sites of SQR and QFR is the stabilization of a semiquinone intermediate. A USQ can be detected by EPR in *E. coli* SQR, as we will see in Chapter 2, and also in *Paracoccus denitrificans* SQR (*202*). In contrast, a menasemiquinone EPR signal cannot be detected in wild-type *E. coli* QFR, suggesting that the intermediate in this enzyme is highly unstable (*198, 203*).

As *E. coli* SQR activity is non-electrogenic (*91*), protons consumed in the reduction of UQ must originate from the cytoplasmic face of the membrane. An ordered water channel that spans the cytoplasm and the Q-site was revealed in the X-ray structure of the enzyme and it is also conserved in the structures of the mitochondrial enzymes (*124, 125*). Disruption of the channel negatively affected quinone reduction rates, bolstering the hypothesis that it functions as the supplier of protons to the Q-site (*204*).

In the di-heme containing complex II homologs, *B. subtilis* SQR and *W. succinogenes* QFR, the quinone-binding site is located on the opposite side of the membrane as the hydrophilic subunits, distal to the [3Fe-4S] cluster, and denoted as a Q_D-site (as opposed to the Q_P-sites mentioned above, proximal to FS3) (*205, 206*). In these enzymes, the hemes certainly lie within the direct pathway of electron

transfer from one active-site to the other. The presence of two active-sites on opposing sides of the membrane should generate or consume Δp, depending on the direction of catalysis. Indeed, the *Bacillus* enzyme catalyzes the pmf-coupled reduction of menaquinone by succinate (*207*). However, the activity of *W. succinogenes* QFR does not appear to be electrogenic, which led to the proposal of the "E-pathway hypothesis", where the transfer of electrons across the two hemes is coupled to the transfer of two protons in the same direction, in order to compensate for the charge transfer (*206, 208*).

The question of whether the type C and type D complex IIs might have a Q_D-site has been controversial. Particularly, two putative Q-sites were observed in the crystal structures of *E. coli* QFR, which bound two MQ molecules; in addition the structure of porcine Complex II revealed two TTFA binding sites (*124, 126*). A Q_D-site in *E. coli* QFR would be especially puzzling, since the lack of a prosthetic group in the membrane domain prohibits electron tunneling to the Q_D-site on a physiological timescale, rendering it redox-inert. However, MQ could not be seen bound at the Q_D-site in later X-ray structures, and more recent analysis of the Q_P-site indicates that only a single redox-active, dissociable Q-site exists in *E. coli* QFR (*198, 209*). In porcine complex II, the TTFA molecule in the Q_D-site is only weakly bound, as suggested by the electron density (*124*). Furthermore, to date, no evidence for a Q_D-site has been provided by any of the X-ray structures of *E. coli* SQR or chicken complex II (*123, 183, 195, 197*). Collectively, structural and kinetic experiments support the presence of only a single Q_P-site in *E. coli* SQR (*109, 210*).

When the structure of *E. coli* SQR was elucidated, the position of the heme off the main electron transfer pathway was very curious (*125*). At least one function of the heme appears to be structural, as SQR could not properly assemble in a heme-deficient strain of *E. coli* (*211, 212*). The distances between cofactors suggest that electrons should be able to tunnel directly from the FAD to the UQ, through the [Fe-S] chain, bypassing the heme altogether. However, pulse radiolysis experiments have indicated that the electrons can quickly equilibrate between the heme, [3Fe-4S] cluster, and the Q-site (*213*). As *E. coli* QFR can catalyze succinate-dependent reduction of UQ, the role of the heme in catalysis is unclear. A popular theory for the function of the heme is in the suppression of ROS. By acting as an electron sink, the heme may reduce the lifetime of the USQ intermediate. Alternatively, the high potential of the heme in *E. coli* SQR could also be drawing electrons away from the FAD, as compared to *E. coli* QFR, the electron distribution at the FAD is significantly lower in SQR (*125*). In both cases, the reduction of highly reactive FSQ intermediates should decrease the number of auto-oxidative reactions with molecular oxygen to form superoxide. The role of the heme is a central theme of this thesis, and will be examined in Chapters 3 and 4.

1.5 Reactive Oxygen Species in the Mitochondrial Respiratory Chain

Since mitochondria are the primary consumers of O_2 in the cell, they are also the primary producers of ROS. The majority of ROS produced by mitochondria originates from the respiratory chain and are in the form of superoxide ($O_2^{\bullet-}$), which can dismutate to hydrogen peroxide (H_2O_2). H_2O_2 can potentially convert into the

highly reactive and highly destructive hydroxyl radical (•OH) (*214*). ROS can be destructive, readily causing oxidative damage to cellular components such as proteins, lipids, and DNA, and may be one of the driving forces behind the aging process (*215, 216*). The $E_{m,7}$ for the $O_2/O_2^{•-}$ couple is -160 mV; however, at physiological O_2 concentrations in the mitochondria, that redox potential can increase into the 100-200 mV range (*217*). Thus, under some conditions, the production of superoxide can be energetically favourable.

Theoretically, any short circuit along the electron transport chain can result in the reduction of O_2 to $O_2^{•-}$. However, most cofactors are shielded from molecular oxygen by the protein milieu; thus, most ROS production arises from solvent-exposed active-sites. There are two major sources of $O_2^{•-}$ in the mitochondria: complex I and complex III. Within complex I, $O_2^{•-}$ is produced primarily when O_2 reacts with the fully reduced form of the FMN cofactor (*218*). Since $O_2^{•-}$ production depends on the concentration of reduced FMN, maximal $O_2^{•-}$ generation at this site occurs when the $NADH/NAD^+$ ratio is very high and when Δp is large. Indeed, a correlation can be observed between high membrane potential and ROS production (*219, 220*). During reverse electron transport through complex I, a secondary source of $O_2^{•-}$ is activated, likely at the Q-site (*221*). $O_2^{•-}$ is also produced at the level of complex III, likely through the Q_o-site, and more so when the Q_i-site is inhibited (*222, 223*). However, the amount of $O_2^{•-}$ produced by complex III is much lower than that produced by complex I (*217*).

Although not a major source of ROS, complex II is also capable of producing $O_2^{•-}$. It has been shown that *E. coli* SQR and QFR are both potential sources of ROS

(*224*). QFR produces much higher levels of ROS than SQR, likely because it normally operates under anaerobic conditions (*225*). Messner and Imlay came to the conclusion that in SQR and QFR, the primary site of $O_2^{\bullet-}$ was the FAD (*224*). In contrast, a separate study by Zhao *et al*. indicated that the Q-site in *E. coli* SQR, and not the FAD, could be the major site of ROS production and importantly, mutations at the Q-site in *E. coli* SQR can significantly increase the yield of $O_2^{\bullet-}$ (*226*). Similar results were obtained in *S. cerevisiae* SQR (*227, 228*) and *Caenorhabditis elegans* SQR (*229, 230*). Most likely, ROS production can arise from either site, as was suggested in *Ascaris suum* complex II where both sites contribute to ROS generation (*231*).

1.6 Human Diseases Associated with Complex II Dysfunction

Since complex II lies at such a critical junction between metabolism and respiration, complex II dysfunction has predictably been implicated in a number of human diseases, although the clinical spectrum of disease is quite varied. Highlighting the importance of complex II activity, homozygous knockouts of the *SDHD* gene in mice are embryonic lethal (*232*).

Mutations in SdhA have been linked to Leigh syndrome, a progressive neurodegenerative disease (*233-235*). Leigh syndrome is associated with general dysfunction of mitochondrial energy conservation, as defects in numerous other mitochondrial proteins can also lead to the identical disease state (*236, 237, 237, 238*). Curiously, mutations in the other complex II structural genes have never been identified in Leigh syndrome patients.

Mutations in complex II have also been associated with a variety of tumor diseases; the most common of these is hereditary paraganglioma, benign tumors of the head and neck; pheochromocytoma, tumors originating from the adrenal medulla; and extra-adrenal paragangliomas that can be found anywhere along the sympathetic nervous system (*239*). More recently, complex II mutations were also identified in patients with Cowden syndrome (*240*), gastrointestinal stromal tumors (*241, 242*), renal cell carcinoma (*243-245*), and thyroid cancer (*246*), although these incidences are much more rare.

The link between complex II dysfunction and paraganglioma/pheochromocytoma was first identified as a mutation in *SDHD* (*247*). Since then, over 300 unique mutations have been identified in complex II-related genes, including genes for the other three complex II subunits as well as in the assembly factor genes, *SDHAF1* and *SDHAF2* (for a full listing of mutations, see the TCA Cycle Gene Mutation Database (*248*)). Patients harboring mutations in *SDHD, SDHB*, and to some extent, *SDHC*, are much more prone to developing paraganglioma (*248*). Why paraganglioma-causing mutations in *SDHA* are so rare is currently unknown. Only a single case of paraganglioma caused by a mutation in *SDHA* has ever been documented (*249*). Paragangliomas generally arise from loss of heterozygosity, and it may be the case that cells are not viable if a complete loss of SdhA activity occurs (*239*). Recently, it was reported that SdhA was a vital component of a mitochondrial ATP-sensitive potassium channel (*250*). However, it is not known if this channel is an essential component of the mitochondria.

The mechanism by which complex II dysfunction can lead to tumorigenesis likely involves hypoxia-inducible factor-1α (HIF-1α). HIF-1α is a transcriptional activator that regulates genes associated with the cellular response to hypoxic conditions, such as those relating to glucose homeostasis, and angiogenesis (*251*). Intracellular levels of HIF-1α are controlled by HIF-prolyl hydroxlases, which hydroxylate HIF-1α, thus marking it for rapid degradation, in an O_2-dependent reaction that concomitantly oxidizes α-ketoglutarate to succinate (*252*). It is known that both succinate and fumarate are capable of inhibiting the activity of HIF-prolyl hydroxlases (*253, 254*). High levels of succinate can result in stabilization of HIF-1α, which can translocate into the nucleus and stimulate cell proliferation. Alternatively, ROS can also increase the stability of HIF-1α, possibly by inhibition of the hydroxylases (*255*). Thus, mutations in complex II that either cause a loss of catalytic activity, or increase the production of ROS can both contribute to the formation of tumors.

Pheochromocytoma formation is also a symptom in a subset of patients with von Hippel-Lindau (VHL) disease (*256*). Tumors associated with VHL disease and complex II dysfunction show similar transcriptional profiles (*257*). Notably, the VHL protein also regulates the degradation of HIF-1α (*251*), further implicating this pathway in complex II-associated tumorigenesis.

Although not as common as those discussed above, decreased Complex II activity has also been shown in a number of other mitochondria-associated diseases such as progressive myopathy (*258*), encephalopyopathy (*140, 259*), isolated

cardiomyopathy (*260*), optic atrophy (*261*), ataxia (*262*), and Kearns-Sayre syndrome (*263*).

1.7 Figures
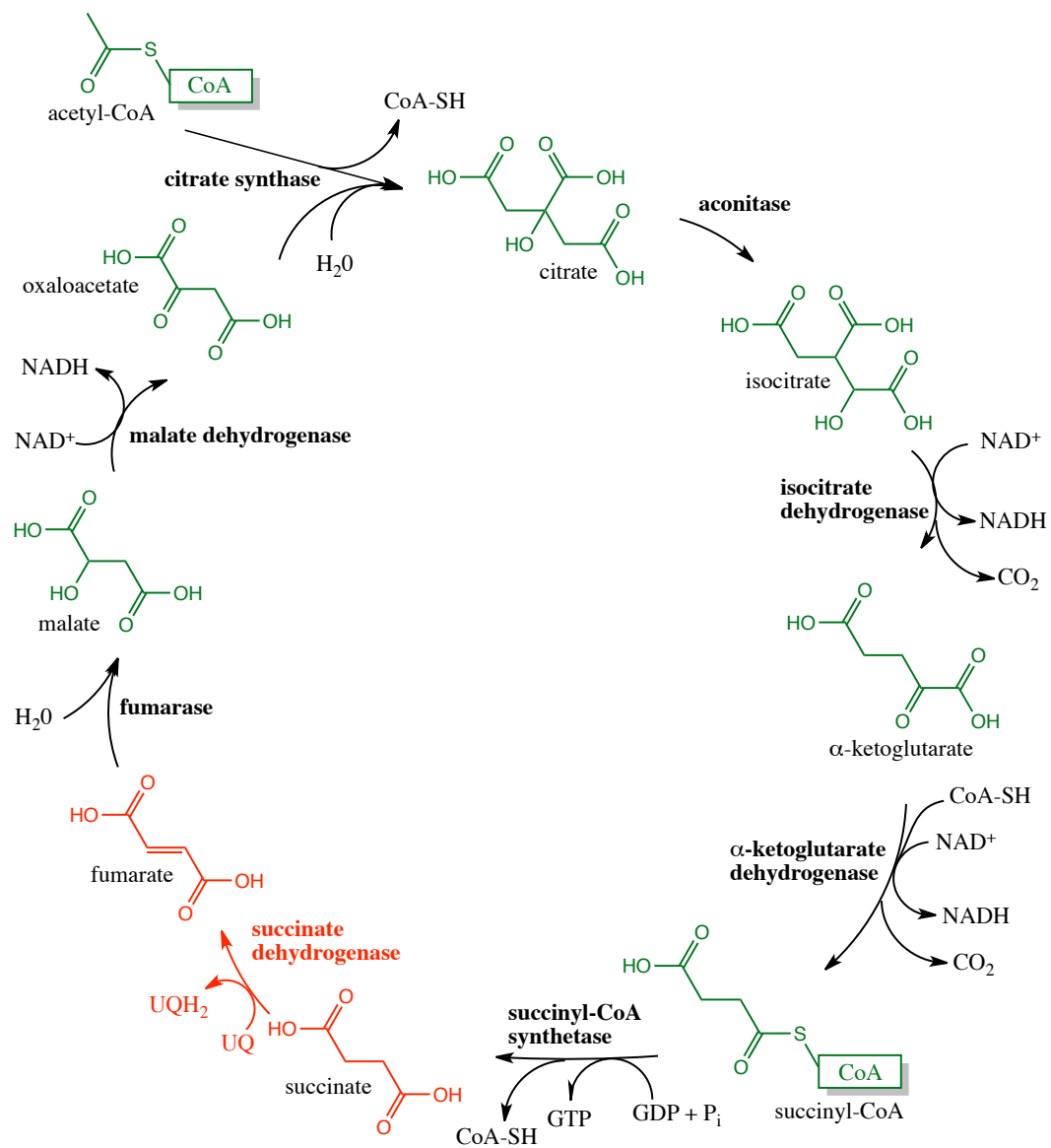
Figure 1.1: TCA cycle. The key part of the pathway catalyzed by complex II

is shown in red.
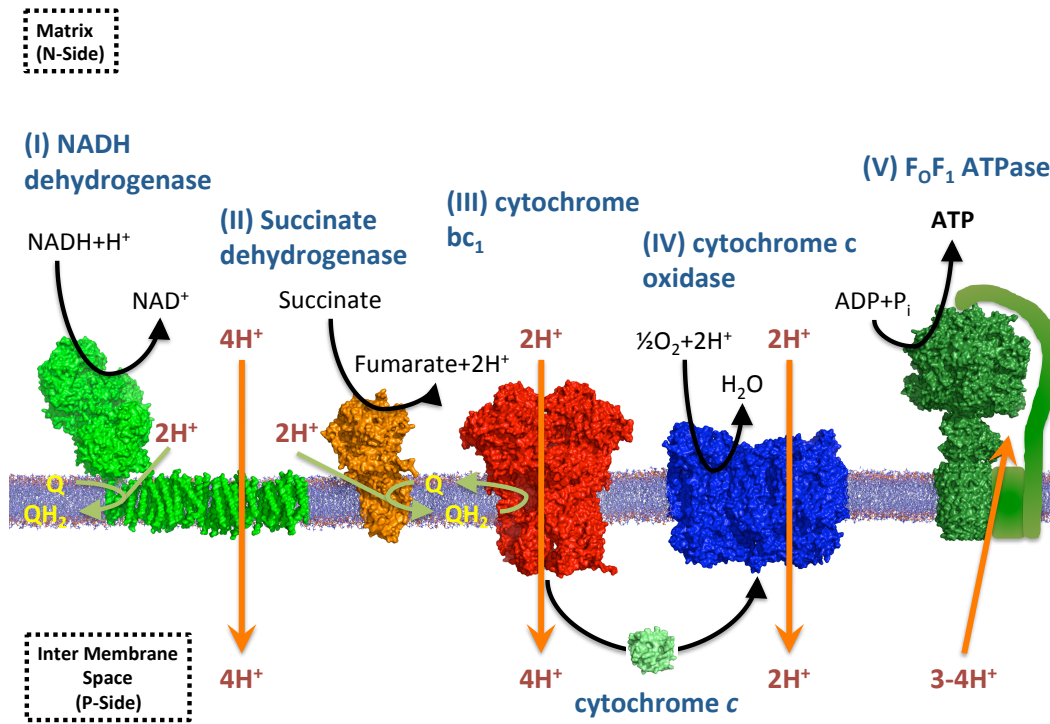
Figure 1.2: Schematic of the mitochondrial respiratory chain. The mitochondrial inner membrane is shown with the five canonical respiratory complexes, along with the direction of proton flow across the membrane. Protons are translocated from the N-side of the membrane to the P-side by complexes I, III, and IV. The activity of complex II is non-electrogenic and is not associated with proton translocation. The proton electrochemical gradient is utilized by complex V to generate ATP.
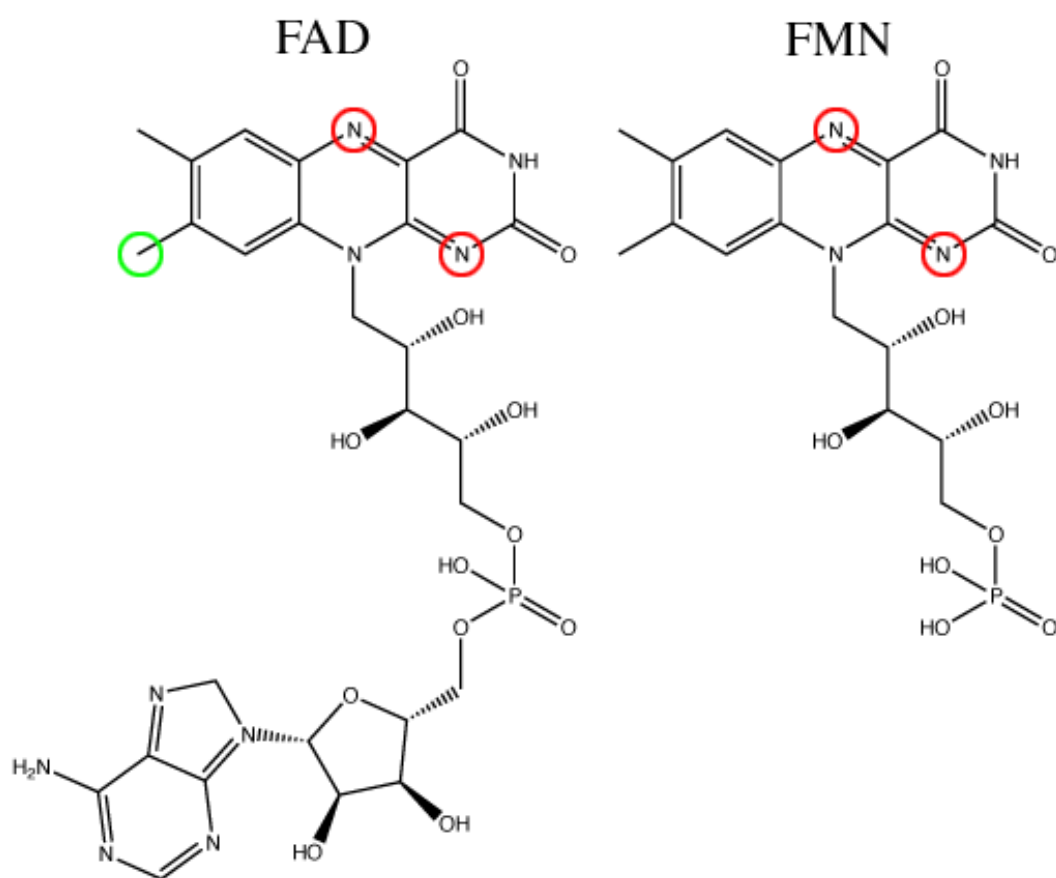
Figure 1.3: The two forms of flavin cofactor. FMN is found in complex I while FAD is the form bound to complex II. In red, the protonatable nitrogens. In green, the site of covalent attachment to complex II.
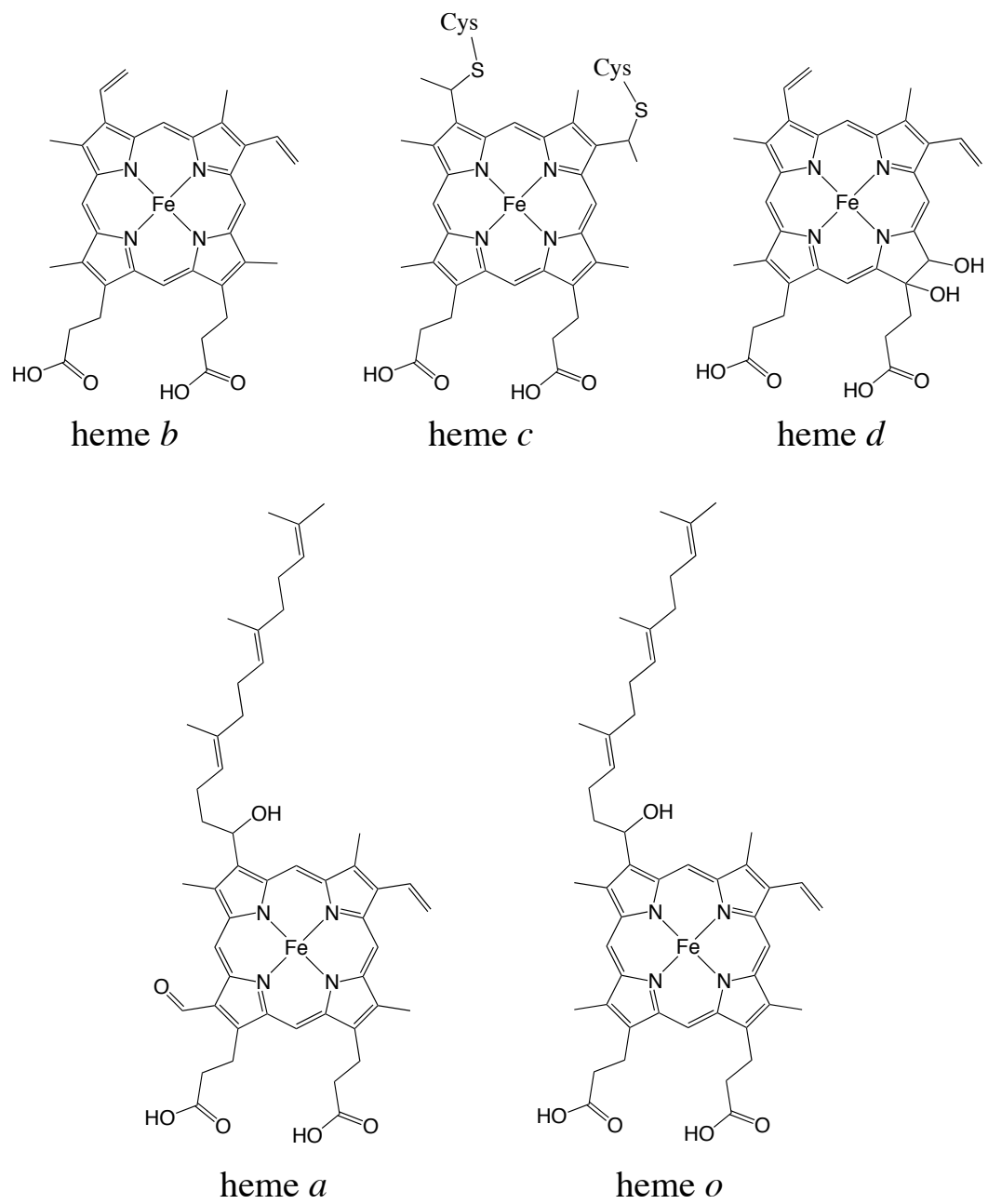
Figure 1.4: Major types of heme cofactors.
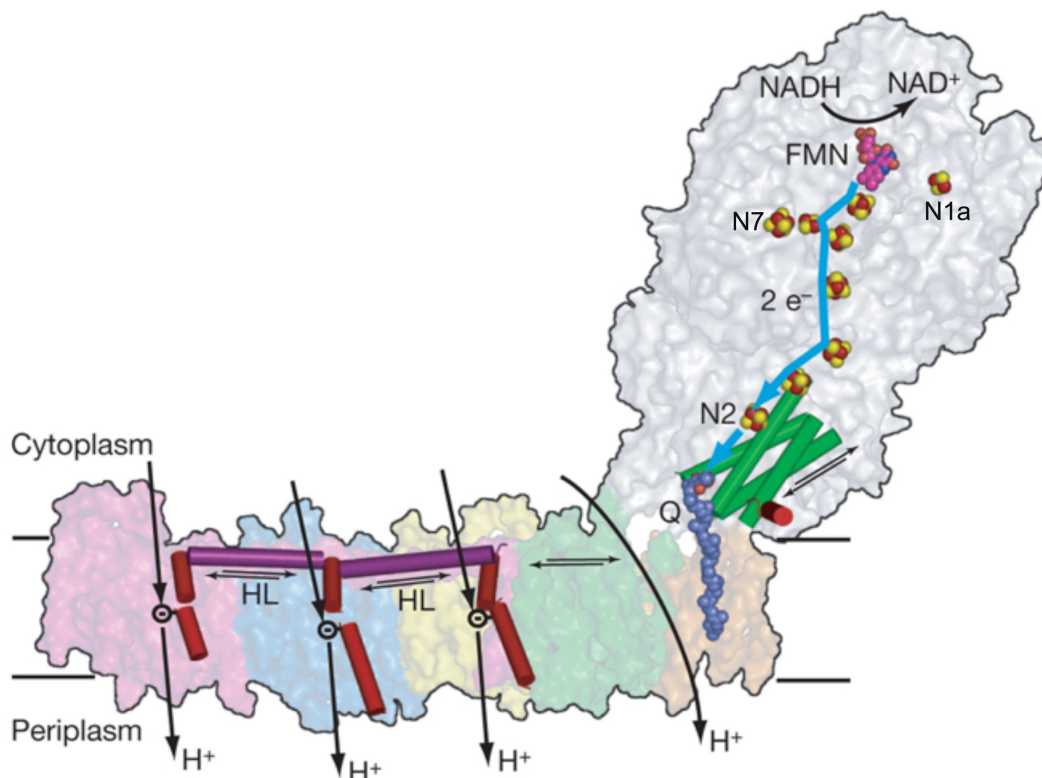
Figure 1.5: The catalytic mechanism of Complex I. Electron transfer through the hydrophilic domain is coupled to the pumping of 4 H+ in the membrane arm at the indicated sites. Notable [Fe-S] clusters N1a and N2 are indicated. Cluster N7 is not conserved in all Complex I structures and is too far from the electron transfer relay for competent electron transfer. Conformational changes associated with Q binding and reduction are translated to the three antiporter-like subunits by the amphipathic helix in magenta. This figure was adapted from Sazanov *et al. (34).*
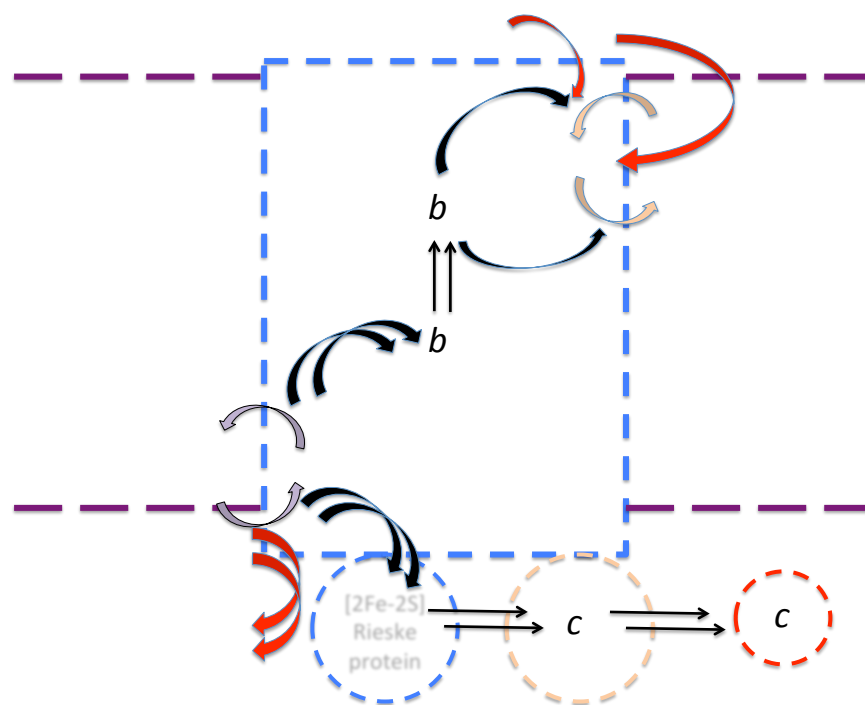
Figure 1.6: The Q-cycle mechanism in Complex III. Two successive turnovers of UQH_2 at the Q_o-site introduce two electrons into the high-potential chain and two electrons into the low-potential chain. The low-potential chain terminates with the reduction of a single UQ at the Q_i-site, while the two electrons in the high-potential chain are used to reduce two molecules of soluble cytochrome *c*. The localization of the two Q-sites on opposite sides of the membrane allow pmf generation by a redox loop mechanism. This figure was adapted from Crofts *et al. (264).*
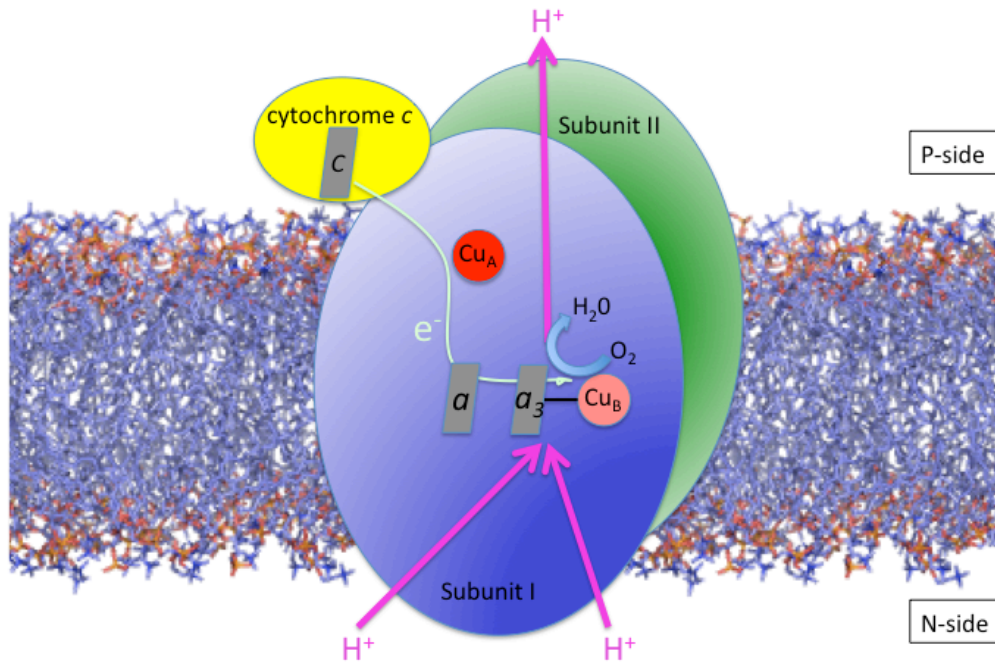
Figure 1.7: Schematic of complex IV catalysis. Electrons flow from cytochrome *c* to the binuclear center where oxygen is reduced to water. Two putative water channels mediate proton uptake from the N-side of the membrane.
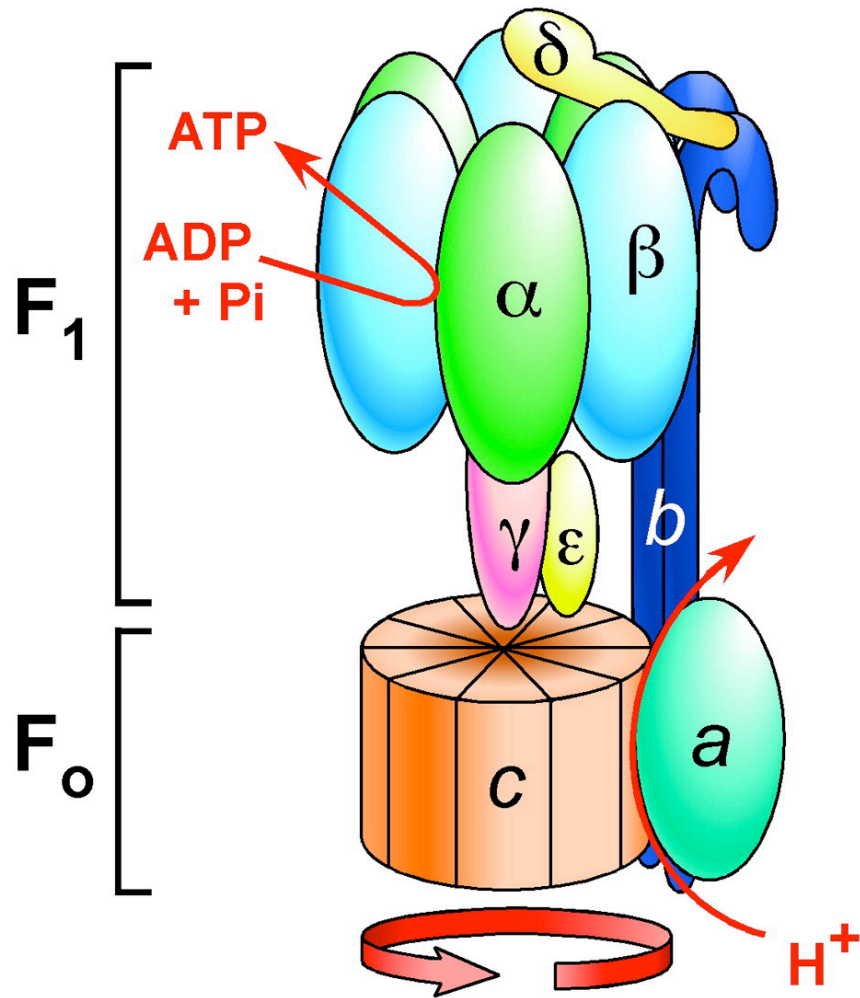
Figure 1.8: Schematic of the rotary mechanism of the F_1F_0-ATPase. Proton flow back into the N-side of the membrane drives rotation of the c-ring, which is coupled to rotation of the αβ-hexamer, the site of ATP synthesis. This figure was adapted from ref. *(265)*.

NADH

Succinate

Glycerol-3-P

Lactate

D-Amino Acids

Pyruvate

Formate

Hydrogen

ubiquinone

menaquinone

demethylmenaquinone

Oxygen

Nitrate

Nitrite

Fumarate

Dimethyl sulfoxide

Trimethylamine N-oxide

Thiosulfate

Figure 1.9: The modular design of the *E. coli* respiratory chain. The substrates on the left are oxidized by the appropriate dehydrogenases while reductases catalyze the terminal reduction of the substrates on the left. The three types of quinones that carry electrons between dehydrogenases and reductases are shown. In *E. coli*, n = 8 but the length of the isoprenoid sidechain can vary depending on the organism.

Figure 1.10: Proton translocation by the *E. coli* respiratory chain using a redox loop mechanism. In this example, the primary dehydrogenase is formate dehydrogenase, while nitrate reductase catalyzes the terminal reduction of nitrate. Proton motive force is generated by a Mitchell redox loop, where vectorial electron transfer across the membrane in one direction results in proton translocation in the opposing direction. This figure is taken as published by Rothery *et al.(266)*

.
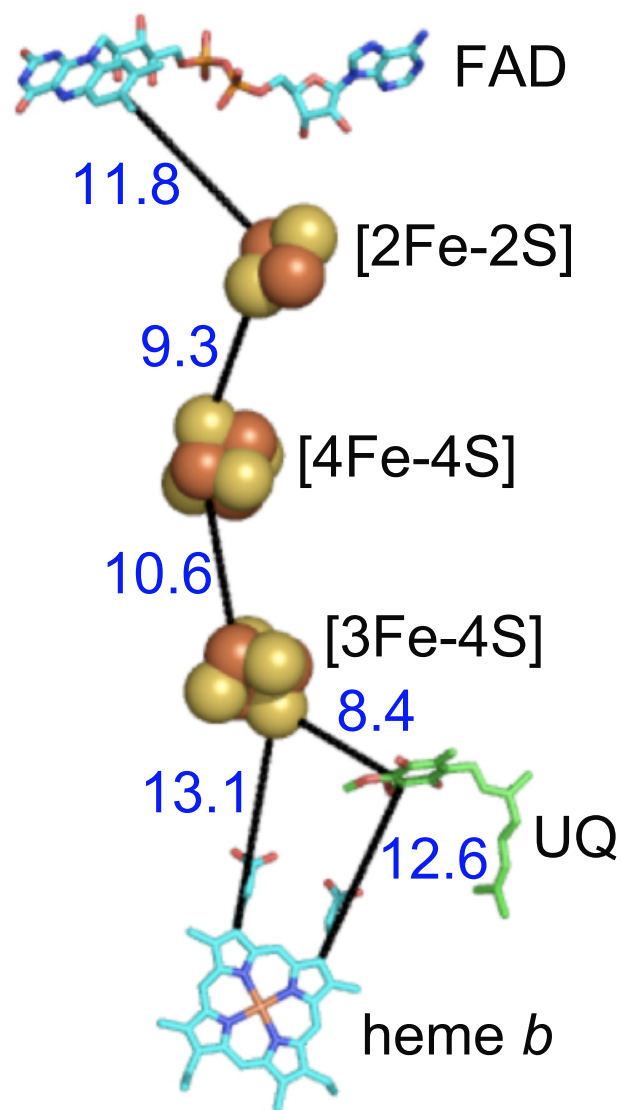
Figure 1.11: Arrangement of redox cofactors in complex II. The distances

shown between cofactors are derived from *E. coli* SQR (PDB: 1NEK *(125)*).
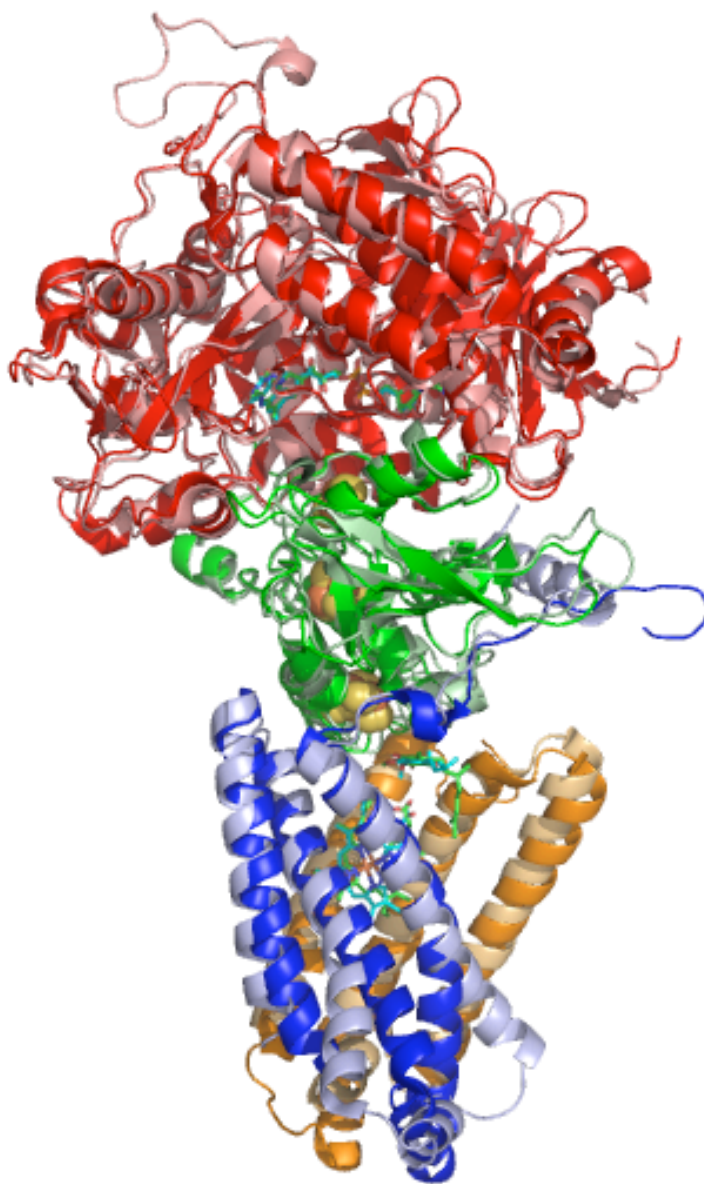
Figure 1.12: Superimposition of the structures of porcine complex II and *E. coli* SQR. PDB structures 1ZOY *(124)* and 1NEK *(125)* were used, respectively. While the SdhAB subunits and redox cofactors align very well, larger divergence in structure is seen in the membrane domains. The two structures were aligned in Pymol, over all backbone atoms.

1.8 References

1. Tornroth-Horsefield, S., and Neutze, R. (2008) Opening and closing the metabolite gate, *Proc Natl Acad Sci U S A 105*, 19565-19566.

2. McBride, H. M., Neuspiel, M., and Wasiak, S. (2006) Mitochondria: more than just a powerhouse, *Curr Biol 16*, R551-60.

3. Emelyanov, V. V. (2001) *Rickettsiaceae*, rickettsia-like endosymbionts, and the origin of mitochondria, *Biosci Rep 21*, 1-17.

4. Cotter, D., Guda, P., Fahy, E., and Subramaniam, S. (2004) MitoProteome: mitochondrial protein sequence database and annotation system, *Nucleic Acids Res 32*, D463-7.

5. Nelson, D. L., and Cox, M. M. (2005) *Lehninger Principles of Biochemistry* 4th ed., W. H. Freeman, New York.

6. Kelly, D. J., and Hughes, N. J. (2001) The citric acid cycle and fatty acid biosynthesis, in *Helicobacter pylori*: *Physiology and Genetics*, Chapter 12, ASM Press, Washington DC.

7. Blattner, F. R., Plunkett, G. r., Bloch, C. A., Perna, N. T., Burland, V., Riley, M., Collado-Vides, J., Glasner, J. D., Rode, C. K., Mayhew, G. F., Gregor, J., Davis, N. W., Kirkpatrick, H. A., Goeden, M. A., Rose, D. J., Mau, B., and Shao, Y. (1997) The complete genome sequence of *Escherichia coli* K-12, *Science 277*, 1453-1462.

8. Huynen, M. A., Dandekar, T., and Bork, P. (1999) Variation and evolution of the citric-acid cycle: a genomic perspective, *Trends Microbiol 7*, 281-291.

9. Nicholls, D. G., and Ferguson, S. J. (2002) *Bioenergetics 3*, Academic Press, San Diego.

10. Mitchell, P. (1961) Coupling of phosphorylation to electron and hydrogen transfer by a chemi-osmotic type of mechanism, *Nature 191*, 144-148.

11. Page, C. C., Moser, C. C., Chen, X., and Dutton, P. L. (1999) Natural engineering principles of electron tunnelling in biological oxidation-reduction, *Nature 402*, 47-52.

12. Barile, M., Brizio, C., Valenti, D., De Virgilio, C., and Passarella, S. (2000) The riboflavin/FAD cycle in rat liver mitochondria, *Eur J Biochem 267*, 4888-4900.

13. Giancaspero, T. A., Locato, V., de Pinto, M. C., De Gara, L., and Barile, M. (2009) The occurrence of riboflavin kinase and FAD synthetase ensures FAD synthesis in tobacco mitochondria and maintenance of cellular redox status, *FEBS J 276*, 219-231.

14. Tzagoloff, A., Jang, J., Glerum, D. M., and Wu, M. (1996) *FLX1* codes for a carrier protein involved in maintaining a proper balance of flavin nucleotides in yeast mitochondria, *J Biol Chem 271*, 7392-7397.

15. Bafunno, V., Giancaspero, T. A., Brizio, C., Bufano, D., Passarella, S., Boles, E., and Barile, M. (2004) Riboflavin uptake and FAD synthesis in *Saccharomyces cerevisiae* mitochondria: involvement of the Flx1p carrier in FAD export, *J Biol Chem 279*, 95-102.

16. Giancaspero, T. A., Wait, R., Boles, E., and Barile, M. (2008) Succinate dehydrogenase flavoprotein subunit expression in *Saccharomyces cerevisiae*-- involvement of the mitochondrial FAD transporter, Flx1p, *FEBS J 275*, 1103-1117.

17. Bacher, A., Eberhardt, S., Fischer, M., Kis, K., and Richter, G. (2000) Biosynthesis of vitamin B_2 (riboflavin), *Annu Rev Nutr 20*, 153-167.

18. Peters, J. W., Stowell, M. H., Soltis, S. M., Finnegan, M. G., Johnson, M. K., and Rees, D. C. (1997) Redox-dependent structural changes in the nitrogenase P-cluster, *Biochemistry 36*, 1181-1187.

19. Lill, R., Dutkiewicz, R., Elsasser, H. P., Hausmann, A., Netz, D. J., Pierik, A. J., Stehling, O., Urzica, E., and Muhlenhoff, U. (2006) Mechanisms of iron-sulfur protein maturation in mitochondria, cytosol and nucleus of eukaryotes, *Biochim Biophys Acta 1763*, 652-667.

20. Hamza, I. (2006) Intracellular trafficking of porphyrins, *ACS Chem Biol 1*, 627-629.

21. Frankenberg, N., Moser, J., and Jahn, D. (2003) Bacterial heme biosynthesis and its biotechnological application, *Appl Microbiol Biotechnol 63*, 115-127.

22. Heinemann, I. U., Jahn, M., and Jahn, D. (2008) The biochemistry of heme biosynthesis, *Arch Biochem Biophys 474*, 238-251.

23. Kadish, K., Smith, K. M., and Guilard, R. (2003) The iron and cobalt pigments: biosynthesis, structure and degradation, in *The Porphyrin Handbook*, *12*, Academic Press, San Diego.

24. Shifman, J. M., Gibney, B. R., Sharp, R. E., and Dutton, P. L. (2000) Heme redox potential control in *de novo* designed four-alpha-helix bundle proteins, *Biochemistry 39*, 14813-14821.

25. Schwarz, G., Mendel, R. R., and Ribbe, M. W. (2009) Molybdenum cofactors, enzymes and pathways, *Nature 460*, 839-847.

26. Carroll, J., Fearnley, I. M., Skehel, J. M., Shannon, R. J., Hirst, J., and Walker, J. E. (2006) Bovine complex I is a complex of 45 different subunits, *J Biol Chem 281*, 32724-32727.

27. Morgner, N., Zickermann, V., Kerscher, S., Wittig, I., Abdrakhmanova, A., Barth, H. D., Brutschy, B., and Brandt, U. (2008) Subunit mass fingerprinting of mitochondrial complex I, *Biochim Biophys Acta 1777*, 1384-1391.

28. Walker, J. E. (1992) The NADH:ubiquinone oxidoreductase (complex I) of respiratory chains, *Q Rev Biophys 25*, 253-324.

29. Hofhaus, G., Weiss, H., and Leonard, K. (1991) Electron microscopic analysis of the peripheral and membrane parts of mitochondrial NADH dehydrogenase (complex I), *J Mol Biol 221*, 1027-1043.

30. Peng, G., Fritzsch, G., Zickermann, V., Schagger, H., Mentele, R., Lottspeich, F., Bostina, M., Radermacher, M., Huber, R., Stetter, K. O., and Michel, H. (2003) Isolation, characterization and electron microscopic single particle analysis of the NADH:ubiquinone oxidoreductase (complex I) from the hyperthermophilic eubacterium *Aquifex aeolicus*, *Biochemistry 42*, 3032-3039.

31. Djafarzadeh, R., Kerscher, S., Zwicker, K., Radermacher, M., Lindahl, M., Schagger, H., and Brandt, U. (2000) Biophysical and structural characterization of proton-translocating NADH-dehydrogenase (complex I) from the strictly aerobic yeast *Yarrowia lipolytica*, *Biochim Biophys Acta 1459*, 230-238.

32. Guenebaut, V., Schlitt, A., Weiss, H., Leonard, K., and Friedrich, T. (1998) Consistent structure between bacterial and mitochondrial NADH:ubiquinone oxidoreductase (complex I), *J Mol Biol 276*, 105-112.

33. Berrisford, J. M., and Sazanov, L. A. (2009) Structural basis for the mechanism of respiratory complex I, *J Biol Chem 284*, 29773-29783.

34. Efremov, R. G., Baradaran, R., and Sazanov, L. A. (2010) The architecture of respiratory complex I, *Nature 465*, 441-445.

35. Sazanov, L. A., and Hinchliffe, P. (2006) Structure of the hydrophilic domain of respiratory complex I from *Thermus thermophilus*, *Science 311*, 1430-1436.

36. Galkin, A., Drose, S., and Brandt, U. (2006) The proton pumping stoichiometry of purified mitochondrial complex I reconstituted into proteoliposomes, *Biochim Biophys Acta 1757*, 1575-1581.

37. Grivermikova, V. G., Kotlyar, A. B., Karliner, J. S., Cecchini, G., and Andrei, D. V. (2007) Redox-dependent change of nucleotide affinity to the active site of the mammalian complex I, *Biochemistry-us 46(38)*, 10971-10978.

38. Chance, B., and Hollunger, G. (1961) The interaction of energy and electron transfer reactions in mitochondria. I. General properties and nature of the products of succinate-linked reduction of pyridine nucleotide, *J Biol Chem 236*, 1534-1543.

39. Brandt, U. (2006) Energy converting NADH:quinone oxidoreductase (complex I), *Annu Rev Biochem 75*, 69-92.

40. Kussmaul, L., and Hirst, J. (2006) The mechanism of superoxide production by NADH:ubiquinone oxidoreductase (complex I) from bovine heart mitochondria, *Proc Natl Acad Sci U S A 103*, 7607-7612.

41. Tocilescu, M. A., Fendel, U., Zwicker, K., Kerscher, S., and Brandt, U. (2007) Exploring the ubiquinone binding cavity of respiratory complex I, *J Biol Chem 282*, 29514-29520.

42. Mathiesen, C., and Hagerhall, C. (2003) The 'antiporter module' of respiratory chain complex I includes the MrpC/NuoK subunit -- a revision of the modular evolution scheme, *FEBS Lett 549*, 7-13.

43. Hunte, C., Zickermann, V., and Brandt, U. (2010) Functional modules and structural basis of conformational coupling in mitochondrial complex I, *Science 329*, 448-451.

44. Treberg, J. R., and Brand, M. D. (2011) A model of the proton translocation mechanism of complex I, *J Biol Chem 286*, 17579-17584.

45. Iwata, S., Lee, J. W., Okada, K., Lee, J. K., Iwata, M., Rasmussen, B., Link, T. A., Ramaswamy, S., and Jap, B. K. (1998) Complete structure of the 11-subunit bovine mitochondrial cytochrome bc_1 complex, *Science 281*, 64-71.

46. Crofts, A. R., and Berry, E. A. (1998) Structure and function of the cytochrome bc_1 complex of mitochondria and photosynthetic bacteria, *Curr Opin Struct Biol 8*, 501-509.

47. Zhang, Z., Huang, L., Shulmeister, V. M., Chi, Y. I., Kim, K. K., Hung, L. W., Crofts, A. R., Berry, E. A., and Kim, S. H. (1998) Electron transfer by domain movement in cytochrome bc_1, *Nature 392*, 677-684.

48. Berry, E. A., Huang, L. S., Saechao, L. K., Pon, N. G., Valkova-Valchanova, M., and Daldal, F. (2004) X-Ray structure of *Rhodobacter capsulatus* cytochrome bc_1: comparison with its mitochondrial and chloroplast counterparts, *Photosynth Res 81*, 251-275.

49. Lange, C., and Hunte, C. (2002) Crystal structure of the yeast cytochrome bc_1 complex with its bound substrate cytochrome *c*, *Proc Natl Acad Sci U S A 99*, 2800-2805.

50. Hunte, C., Palsdottir, H., and Trumpower, B. L. (2003) Protonmotive pathways and mechanisms in the cytochrome bc_1 complex, *FEBS Lett 545*, 39-46.

51. Crofts, A. R., Holland, J. T., Victoria, D., Kolling, D. R., Dikanov, S. A., Gilbreth, R., Lhee, S., Kuras, R., and Kuras, M. G. (2008) The Q-cycle reviewed: How well does a monomeric mechanism of the bc_1 complex account for the function of a dimeric complex?, *Biochim Biophys Acta 1777*, 1001-1019.

52. Crofts, A. R., Meinhardt, S. W., Jones, K. R., and Snozzi, M. (1983) The role of the quinone pool in the cyclic electron-transfer chain of *Rhodopseudomonas sphaeroides*: a modified Q-cycle mechanism, *Biochim Biophys Acta 723*, 202-218.

53. Crofts, A. R., Shinkarev, V. P., Kolling, D. R., and Hong, S. (2003) The modified Q-cycle explains the apparent mismatch between the kinetics of reduction of cytochromes c_1 and b_H in the bc_1 complex, *J Biol Chem 278*, 36191-36201.

54. Mitchell, P. (1976) Possible molecular mechanisms of the protonmotive function of cytochrome systems, *J Theor Biol 62*, 327-367.

55. Junemann, S., Heathcote, P., and Rich, P. R. (1998) On the mechanism of quinol oxidation in the bc_1 complex, *J Biol Chem 273*, 21603-21607.

56. Trumpower, B. L. (2002) A concerted, alternating sites mechanism of ubiquinol oxidation by the dimeric cytochrome bc_1 complex, *Biochim Biophys Acta 1555*, 166-173.

57. Osyczka, A., Moser, C. C., Daldal, F., and Dutton, P. L. (2004) Reversible redox energy coupling in electron transfer chains, *Nature 427*, 607-612.

58. Crofts, A. R. (2004) The cytochrome bc_1 complex: function in the context of structure, *Annu Rev Physiol 66*, 689-733.

59. Mitchell, P. (1979) Keilin's respiratory chain concept and its chemiosmotic consequences, *Science 206*, 1148-1159.

60. Tsukihara, T., Aoyama, H., Yamashita, E., Tomizaki, T., Yamaguchi, H., Shinzawa-Itoh, K., Nakashima, R., Yaono, R., and Yoshikawa, S. (1996) The whole structure of the 13-subunit oxidized cytochrome *c* oxidase at 2.8 Å, *Science 272*, 1136-1144.

61. Cao, J., Shapleigh, J., Gennis, R., Revzin, A., and Ferguson-Miller, S. (1991) The gene encoding cytochrome *c* oxidase subunit II from *Rhodobacter sphaeroides*; comparison of the deduced amino acid sequence with sequences of corresponding peptides from other species, *Gene 101*, 133-137.

62. Shapleigh, J. P., and Gennis, R. B. (1992) Cloning, sequencing and deletion from the chromosome of the gene encoding subunit I of the aa_3-type cytochrome *c* oxidase of *Rhodobacter sphaeroides*, *Mol Microbiol 6*, 635-642.

63. Svensson-Ek, M., Abramson, J., Larsson, G., Tornroth, S., Brzezinski, P., and Iwata, S. (2002) The X-ray crystal structures of wild-type and EQ(I-286) mutant cytochrome *c* oxidases from *Rhodobacter sphaeroides*, *J Mol Biol 321*, 329-339.

64. Harrenga, A., and Michel, H. (1999) The cytochrome *c* oxidase from *Paracoccus denitrificans* does not change the metal center ligation upon reduction, *J Biol Chem 274*, 33296-33299.

65. Flock, D., and Helms, V. (2002) Protein--protein docking of electron transfer complexes: cytochrome *c* oxidase and cytochrome *c*, *Proteins 47*, 75-85.

66. Kaila, V. R., Verkhovsky, M. I., and Wikstrom, M. (2010) Proton-coupled electron transfer in cytochrome oxidase, *Chem Rev 110*, 7062-7081.

67. Wikstrom, M. K. (1977) Proton pump coupled to cytochrome *c* oxidase in mitochondria, *Nature 266*, 271-273.

68. Gennis, R. B. (1998) Multiple proton-conducting pathways in cytochrome oxidase and a proposed role for the active-site tyrosine, *Bba-bioenergetics 1365(1-2)*, 241-248.

69. Wikstrom, M., Verkhovsky, M. I., and Hummer, G. (2003) Water-gated mechanism of proton translocation by cytochrome *c* oxidase, *Bba-bioenergetics 1604(2)*, 61-65.

70. Kaila, V. R. I., Sharma, V., and Wikstrom, M. (2011) The identity of the transient proton loading site of the proton-pumping mechanism of cytochrome *c* oxidase, *Bba-bioenergetics 1807(1)*, 80-84.

71. Daskalakis, V., Farantos, S. C., Guallar, V., and Varotsis, C. (2011) Regulation of electron and proton transfer by the protein matrix of cytochrome *c* oxidase, *J Phys Chem B 115(13)*, 3648-3655.

72. Okuno, D., Iino, R., and Noji, H. (2011) Rotation and structure of F_0F_1-ATP synthase, *J Biochem 149(6)*, 655-664.

73. Rees, D. M., Leslie, A. G., and Walker, J. E. (2009) The structure of the membrane extrinsic region of bovine ATP synthase, *Proc Natl Acad Sci U S A 106*, 21597-21601.

74. Dickson, V. K., Silvester, J. A., Fearnley, I. M., Leslie, A. G., and Walker, J. E. (2006) On the structure of the stator of the mitochondrial ATP synthase, *EMBO J 25*, 2911-2918.

75. Gabellieri, E., Strambini, G. B., Baracca, A., and Solaini, G. (1997) Structural mapping of the epsilon-subunit of mitochondrial H^+-ATPase complex (F_1), *Biophys J 72*, 1818-1827.

76. Abrahams, J. P., Leslie, A. G., Lutter, R., and Walker, J. E. (1994) Structure at 2.8 Å resolution of F_1-ATPase from bovine heart mitochondria, *Nature 370*, 621-628.

77. Bottcher, B., Bertsche, I., Reuter, R., and Graber, P. (2000) Direct visualisation of conformational changes in EF(0)F(1) by electron microscopy, *J Mol Biol 296*, 449-457.

78. Rubinstein, J. L., Walker, J. E., and Henderson, R. (2003) Structure of the mitochondrial ATP synthase by electron cryomicroscopy, *EMBO J 22*, 6182-6192.

79. Meier, T., Ferguson, S. A., Cook, G. M., Dimroth, P., and Vonck, J. (2006) Structural investigations of the membrane-embedded rotor ring of the F-ATPase from *Clostridium paradoxum*, *J Bacteriol 188*, 7759-7764.

80. Stock, D., Leslie, A. G., and Walker, J. E. (1999) Molecular architecture of the rotary motor in ATP synthase, *Science 286*, 1700-1705.

81. Muench, S. P., Trinick, J., and Harrison, M. A. (2011) Structural divergence of the rotary ATPases, *Q Rev Biophys* 1-46.

82. Jiang, W., Hermolin, J., and Fillingame, R. H. (2001) The preferred stoichiometry of c subunits in the rotary motor sector of *Escherichia coli* ATP synthase is 10, *Proc Natl Acad Sci U S A 98*, 4966-4971.

83. Vik, S. B., and Antonio, B. J. (1994) A mechanism of proton translocation by F_1F_0 ATP synthases suggested by double mutants of the a subunit, *J Biol Chem 269*, 30364-30369.

84. Junge, W., Sielaff, H., and Engelbrecht, S. (2009) Torque generation and elastic power transmission in the rotary F_0F_1-ATPase, *Nature 459*, 364-370.

85. Boyer, P. D. (1997) The ATP synthase--a splendid molecular machine, *Annu Rev Biochem 66*, 717-749.

86. Hirono-Hara, Y., Noji, H., Nishiura, M., Muneyuki, E., Hara, K. Y., Yasuda, R., Kinosita, K. J., and Yoshida, M. (2001) Pause and rotation of F_1-ATPase during catalysis, *Proc Natl Acad Sci U S A 98*, 13649-13654.

87. Pu, J., and Karplus, M. (2008) How subunit coupling produces the gamma-subunit rotary motion in F_1-ATPase, *Proc Natl Acad Sci U S A 105*, 1192-1197.

88. Pogoryelov, D., Yu, J., Meier, T., Vonck, J., Dimroth, P., and Muller, D. J. (2005) The c_{15} ring of the *Spirulina platensis* F-ATP synthase: F_1/F_0 symmetry mismatch is not obligatory, *EMBO Rep 6*, 1040-1044.

89. Matthies, D., Preiss, L., Klyszejko, A. L., Muller, D. J., Cook, G. M., Vonck, J., and Meier, T. (2009) The c_{13} ring from a thermoalkaliphilic ATP synthase reveals an extended diameter due to a special structural region, *J Mol Biol 388*, 611-618.

90. Clark, D. P. (1989) The fermentation pathways of *Escherichia coli*, *FEMS Microbiol Rev 5*, 223-234.

91. Unden, G., and Bongaerts, J. (1997) Alternative respiratory pathways of *Escherichia coli*: energetics and transcriptional regulation in response to electron acceptors, *Biochim Biophys Acta 1320*, 217-234.

92. Unden, G. (1988) Differential roles for menaquinone and demethylmenaquinone in anaerobic electron transport of *E. coli* and their *fnr*-independent expression, *Arch Microbiol 150*, 499-503.

93. Szkopinska, A. (2000) Ubiquinone. Biosynthesis of quinone ring and its isoprenoid side chain. Intracellular localization, *Acta Biochim Pol 47*, 469-480.

94. Lin, E. C., and Iuchi, S. (1991) Regulation of gene expression in fermentative and respiratory systems in *Escherichia coli* and related bacteria, *Annu Rev Genet 25*, 361-387.

95. Calhoun, M. W., Oden, K. L., Gennis, R. B., de Mattos, M. J., and Neijssel, O. M. (1993) Energetic efficiency of *Escherichia coli*: effects of mutations in components of the aerobic respiratory chain, *J Bacteriol 175*, 3020-3025.

96. Spiro, S., and Guest, J. R. (1990) FNR and its role in oxygen-regulated gene expression in *Escherichia coli*, *FEMS Microbiol Rev 6*, 399-428.

97. Sutton, V. R., Mettert, E. L., Beinert, H., and Kiley, P. J. (2004) Kinetic analysis of the oxidative conversion of the $[4Fe\text{-}4S]^{2+}$ cluster of FNR to a $[2Fe\text{-}2S]^{2+}$ Cluster, *J Bacteriol 186*, 8018-8025.

98. Blake, T., Barnard, A., Busby, S. J., and Green, J. (2002) Transcription activation by FNR: evidence for a functional activating region 2, *J Bacteriol 184*, 5855-5861.

99. Meng, W., Green, J., and Guest, J. R. (1997) FNR-dependent repression of *ndh* gene expression requires two upstream FNR-binding sites, *Microbiology 143*, 1521-1532.

100. Green, J., Bennett, B., Jordan, P., Ralph, E. T., Thomson, A. J., and Guest, J. R. (1996) Reconstitution of the [4Fe-4S] cluster in FNR and demonstration of the aerobic-anaerobic transcription switch *in vitro*, *Biochem J 316*, 887-892.

101. Dibden, D. P., and Green, J. (2005) *In vivo* cycling of the *Escherichia coli* transcription factor FNR between active and inactive states, *Microbiology 151*, 4063-4070.

102. Bekker, M., Alexeeva, S., Laan, W., Sawers, G., Teixeira de Mattos, J., and Hellingwerf, K. (2010) The ArcBA two-component system of *Escherichia coli* is regulated by the redox state of both the ubiquinone and the menaquinone pool, *J Bacteriol 192*, 746-754.

103. Malpica, R., Franco, B., Rodriguez, C., Kwon, O., and Georgellis, D. (2004) Identification of a quinone-sensitive redox switch in the ArcB sensor kinase, *Proc Natl Acad Sci U S A 101*, 13318-13323.

104. Stewart, V. (1993) Nitrate regulation of anaerobic respiratory gene expression in *Escherichia coli*, *Mol Microbiol 9*, 425-434.

105. Cheung, J., and Hendrickson, W. A. (2009) Structural analysis of ligand stimulation of the histidine kinase NarX, *Structure 17*, 190-201.

106. Janausch, I. G., Garcia-Moreno, I., and Unden, G. (2002) Function of DcuS from *Escherichia coli* as a fumarate-stimulated histidine protein kinase *in vitro*, *J Biol Chem 277*, 39809-39814.

107. Zientz, E., Bongaerts, J., and Unden, G. (1998) Fumarate regulation of gene expression in *Escherichia coli* by the DcuSR (*dcuSR* genes) two-component regulatory system, *J Bacteriol 180*, 5421-5425.

108. Maklashina, E., Berthold, D. A., and Cecchini, G. (1998) Anaerobic expression of *Escherichia coli* succinate dehydrogenase: functional replacement of fumarate reductase in the respiratory chain during anaerobic growth, *J Bacteriol 180*, 5989-5996.

109. Maklashina, E., and Cecchini, G. (1999) Comparison of catalytic activity and inhibitors of quinone reactions of succinate dehydrogenase (Succinate-ubiquinone oxidoreductase) and fumarate reductase (Menaquinol-fumarate oxidoreductase) from *Escherichia coli*, *Arch Biochem Biophys 369*, 223-232.

110. Guest, J. R. (1981) Partial replacement of succinate dehydrogenase function by phage- and plasmid-specified fumarate reductase in *Escherichia coli*, *J Gen Microbiol 122*, 171-179.

111. Park, S. J., Tseng, C. P., and Gunsalus, R. P. (1995) Regulation of succinate dehydrogenase (*sdhCDAB*) operon expression in *Escherichia coli* in response to carbon supply and anaerobiosis: role of ArcA and Fnr, *Mol Microbiol 15*, 473-482.

112. Shen, J., and Gunsalus, R. P. (1997) Role of multiple ArcA recognition sites in anaerobic regulation of succinate dehydrogenase (*sdhCDAB*) gene expression in *Escherichia coli*, *Mol Microbiol 26*, 223-236.

113. Jones, H. M., and Gunsalus, R. P. (1987) Regulation of *Escherichia coli* fumarate reductase (*frdABCD*) operon expression by respiratory electron acceptors and the *fnr* gene product, *J Bacteriol 169*, 3340-3349.

114. Golby, P., Davies, S., Kelly, D. J., Guest, J. R., and Andrews, S. C. (1999) Identification and characterization of a two-component sensor-kinase and response-regulator system (DcuS-DcuR) controlling gene expression in response to C_4-dicarboxylates in *Escherichia coli*, *J Bacteriol 181*, 1238-1248.

115. Gutowski, S. J., and Rosenberg, H. (1975) Succinate uptake and related proton movements in *Escherichia coli* K12, *Biochem J 152*, 647-654.

116. Six, S., Andrews, S. C., Unden, G., and Guest, J. R. (1994) *Escherichia coli* possesses two homologous anaerobic C_4-dicarboxylate membrane transporters (DcuA and DcuB) distinct from the aerobic dicarboxylate transport system (Dct), *J Bacteriol 176*, 6470-6478.

117. Zientz, E., Six, S., and Unden, G. (1996) Identification of a third secondary carrier (DcuC) for anaerobic C_4-dicarboxylate transport in *Escherichia coli*: roles of the three Dcu carriers in uptake and exchange, *J Bacteriol 178*, 7241-7247.

118. Golby, P., Kelly, D. J., Guest, J. R., and Andrews, S. C. (1998) Transcriptional regulation and organization of the *dcuA* and *dcuB* genes, encoding homologous anaerobic C$_4$-dicarboxylate transporters in *Escherichia coli*, *J Bacteriol 180*, 6586-6596.

119. Zientz, E., Janausch, I. G., Six, S., and Unden, G. (1999) Functioning of DcuC as the C$_4$-dicarboxylate carrier during glucose fermentation by *Escherichia coli*, *J Bacteriol 181*, 3716-3720.

120. Au, H. C., and Scheffler, I. E. (1998) Promoter analysis of the human succinate dehydrogenase iron-protein gene--both nuclear respiratory factors NRF-1 and NRF-2 are required, *Eur J Biochem 251*, 164-174.

121. Scarpulla, R. C. (2002) Transcriptional activators and coactivators in the nuclear control of mitochondrial function in mammalian cells, *Gene 286*, 81-89.

122. Piantadosi, C. A., and Suliman, H. B. (2008) Transcriptional Regulation of SDHa flavoprotein by nuclear respiratory factor-1 prevents pseudo-hypoxia in aerobic cardiac cells, *J Biol Chem 283*, 10967-10977.

123. Huang, L. S., Sun, G., Cobessi, D., Wang, A. C., Shen, J. T., Tung, E. Y., Anderson, V. E., and Berry, E. A. (2006) 3-nitropropionic acid is a suicide inhibitor of mitochondrial respiration that, upon oxidation by complex II, forms a covalent adduct with a catalytic base arginine in the active site of the enzyme, *J Biol Chem 281*, 5965-5972.

124. Sun, F., Huo, X., Zhai, Y., Wang, A., Xu, J., Su, D., Bartlam, M., and Rao, Z. (2005) Crystal structure of mitochondrial respiratory membrane protein complex II, *Cell 121*, 1043-1057.

125. Yankovskaya, V., Horsefield, R., Tornroth, S., Luna-Chavez, C., Miyoshi, H., Leger, C., Byrne, B., Cecchini, G., and Iwata, S. (2003) Architecture of succinate dehydrogenase and reactive oxygen species generation, *Science 299*, 700-704.

126. Iverson, T. M., Luna-Chavez, C., Cecchini, G., and Rees, D. C. (1999) Structure of the *Escherichia coli* fumarate reductase respiratory complex, *Science 284*, 1961-1966.

127. Lemos, R. S., Fernandes, A. S., Pereira, M. M., Gomes, C. M., and Teixeira, M. (2002) Quinol:fumarate oxidoreductases and succinate:quinone

oxidoreductases: phylogenetic relationships, metal centres and membrane attachment, *Biochim Biophys Acta 1553*, 158-170.

128. Lancaster, C. R. (2002) Succinate:quinone oxidoreductases: an overview, *Biochim Biophys Acta 1553*, 1-6.

129. Schafer, G., Anemuller, S., and Moll, R. (2002) Archaeal complex II: 'classical' and 'non-classical' succinate:quinone reductases with unusual features, *Biochim Biophys Acta 1553*, 57-73.

130. Kolaj-Robin, O., O'Kane, S. R., Nitschke, W., Leger, C., Baymann, F., and Soulimane, T. (2011) Biochemical and biophysical characterization of succinate: quinone reductase from *Thermus thermophilus*, *Biochim Biophys Acta 1807*, 68-79.

131. Hederstedt, L. (2002) Succinate:quinone oxidoreductase in the bacteria *Paracoccus denitrificans* and *Bacillus subtilis*, *Biochim Biophys Acta 1553*, 74-83.

132. Lancaster, C. R., Kroger, A., Auer, M., and Michel, H. (1999) Structure of fumarate reductase from *Wolinella succinogenes* at 2.2 Å resolution, *Nature 402*, 377-385.

133. Wickstrom, D., Wagner, S., Baars, L., Ytterberg, A. J., Klepsch, M., van Wijk, K. J., Luirink, J., and de Gier, J. W. (2011) Consequences of depletion of the signal recognition particle in *Escherichia coli*, *J Biol Chem 286*, 4598-4609.

134. Xie, K., and Dalbey, R. E. (2008) Inserting proteins into the bacterial cytoplasmic membrane using the Sec and YidC translocases, *Nat Rev Microbiol 6*, 234-244.

135. Huo, X., Su, D., Wang, A., Zhai, Y., Xu, J., Li, X., Bartlam, M., Sun, F., and Rao, Z. (2007) Preliminary molecular characterization and crystallization of mitochondrial respiratory complex II from porcine heart, *FEBS J 274*, 1524-1529.

136. Sodergren, E. J., Hsu, P. Y., and DeMoss, J. A. (1988) Roles of the *narJ* and *narI* gene products in the expression of nitrate reductase in *Escherichia coli*, *J Biol Chem 263*, 16156-16162.

137. Pommier, J., Mejean, V., Giordano, G., and Iobbi-Nivol, C. (1998) TorD, a cytoplasmic chaperone that interacts with the unfolded trimethylamine N-

oxide reductase enzyme (TorA) in *Escherichia coli*, *J Biol Chem 273*, 16615-16620.

138. Sambasivarao, D., and Weiner, J. H. (1991) Dimethyl sulfoxide reductase of *Escherichia coli*: an investigation of function and assembly by use of *in vivo* complementation, *J Bacteriol 173*, 5935-5943.

139. Luke, I., Butland, G., Moore, K., Buchanan, G., Lyall, V., Fairhurst, S. A., Greenblatt, J. F., Emili, A., Palmer, T., and Sargent, F. (2008) Biosynthesis of the respiratory formate dehydrogenases from *Escherichia coli*: characterization of the FdhE protein, *Arch Microbiol 190*, 685-696.

140. Ghezzi, D., Goffrini, P., Uziel, G., Horvath, R., Klopstock, T., Lochmuller, H., D'Adamo, P., Gasparini, P., Strom, T. M., Prokisch, H., Invernizzi, F., Ferrero, I., and Zeviani, M. (2009) *SDHAF1*, encoding a LYR complex-II specific assembly factor, is mutated in SDH-defective infantile leukoencephalopathy, *Nat Genet 41*, 654-656.

141. Cardol, P., Vanrobaeys, F., Devreese, B., Van Beeumen, J., Matagne, R. F., and Remacle, C. (2004) Higher plant-like subunit composition of mitochondrial complex I from *Chlamydomonas reinhardtii*: 31 conserved components among eukaryotes, *Biochim Biophys Acta 1658*, 212-224.

142. Wiedemann, N., Urzica, E., Guiard, B., Muller, H., Lohaus, C., Meyer, H. E., Ryan, M. T., Meisinger, C., Muhlenhoff, U., Lill, R., and Pfanner, N. (2006) Essential role of Isd11 in mitochondrial iron-sulfur cluster synthesis on Isu scaffold proteins, *EMBO J 25*, 184-195.

143. Ye, Z., and Connor, J. R. (2000) cDNA cloning by amplification of circularized first strand cDNAs reveals non-IRE-regulated iron-responsive mRNAs, *Biochem Biophys Res Commun 275*, 223-227.

144. Hao, H. X., Khalimonchuk, O., Schraders, M., Dephoure, N., Bayley, J. P., Kunst, H., Devilee, P., Cremers, C. W., Schiffman, J. D., Bentz, B. G., Gygi, S. P., Winge, D. R., Kremer, H., and Rutter, J. (2009) *SDH5*, a gene required for flavination of succinate dehydrogenase, is mutated in paraganglioma, *Science 325*, 1139-1142.

145. Robinson, K. M., Rothery, R. A., Weiner, J. H., and Lemire, B. D. (1994) The covalent attachment of FAD to the flavoprotein of *Saccharomyces cerevisiae* succinate dehydrogenase is not necessary for import and assembly into mitochondria, *Eur J Biochem 222*, 983-990.

146. Blaut, M., Whittaker, K., Valdovinos, A., Ackrell, B. A., Gunsalus, R. P., and Cecchini, G. (1989) Fumarate reductase mutants of *Escherichia coli* that lack covalently bound flavin, *J Biol Chem 264*, 13599-13604.

147. Heuts, D. P., Scrutton, N. S., McIntire, W. S., and Fraaije, M. W. (2009) What's in a covalent bond? On the role and formation of covalently bound flavin cofactors, *FEBS J 276*, 3405-3427.

148. Hederstedt, L. (1983) Succinate dehydrogenase mutants of *Bacillus subtilis* lacking covalently bound flavin in the flavoprotein subunit, *Eur J Biochem 132*, 589-593.

149. Thony-Meyer, L. (1997) Biogenesis of respiratory cytochromes in bacteria, *Microbiol Mol Biol Rev 61*, 337-376.

150. Kranz, R. G., Richard-Fogal, C., Taylor, J. S., and Frawley, E. R. (2009) Cytochrome *c* biogenesis: mechanisms for covalent modifications and trafficking of heme and for heme-iron redox control, *Microbiol Mol Biol Rev 73*, 510-28, Table of Contents.

151. Goldstein, L., Teng, Z. P., Zeserson, E., Patel, M., and Regan, R. F. (2003) Hemin induces an iron-dependent, oxidative injury to human neuron-like cells, *J Neurosci Res 73*, 113-121.

152. Severance, S., and Hamza, I. (2009) Trafficking of heme and porphyrins in metazoa, *Chem Rev 109*, 4596-4616.

153. Pequignot, M. O., Dey, R., Zeviani, M., Tiranti, V., Godinot, C., Poyau, A., Sue, C., Di Mauro, S., Abitbol, M., and Marsac, C. (2001) Mutations in the *SURF1* gene associated with Leigh syndrome and cytochrome *c* oxidase deficiency, *Hum Mutat 17*, 374-381.

154. Hannappel, A., Bundschuh, F. A., and Ludwig, B. (2011) Characterization of heme-binding properties of *Paracoccus denitrificans* Surf1 proteins, *FEBS J 278*, 1769-1778.

155. Bundschuh, F. A., Hannappel, A., Anderka, O., and Ludwig, B. (2009) Surf1, associated with Leigh syndrome in humans, is a heme-binding protein in bacterial oxidase biogenesis, *J Biol Chem 284*, 25735-25741.

156. Zhu, Z., Yao, J., Johns, T., Fu, K., De Bie, I., Macmillan, C., Cuthbert, A. P., Newbold, R. F., Wang, J., Chevrette, M., Brown, G. K., Brown, R. M., and Shoubridge, E. A. (1998) *SURF1*, encoding a factor involved in the biogenesis of cytochrome *c* oxidase, is mutated in Leigh syndrome, *Nat Genet 20*, 337-343.

157. Werner, C., Richter, O. M., and Ludwig, B. (2010) A novel heme *a* insertion factor gene cotranscribes with the *Thermus thermophilus* cytochrome ba_3 oxidase locus, *J Bacteriol 192*, 4712-4719.

158. Chakravarti, R., Aulak, K. S., Fox, P. L., and Stuehr, D. J. (2010) GAPDH regulates cellular heme insertion into inducible nitric oxide synthase, *Proc Natl Acad Sci U S A 107*, 18004-18009.

159. Reid, G. A., Miles, C. S., Moysey, R. K., Pankhurst, K. L., and Chapman, S. K. (2000) Catalysis in fumarate reductase, *Biochim Biophys Acta 1459*, 310-315.

160. Tomasiak, T. M., Archuleta, T. L., Andrell, J., Luna-Chavez, C., Davis, T. A., Sarwar, M., Ham, A. J., McDonald, W. H., Yankovskaya, V., Stern, H. A., Johnston, J. N., Maklashina, E., Cecchini, G., and Iverson, T. M. (2011) Geometric restraint drives on- and off-pathway catalysis by the *Escherichia coli* menaquinol:fumarate reductase, *J Biol Chem 286*, 3047-3056.

161. Ackrell, B. A., Cochran, B., and Cecchini, G. (1989) Interactions of oxaloacetate with *Escherichia coli* fumarate reductase, *Arch Biochem Biophys 268*, 26-34.

162. Kotliar, A. B., and Vinogradov, A. D. (1984) [Interaction of succinate dehydrogenase and oxaloacetate], *Biokhimiia 49*, 667-675.

163. Belikova, I., and Kotliar, A. B. (1988) [Malate oxidation by mitochondrial succinate:ubiquinone-reductase], *Biokhimiia 53*, 668-676.

164. Ackrell, B. A., Kearney, E. B., and Edmondson, D. (1975) Mechanism of the reductive activation of succinate dehydrogenase, *J Biol Chem 250*, 7114-7119.

165. Walker, W. H., and Singer, T. P. (1970) Identification of the covalently bound flavin of succinate dehydrogenase as 8-alpha-(histidyl) flavin adenine dinucleotide, *J Biol Chem 245*, 4224-4225.

166. Maklashina, E., Iverson, T. M., Sher, Y., Kotlyar, V., Andrell, J., Mirza, O., Hudson, J. M., Armstrong, F. A., Rothery, R. A., Weiner, J. H., and Cecchini, G. (2006) Fumarate reductase and succinate oxidase activity of *Escherichia coli* complex II homologs are perturbed differently by mutation of the flavin binding domain, *J Biol Chem 281*, 11357-11365.

167. Hudson, J. M., Heffron, K., Kotlyar, V., Sher, Y., Maklashina, E., Cecchini, G., and Armstrong, F. A. (2005) Electron transfer and catalytic control by the iron-sulfur clusters in a respiratory enzyme, *E. coli* fumarate reductase, *J Am Chem Soc 127*, 6977-6989.

168. Ohnishi, T., King, T. E., Salerno, J. C., Blum, H., Bowyer, J. R., and Maida, T. (1981) Thermodynamic and electron paramagnetic resonance characterization of flavin in succinate dehydrogenase, *J Biol Chem 256*, 5577-5582.

169. Sucheta, A., Ackrell, B. A., Cochran, B., and Armstrong, F. A. (1992) Diode-like behaviour of a mitochondrial electron-transport enzyme, *Nature 356*, 361-362.

170. Leger, C., Heffron, K., Pershad, H. R., Maklashina, E., Luna-Chavez, C., Cecchini, G., Ackrell, B. A., and Armstrong, F. A. (2001) Enzyme electrokinetics: energetics of succinate oxidation by fumarate reductase and succinate dehydrogenase, *Biochemistry 40*, 11234-11245.

171. Ackrell, B. A., Armstrong, F. A., Cochran, B., Sucheta, A., and Yu, T. (1993) Classification of fumarate reductases and succinate dehydrogenases based upon their contrasting behaviour in the reduced benzylviologen/fumarate assay, *FEBS Lett 326*, 92-94.

172. Lancaster, C. R., Gross, R., and Simon, J. (2001) A third crystal form of *Wolinella succinogenes* quinol:fumarate reductase reveals domain closure at the site of fumarate reduction, *Eur J Biochem 268*, 1820-1827.

173. Tomasiak, T. M., Maklashina, E., Cecchini, G., and Iverson, T. M. (2008) A threonine on the active site loop controls transition state formation in *Escherichia coli* respiratory complex II, *J Biol Chem 283*, 15460-15468.

174. Coles, C. J., Edmondson, D. E., and Singer, T. P. (1979) Inactivation of succinate dehydrogenase by 3-nitropropionate, *J Biol Chem 254*, 5161-5167.

175. Cimen, H., Han, M. J., Yang, Y., Tong, Q., Koc, H., and Koc, E. C. (2010) Regulation of succinate dehydrogenase activity by SIRT3 in mammalian mitochondria, *Biochemistry 49*, 304-311.

176. Tomitsuka, E., Kita, K., and Esumi, H. (2009) Regulation of succinate-ubiquinone reductase and fumarate reductase activities in human complex II by phosphorylation of its flavoprotein subunit, *Proc Jpn Acad Ser B Phys Biol Sci 85*, 258-265.

177. Condon, C., Cammack, R., Patil, D. S., and Owen, P. (1985) The succinate dehydrogenase of *Escherichia coli*. Immunochemical resolution and biophysical characterization of a 4-subunit enzyme complex, *J Biol Chem 260*, 9427-9434.

178. Hagerhall, C. (1997) Succinate: quinone oxidoreductases. Variations on a conserved theme, *Biochim Biophys Acta 1320*, 107-141.

179. Manodori, A., Cecchini, G., Schroder, I., Gunsalus, R. P., Werth, M. T., and Johnson, M. K. (1992) [3Fe-4S] to [4Fe-4S] cluster conversion in *Escherichia coli* fumarate reductase by site-directed mutagenesis, *Biochemistry 31*, 2703-2712.

180. Hagerhall, C., Sled, V., Hederstedt, L., and Ohnishi, T. (1995) The trinuclear iron-sulfur cluster S3 in *Bacillus subtilis* succinate:menaquinone reductase; effects of a mutation in the putative cluster ligation motif on enzyme activity and EPR properties, *Biochim Biophys Acta 1229*, 356-362.

181. Anemuller, S., Hettmann, T., Moll, R., Teixeira, M., and Schafer, G. (1995) EPR characterization of an archaeal succinate dehydrogenase in the membrane-bound state, *Eur J Biochem 232*, 563-568.

182. Cheng, V. W., Ma, E., Zhao, Z., Rothery, R. A., and Weiner, J. H. (2006) The iron-sulfur clusters in *Escherichia coli* succinate dehydrogenase direct electron flow, *J Biol Chem 281*, 27662-27668.

183. Ruprecht, J., Iwata, S., Rothery, R. A., Weiner, J. H., Maklashina, E., and Cecchini, G. (2011) Perturbation of the quinone-binding site of complex II alters the electronic properties of the proximal [3Fe-4S] iron-sulfur cluster, *J Biol Chem 286*, 12756-12765.

184. Guigliarelli, B., Magalon, A., Asso, M., Bertrand, P., Frixon, C., Giordano, G., and Blasco, F. (1996) Complete coordination of the four Fe-S centers of the beta subunit from *Escherichia coli* nitrate reductase. Physiological, biochemical, and EPR characterization of site-directed mutants lacking the highest or lowest potential [4Fe-4S] clusters, *Biochemistry 35*, 4828-4836.

185. Cammack, R., Patil, D. S., and Weiner, J. H. (1986) Evidence that centre 2 in *Escherichia coli* fumarate reductase is a [4Fe-4S]cluster, *Biochim Biophys Acta 870*, 545-551.

186. Cammack, R., and Weiner, J. H. (1990) Electron paramagnetic resonance spectroscopic characterization of dimethyl sulfoxide reductase of *Escherichia coli*, *Biochemistry 29*, 8410-8416.

187. Jeuken, L. J., Jones, A. K., Chapman, S. K., Cecchini, G., and Armstrong, F. A. (2002) Electron-transfer mechanisms through biological redox chains in multicenter enzymes, *J Am Chem Soc 124*, 5702-5713.

188. Cheng, V. W., Rothery, R. A., Bertero, M. G., Strynadka, N. C., and Weiner, J. H. (2005) Investigation of the environment surrounding iron-sulfur cluster 4 of *Escherichia coli* dimethylsulfoxide reductase, *Biochemistry 44*, 8068-8077.

189. Kita, K., Vibat, C. R., Meinhardt, S., Guest, J. R., and Gennis, R. B. (1989) One-step purification from *Escherichia coli* of complex II (succinate: ubiquinone oxidoreductase) associated with succinate-reducible cytochrome b_{556}, *J Biol Chem 264*, 2672-2677.

190. Yang, X., Yu, L., and Yu, C. A. (1997) Resolution and reconstitution of succinate-ubiquinone reductase from *Escherichia coli*, *J Biol Chem 272*, 9683-9689.

191. Yu, L., Xu, J. X., Haley, P. E., and Yu, C. A. (1987) Properties of bovine heart mitochondrial cytochrome b_{560}, *J Biol Chem 262*, 1137-1143.

192. Oyedotun, K. S., Yau, P. F., and Lemire, B. D. (2004) Identification of the heme axial ligands in the cytochrome b_{562} of the *Saccharomyces cerevisiae* succinate dehydrogenase, *J Biol Chem 279*, 9432-9439.

193. Maklashina, E., Rajagukguk, S., McIntire, W. S., and Cecchini, G. (2010) Mutation of the heme axial ligand of *Escherichia coli* succinate-quinone reductase:

Implications for heme ligation in mitochondrial complex II from yeast, *Biochim Biophys Acta 1797*, 747-754.

194. Lemire, B. D., and Oyedotun, K. S. (2002) The *Saccharomyces cerevisiae* mitochondrial succinate:ubiquinone oxidoreductase, *Biochim Biophys Acta 1553*, 102-116.

195. Ruprecht, J., Yankovskaya, V., Maklashina, E., Iwata, S., and Cecchini, G. (2009) Structure of *Escherichia coli* succinate:quinone oxidoreductase with an occupied and empty quinone-binding site, *J Biol Chem 284*, 29836-29846.

196. Silkin, Y., Oyedotun, K. S., and Lemire, B. D. (2007) The role of Sdh4p Tyr-89 in ubiquinone reduction by the *Saccharomyces cerevisiae* succinate dehydrogenase, *Biochim Biophys Acta 1767*, 143-150.

197. Horsefield, R., Yankovskaya, V., Sexton, G., Whittingham, W., Shiomi, K., Omura, S., Byrne, B., Cecchini, G., and Iwata, S. (2006) Structural and computational analysis of the quinone-binding site of complex II (succinate-ubiquinone oxidoreductase): a mechanism of electron transfer and proton conduction during ubiquinone reduction, *J Biol Chem 281*, 7309-7316.

198. Rothery, R. A., Seime, A. M., Spiers, A. M., Maklashina, E., Schroder, I., Gunsalus, R. P., Cecchini, G., and Weiner, J. H. (2005) Defining the Q-site of *Escherichia coli* fumarate reductase by site-directed mutagenesis, fluorescence quench titrations and EPR spectroscopy, *FEBS J 272*, 313-326.

199. Ramsay, R. R., Ackrell, B. A., Coles, C. J., Singer, T. P., White, G. A., and Thorn, G. D. (1981) Reaction site of carboxanilides and of thenoyltrifluoroacetone in complex II, *Proc Natl Acad Sci U S A 78*, 825-828.

200. Afanas'eva, E. V., and Kostyrko, V. A. (1986) Pentachlorophenol inhibition of succinate oxidation by the respiratory chain in submitochondrial particles from the bovine heart, *Biokhimiia 51*, 823-829.

201. Yankovskaya, V., Sablin, S. O., Ramsay, R. R., Singer, T. P., Ackrell, B. A., Cecchini, G., and Miyoshi, H. (1996) Inhibitor probes of the quinone binding sites of mammalian complex II and *Escherichia coli* fumarate reductase, *J Biol Chem 271*, 21020-21024.

202. Waldeck, A. R., Stowell, M. H., Lee, H. K., Hung, S. C., Matsson, M., Hederstedt, L., Ackrell, B. A., and Chan, S. I. (1997) Electron paramagnetic resonance studies of succinate:ubiquinone oxidoreductase from *Paracoccus denitrificans*. Evidence for a magnetic interaction between the 3Fe-4S cluster and cytochrome *b*, *J Biol Chem 272*, 19373-19382.

203. Hagerhall, C., Magnitsky, S., Sled, V. D., Schroder, I., Gunsalus, R. P., Cecchini, G., and Ohnishi, T. (1999) An *Escherichia coli* mutant quinol:fumarate reductase contains an EPR-detectable semiquinone stabilized at the proximal quinone-binding site, *J Biol Chem 274*, 26157-26164.

204. Cheng, V. W., Johnson, A., Rothery, R. A., and Weiner, J. H. (2008) Alternative sites for proton entry from the cytoplasm to the quinone binding site in *Escherichia coli* succinate dehydrogenase, *Biochemistry 47*, 9107-9116.

205. Matsson, M., Tolstoy, D., Aasa, R., and Hederstedt, L. (2000) The distal heme center in *Bacillus subtilis* succinate:quinone reductase is crucial for electron transfer to menaquinone, *Biochemistry 39*, 8617-8624.

206. Lancaster, C. R. (2002) *Wolinella succinogenes* quinol:fumarate reductase-2.2-Å resolution crystal structure and the E-pathway hypothesis of coupled transmembrane proton and electron transfer, *Biochim Biophys Acta 1565*, 215-231.

207. Madej, M. G., Nasiri, H. R., Hilgendorff, N. S., Schwalbe, H., Unden, G., and Lancaster, C. R. (2006) Experimental evidence for proton motive force-dependent catalysis by the diheme-containing succinate:menaquinone oxidoreductase from the Gram-positive bacterium *Bacillus licheniformis*, *Biochemistry 45*, 15049-15055.

208. Lancaster, C. R., Haas, A. H., Madej, M. G., and Mileni, M. (2006) Recent progress on obtaining theoretical and experimental support for the "E-pathway hypothesis" of coupled transmembrane electron and proton transfer in dihaem-containing quinol:fumarate reductase, *Biochim Biophys Acta 1757*, 988-995.

209. Iverson, T. M., Luna-Chavez, C., Croal, L. R., Cecchini, G., and Rees, D. C. (2002) Crystallographic studies of the *Escherichia coli* quinol-fumarate reductase with inhibitors bound to the quinol-binding site, *J Biol Chem 277*, 16124-16130.

210. Maklashina, E., and Cecchini, G. (2010) The quinone-binding and catalytic site of complex II, *Biochim Biophys Acta*

211. Nakamura, K., Yamaki, M., Sarada, M., Nakayama, S., Vibat, C. R., Gennis, R. B., Nakayashiki, T., Inokuchi, H., Kojima, S., and Kita, K. (1996) Two hydrophobic subunits are essential for the heme *b* ligation and functional assembly of complex II (succinate-ubiquinone oxidoreductase) from *Escherichia coli*, *J Biol Chem 271*, 521-527.

212. Nihei, C., Nakayashiki, T., Nakamura, K., Inokuchi, H., Gennis, R. B., Kojima, S., and Kita, K. (2001) Abortive assembly of succinate-ubiquinone reductase (complex II) in a ferrochelatase-deficient mutant of *Escherichia coli*, *Mol Genet Genomics 265*, 394-404.

213. Anderson, R. F., Hille, R., Shinde, S. S., and Cecchini, G. (2005) Electron transfer within complex II. Succinate:ubiquinone oxidoreductase of *Escherichia coli*, *J Biol Chem 280*, 33331-33337.

214. Paradies, G., Petrosillo, G., Paradies, V., and Ruggiero, F. M. (2010) Oxidative stress, mitochondrial bioenergetics, and cardiolipin in aging, *Free Radic Biol Med 48*, 1286-1295.

215. HARMAN, D. (1956) Aging: a theory based on free radical and radiation chemistry, *J Gerontol 11*, 298-300.

216. Pak, J. W., Herbst, A., Bua, E., Gokey, N., McKenzie, D., and Aiken, J. M. (2003) Mitochondrial DNA mutations as a fundamental mechanism in physiological declines associated with aging, *Aging Cell 2*, 1-7.

217. Murphy, M. P. (2009) How mitochondria produce reactive oxygen species, *Biochem J 417*, 1-13.

218. Hirst, J., King, M. S., and Pryde, K. R. (2008) The production of reactive oxygen species by complex I, *Biochem Soc Trans 36*, 976-980.

219. Korshunov, S. S., Skulachev, V. P., and Starkov, A. A. (1997) High protonic potential actuates a mechanism of production of reactive oxygen species in mitochondria, *FEBS Lett 416*, 15-18.

220. Votyakova, T. V., and Reynolds, I. J. (2001) DeltaPsi(m)-Dependent and -independent production of reactive oxygen species by rat brain mitochondria, *J Neurochem 79*, 266-277.

221. Lambert, A. J., and Brand, M. D. (2004) Superoxide production by NADH:ubiquinone oxidoreductase (complex I) depends on the pH gradient across the mitochondrial inner membrane, *Biochem J 382*, 511-517.

222. Turrens, J. F., Alexandre, A., and Lehninger, A. L. (1985) Ubisemiquinone is the electron donor for superoxide formation by complex III of heart mitochondria, *Arch Biochem Biophys 237*, 408-414.

223. Zhang, L., Yu, L., and Yu, C. A. (1998) Generation of superoxide anion by succinate-cytochrome *c* reductase from bovine heart mitochondria, *J Biol Chem 273*, 33972-33976.

224. Messner, K. R., and Imlay, J. A. (2002) Mechanism of superoxide and hydrogen peroxide formation by fumarate reductase, succinate dehydrogenase, and aspartate oxidase, *J Biol Chem 277*, 42563-42571.

225. Imlay, J. A. (1995) A metabolic enzyme that rapidly produces superoxide, fumarate reductase of *Escherichia coli*, *J Biol Chem 270*, 19767-19777.

226. Zhao, Z., Rothery, R. A., and Weiner, J. H. (2006) Effects of site-directed mutations in *Escherichia coli* succinate dehydrogenase on the enzyme activity and production of superoxide radicals, *Biochem Cell Biol 84*, 1013-1021.

227. Guo, J., and Lemire, B. D. (2003) The ubiquinone-binding site of the *Saccharomyces cerevisiae* succinate-ubiquinone oxidoreductase is a source of superoxide, *J Biol Chem 278*, 47629-47635.

228. Szeto, S. S., Reinke, S. N., Sykes, B. D., and Lemire, B. D. (2007) Ubiquinone-binding site mutations in the *Saccharomyces cerevisiae* succinate dehydrogenase generate superoxide and lead to the accumulation of succinate, *J Biol Chem 282*, 27518-27526.

229. Ishii, N., Fujii, M., Hartman, P. S., Tsuda, M., Yasuda, K., Senoo-Matsuda, N., Yanase, S., Ayusawa, D., and Suzuki, K. (1998) A mutation in succinate dehydrogenase cytochrome *b* causes oxidative stress and ageing in nematodes, *Nature 394*, 694-697.

230. Senoo-Matsuda, N., Yasuda, K., Tsuda, M., Ohkubo, T., Yoshimura, S., Nakazawa, H., Hartman, P. S., and Ishii, N. (2001) A defect in the cytochrome *b* large subunit in complex II causes both superoxide anion overproduction and abnormal energy metabolism in *Caenorhabditis elegans*, *J Biol Chem 276*, 41553-41558.

231. Paranagama, M. P., Sakamoto, K., Amino, H., Awano, M., Miyoshi, H., and Kita, K. (2010) Contribution of the FAD and quinone binding sites to the production of reactive oxygen species from *Ascaris suum* mitochondrial complex II, *Mitochondrion 10*, 158-165.

232. Piruat, J. I., Pintado, C. O., Ortega-Saenz, P., Roche, M., and Lopez-Barneo, J. (2004) The mitochondrial *SDHD* gene is required for early embryogenesis, and its partial deficiency results in persistent carotid body glomus cell activation with full responsiveness to hypoxia, *Mol Cell Biol 24*, 10933-10940.

233. Bourgeron, T., Rustin, P., Chretien, D., Birch-Machin, M., Bourgeois, M., Viegas-Pequignot, E., Munnich, A., and Rotig, A. (1995) Mutation of a nuclear succinate dehydrogenase gene results in mitochondrial respiratory chain deficiency, *Nat Genet 11*, 144-149.

234. Horvath, R., Abicht, A., Holinski-Feder, E., Laner, A., Gempel, K., Prokisch, H., Lochmuller, H., Klopstock, T., and Jaksch, M. (2006) Leigh syndrome caused by mutations in the flavoprotein (Fp) subunit of succinate dehydrogenase (SDHA), *J Neurol Neurosurg Psychiatry 77*, 74-76.

235. Parfait, B., Chretien, D., Rotig, A., Marsac, C., Munnich, A., and Rustin, P. (2000) Compound heterozygous mutations in the flavoprotein gene of the respiratory chain complex II in a patient with Leigh syndrome, *Hum Genet 106*, 236-243.

236. Sorbi, S., and Blass, J. P. (1982) Abnormal activation of pyruvate dehydrogenase in Leigh disease fibroblasts, *Neurology 32*, 555-558.

237. Lebon, S., Minai, L., Chretien, D., Corcos, J., Serre, V., Kadhom, N., Steffann, J., Pauchard, J. Y., Munnich, A., Bonnefont, J. P., and Rotig, A. (2007) A novel mutation of the *NDUFS7* gene leads to activation of a cryptic exon and impaired assembly of mitochondrial complex I in a patient with Leigh syndrome, *Mol Genet Metab 92*, 104-108.

238. Adams, P. L., Lightowlers, R. N., and Turnbull, D. M. (1997) Molecular analysis of cytochrome *c* oxidase deficiency in Leigh's syndrome, *Ann Neurol 41*, 268-270.

239. Hensen, E. F., and Bayley, J. P. (2011) Recent advances in the genetics of SDH-related paraganglioma and pheochromocytoma, *Fam Cancer 10*, 355-363.

240. Ni, Y., Zbuk, K. M., Sadler, T., Patocs, A., Lobo, G., Edelman, E., Platzer, P., Orloff, M. S., Waite, K. A., and Eng, C. (2008) Germline mutations and variants in the succinate dehydrogenase genes in Cowden and Cowden-like syndromes, *Am J Hum Genet 83*, 261-268.

241. Janeway, K. A., Kim, S. Y., Lodish, M., Nose, V., Rustin, P., Gaal, J., Dahia, P. L., Liegl, B., Ball, E. R., Raygada, M., Lai, A. H., Kelly, L., Hornick, J. L., O'Sullivan, M., de Krijger, R. R., Dinjens, W. N., Demetri, G. D., Antonescu, C. R., Fletcher, J. A., Helman, L., and Stratakis, C. A. (2011) Defects in succinate dehydrogenase in gastrointestinal stromal tumors lacking KIT and PDGFRA mutations, *Proc Natl Acad Sci U S A 108*, 314-318.

242. Pantaleo, M. A., Astolfi, A., Indio, V., Moore, R., Thiessen, N., Heinrich, M. C., Gnocchi, C., Santini, D., Catena, F., Formica, S., Martelli, P. L., Casadio, R., Pession, A., and Biasco, G. (2011) SDHA Loss-of-Function Mutations in KIT-PDGFRA Wild-Type Gastrointestinal Stromal Tumors Identified by Massively Parallel Sequencing, *J Natl Cancer Inst*

243. Housley, S. L., Lindsay, R. S., Young, B., McConachie, M., Mechan, D., Baty, D., Christie, L., Rahilly, M., Qureshi, K., and Fleming, S. (2010) Renal carcinoma with giant mitochondria associated with germ-line mutation and somatic loss of the succinate dehydrogenase B gene, *Histopathology 56*, 405-408.

244. Ricketts, C., Woodward, E. R., Killick, P., Morris, M. R., Astuti, D., Latif, F., and Maher, E. R. (2008) Germline *SDHB* mutations and familial renal cell carcinoma, *J Natl Cancer Inst 100*, 1260-1262.

245. Vanharanta, S., Buchta, M., McWhinney, S. R., Virta, S. K., Peczkowska, M., Morrison, C. D., Lehtonen, R., Januszewicz, A., Jarvinen, H., Juhola, M., Mecklin, J. P., Pukkala, E., Herva, R., Kiuru, M., Nupponen, N. N., Aaltonen, L. A., Neumann, H. P., and Eng, C. (2004) Early-onset renal cell carcinoma as a novel extraparaganglial component of SDHB-associated heritable paraganglioma, *Am J Hum Genet 74*, 153-159.

246. Neumann, H. P., Pawlu, C., Peczkowska, M., Bausch, B., McWhinney, S. R., Muresan, M., Buchta, M., Franke, G., Klisch, J., Bley, T. A., Hoegerle, S., Boedeker, C. C., Opocher, G., Schipper, J., Januszewicz, A., and Eng, C. (2004) Distinct clinical features of paraganglioma syndromes associated with *SDHB* and *SDHD* gene mutations, *JAMA 292*, 943-951.

247. Baysal, B. E., Ferrell, R. E., Willett-Brozick, J. E., Lawrence, E. C., Myssiorek, D., Bosch, A., van der Mey, A., Taschner, P. E., Rubinstein, W. S., Myers, E. N., Richard, C. W. r., Cornelisse, C. J., Devilee, P., and Devlin, B. (2000) Mutations in *SDHD*, a mitochondrial complex II gene, in hereditary paraganglioma, *Science 287*, 848-851.

248. Bayley, J. P., Devilee, P., and Taschner, P. E. (2005) The SDH mutation database: an online resource for succinate dehydrogenase sequence variants involved in pheochromocytoma, paraganglioma and mitochondrial complex II deficiency, *BMC Med Genet 6*, 39.

249. Burnichon, N., Briere, J. J., Libe, R., Vescovo, L., Riviere, J., Tissier, F., Jouanno, E., Jeunemaitre, X., Benit, P., Tzagoloff, A., Rustin, P., Bertherat, J., Favier, J., and Gimenez-Roqueplo, A. P. (2010) *SDHA* is a tumor suppressor gene causing paraganglioma, *Hum Mol Genet 19*, 3011-3020.

250. Ardehali, H., Chen, Z., Ko, Y., Mejia-Alvarez, R., and Marban, E. (2004) Multiprotein complex containing succinate dehydrogenase confers mitochondrial ATP-sensitive K$^+$ channel activity, *Proc Natl Acad Sci U S A 101*, 11880-11885.

251. Cantley, J., Grey, S. T., Maxwell, P. H., and Withers, D. J. (2010) The hypoxia response pathway and beta-cell function, *Diabetes Obes Metab 12 Suppl 2*, 159-167.

252. Bruick, R. K., and McKnight, S. L. (2001) A conserved family of prolyl-4-hydroxylases that modify HIF, *Science 294*, 1337-1340.

253. Koivunen, P., Hirsila, M., Remes, A. M., Hassinen, I. E., Kivirikko, K. I., and Myllyharju, J. (2007) Inhibition of hypoxia-inducible factor (HIF) hydroxylases by citric acid cycle intermediates: possible links between cell metabolism and stabilization of HIF, *J Biol Chem 282*, 4524-4532.

254. Selak, M. A., Armour, S. M., MacKenzie, E. D., Boulahbel, H., Watson, D. G., Mansfield, K. D., Pan, Y., Simon, M. C., Thompson, C. B., and Gottlieb, E. (2005) Succinate links TCA cycle dysfunction to oncogenesis by inhibiting HIF-alpha prolyl hydroxylase, *Cancer Cell 7*, 77-85.

255. Mansfield, K. D., Guzy, R. D., Pan, Y., Young, R. M., Cash, T. P., Schumacker, P. T., and Simon, M. C. (2005) Mitochondrial dysfunction resulting from loss of cytochrome c impairs cellular oxygen sensing and hypoxic HIF-alpha activation, *Cell Metab 1*, 393-399.

256. Tischler, A. S. (2008) Pheochromocytoma and extra-adrenal paraganglioma: updates, *Arch Pathol Lab Med 132*, 1272-1284.

257. Dahia, P. L., Ross, K. N., Wright, M. E., Hayashida, C. Y., Santagata, S., Barontini, M., Kung, A. L., Sanso, G., Powers, J. F., Tischler, A. S., Hodin, R., Heitritter, S., Moore, F., Dluhy, R., Sosa, J. A., Ocal, I. T., Benn, D. E., Marsh, D. J., Robinson, B. G., Schneider, K., Garber, J., Arum, S. M., Korbonits, M., Grossman, A., Pigny, P., Toledo, S. P., Nose, V., Li, C., and Stiles, C. D. (2005) A HIF-1alpha regulatory loop links hypoxia and mitochondrial signals in pheochromocytomas, *PLoS Genet 1*, 72-80.

258. Rodrigues Ade, S., Kiyomoto, B. H., Oliveira, A. S., Gabbai, A. A., Schmidt, B., and Tengan, C. H. (2008) Progressive myopathy with a combined respiratory chain defect including Complex II, *J Neurol Sci 264*, 182-186.

259. Riggs, J. E., Schochet, S. S. J., Fakadej, A. V., Papadimitriou, A., DiMauro, S., Crosby, T. W., Gutmann, L., and Moxley, R. T. (1984) Mitochondrial

encephalomyopathy with decreased succinate-cytochrome *c* reductase activity, *Neurology 34*, 48-53.

260. Rustin, P., Chretien, D., Bourgeron, T., LeBidois, J., Sidi, D., Rotig, A., and Munnich, A. (1993) Investigation of respiratory chain activity in human heart, *Biochem Med Metab Biol 50*, 120-126.

261. Birch-Machin, M. A., Taylor, R. W., Cochran, B., Ackrell, B. A., and Turnbull, D. M. (2000) Late-onset optic atrophy, ataxia, and myopathy associated with a mutation of a complex II gene, *Ann Neurol 48*, 330-335.

262. Taylor, R. W., Birch-Machin, M. A., Schaefer, J., Taylor, L., Shakir, R., Ackrell, B. A., Cochran, B., Bindoff, L. A., Jackson, M. J., Griffiths, P., and Turnbull, D. M. (1996) Deficiency of complex II of the mitochondrial respiratory chain in late-onset optic atrophy and ataxia, *Ann Neurol 39*, 224-232.

263. Rivner, M. H., Shamsnia, M., Swift, T. R., Trefz, J., Roesel, R. A., Carter, A. L., Yanamura, W., and Hommes, F. A. (1989) Kearns-Sayre syndrome and complex II deficiency, *Neurology 39*, 693-696.

264. Crofts, A. R., Lhee, S., Crofts, S. B., Cheng, J., and Rose, S. (2006) Proton pumping in the bc_1 complex: a new gating mechanism that prevents short circuits, *Biochim Biophys Acta 1757*, 1019-1034.

265. Nakanishi-Matsui, M., Sekiya, M., Nakamoto, R. K., and Futai, M. (2010) The mechanism of rotating proton pumping ATPases, *Biochim Biophys Acta 1797*, 1343-1352.

266. Rothery, R. A., Workun, G. J., and Weiner, J. H. (2008) The prokaryotic complex iron-sulfur molybdoenzyme family, *Biochim Biophys Acta 1778*, 1897-1929.

Chapter 2: The Quinone Binding Site in *Escherichia coli* Succinate Dehydrogenase is Required for Electron Transfer to the Heme *b**

2.1 Introduction

Escherichia coli SQR is responsible for the oxidation of succinate to fumarate coupled with quinone reduction during aerobic growth. The electrons from succinate oxidation are ultimately transferred via the [3Fe-4S] cluster to reduce a bound ubiquinone (UQ) at the Q_p-site. Still, the electron transfer pathway through the enzyme is highly ambiguous. Limitations in electron tunneling efficiency dictate that electrons must travel in a non-deviant path from the FAD to the [3Fe-4S] cluster through each of the other [Fe-S] clusters. The edge-to-edge distances from the [3Fe-4S] cluster to the Q_p-site and the conjugated porphyrin ring of the heme are 6.8 and 13.1 Å, respectively. These distances are well within the limit for effective electron tunneling of 14 Å (*1*), and it is unknown what role the heme may have in the electron transfer pathway, as electrons are fully capable of traveling directly to a UQ bound at the Q_p-site. It has been determined that the heme performs a structural role in stabilizing the holoenzyme (*2*), but the question of it participating in the electron transfer pathway has not been adequately addressed. It should be noted that using pulse radiolysis it has been suggested that the heme can participate in fast electron equilibration between the [3Fe-4S] cluster and quinone in the *E. coli* SQR (*3*). It is notable that in other members of the complex II superfamily, there may be no heme present (*E. coli* menaquinol:fumarate oxidoreductase), and in others there are two hemes present (*Bacillus subtilis* SQR and *Wolinella succinogenes* menaquinol: fumarate oxidoreductase) (*4*). In the case of *B. subtilis* SQR, it has been demonstrated that both hemes undergo redox cycling

during enzyme turnover (*5*). However, the structure of the *B. subtilis* SQR membrane domain is radically different compared with the *E. coli* SQR.

In mitochondrial Complex II, mutations in residues at and around the heme cofactor, as well as those surrounding the Q-site, have been implicated in human disease and oxygen hypersensitivity in *Caenorhabditis elegans* (*6-8*). Individuals with hereditary paragangliomas as well as pheochromocytomas tend to also have mutations in key conserved residues in these areas of their Complex II (*9, 10*). That these residues are often conserved between the human and *E. coli* enzymes is a testament to the usefulness of the latter as a model system to mimic disease-associated mutations.

In this study, we have examined the role of the heme within *E. coli* SQR. We demonstrate that it undergoes succinate-dependent reduction. However, optimal heme reduction by succinate requires the presence of a fully functional Q_p-site. Mutations to Q-site residues $SdhC^{S27}$, $SdhC^{R31}$, $SdhD^{D82}$, and $SdhD^{Y83}$ impair electron transfer to the heme. Additionally, we show that enzyme turnover and subsequent quinone reduction likely involve a radical semiquinone (SQ) species. These studies are a key step in the elucidation of the electron transfer mechanisms between key areas within the membrane domain of Complex II.

2.2 Materials and Methods

Bacterial Strains and Plasmids—Expression of wild-type and mutant SdhCDAB was carried out using the *E. coli* strain DW35 (($\Delta frdABCD$, *sdhC*::*kan*), laboratory collection) as the host that has been previously described (*11*). Wild-type SdhCDAB

was expressed from plasmid pFAS ($p_{FRD}sdh$C⁺D⁺A⁺B⁺) under the control of the fumarate reductase promoter (*12*). All cloning procedures were performed in TG1 cells (K12, Δ(*lacproAB*), *supE, thi, hsd* Δ5 F′[*traD*36 *proA⁺B⁺lacI*q *lacZ* ΔM15]) (Amersham Biosciences).

Site-directed Mutagenesis of Q-site Mutants—The 3.7-kb SphI/KpnI fragment of pFAS was excised and placed into vector pTZ18R [AmpR*lacZ′*] (Pharmacia), and this construct was used as a template for the mutagenesis reaction. Mutants were created with the QuikChange site-directed mutagenesis kit from Stratagene using 20-mer oligos as the mutagenic primers. All mutants were verified by sequencing (DNA core facility, University of Alberta). Mutagenized fragments were subcloned back into pFAS and transformed into *E. coli* DW35 for expression. All cloning procedures were performed in accordance with methods described in Sambrook and Russell (*13*).

Growth Conditions—*E. coli* DW35 expressing the appropriate SdhCDAB enzymes from recombinant plasmids were grown under microaerobic conditions. A 25 ml culture of Terrific Broth containing 100 μg ml⁻¹ ampicillin, 100 μg ml⁻¹ streptomycin, and 50 μg ml⁻¹ kanamycin was grown overnight under standard aerobic conditions. This was used to inoculate 2-liter cultures (in 4-liter Erlenmeyer flasks), which were then grown overnight at 37 °C with moderate shaking, each with antibiotics identical to those of the inoculum. The cells were harvested and washed once in 100

mM MOPS/ 5 mM EDTA, pH 7, buffer before freezing in liquid nitrogen and storing at −70 °C.

Growth Studies—The ability of mutant SQR to support growth in the presence of succinate was determined by growing *E. coli* DW35 expressing each of the mutants in minimal medium containing 20 mM succinate at 37 °C and monitoring cell turbidity with a Klett-Summerson spectrophotometer (red filter number 66). Growth studies were also done in glycerol-fumarate minimal medium as previously described (*14*).

Preparation of Membranes—Cells were lysed by two passages through a French press at 15,000 psi. The bacterial inner membrane fraction was concentrated by subjecting the cell lysate to a low speed centrifugation at 15,000 × *g* followed by high speed centrifugation steps at 150,000 × *g* as previously described (*15*). A 52% sucrose gradient was used to separate the inner membrane from the outer membrane, and following this step the *E. coli* SQR within the membranes was activated with 1 mM malonate at 30 °C for 20 min to release an oxaloacetate molecule bound to the active site FAD (*16*). Final membrane preparations were aliquotted into 300 μl batches, frozen in liquid nitrogen, and stored at −70 °C.

Analytical Methods—Protein concentrations were determined by a modified Lowry assay (*17*), and SdhCDAB concentration was determined through a covalently bound flavin assay (*18*).

Measurement of Enzyme Activity—Enzyme activity was assayed in 100 mM MOPS/ 5 mM EDTA, pH 7, degassed buffer at 23 °C.

Succinate-Q_0 Assay—This assay was performed anaerobically using a combination of 20 mM glucose in the buffer and the addition of 25 units of glucose oxidase/catalase (Sigma) as an oxygen scavenger. The absorbance decrease at 410 nm was measured in the presence of 10 mM succinate and 0.7 mM Q_0 (ϵ_{410} = 0.73 mM^{-1} cm^{-1}).

Plumbagin-Fumarate Assay—This assay was performed, as described ([*19*]), anaerobically in the presence of 10 mM fumarate and 0.35 mM plumbagin (5-hydroxy-2-methyl-naphthalene-1,4-dione) (ϵ_{419} = 2.81 mM^{-1} cm^{-1}). A combination of 20 mM glucose in the assay buffer and 25 units of glucose oxidase/catalase was used as well.

PMS-MTT Assay—The ability of the enzyme to pass electrons from succinate to 3-(4,5-dimethylthiazolyl-2-)2,5,di-phenyltetrazolium bromide was assayed as previously described ([*20*]) by monitoring the absorbance increase at 570 nm in the presence of 4 mM succinate, 0.75 mM phenazine methosulfate, and 0.075 mM 3-(4,5-dimethylthiazolyl-2-)2,5,di-phenyltetrazolium bromide (ϵ_{570} = 17 mM^{-1} cm^{-1}). All spectroscopic measurements were performed with a Hewlett Packard 8453 UV-VIS diode array spectrophotometer.

Heme Reduction Assay—The ability of the heme to be reduced in the presence of succinate was monitored spectrophotometrically. Membrane vesicles were injected into a cuvette containing degassed 100 mM MOPS/ 5 mM EDTA/ 20 mM glucose buffer to a final concentration of 0.5 mg ml^{-1}. 25 units of glucose oxidase/catalase were added to ensure a totally anaerobic solution. The absorbance of the heme at 560 nm was monitored using a three-point drop method with the data points at 500 and 575 nm. A base-line absorbance reading was established for 30 s prior to the addition of succinate into the cuvette to a final concentration of 8.7 mM. All readings were performed with a Hewlett Packard 8453 UV-VIS diode array spectrophotometer.

EPR Spectroscopy—In preliminary studies of "as is" air-oxidized membranes, samples containing 180 µl of membrane vesicles in 100 mM MOPS/ 5 mM EDTA, pH 7, of roughly 30 mg ml^{-1} protein were prepared. To simulate turnover conditions, 30 µl of 150 mM succinate was added to 150 µl of the same membranes and incubated at 23 °C for 30 s prior to freezing. For potentiometric titrations, membrane vesicles were prepared in 100 mM Tricine/ 5 mM EDTA buffer, pH 8, at a protein concentration of ~20 mg ml^{-1}. Titrations were carried out in an anaerobic vessel at 25 °C as previously described (*14*). The following redox dyes were added to a final concentration of 25 µM: dichlorophenolindophenol, 1,2-naphthoquinone, toluylene blue, phenazine methosulfate, thionine, methylene blue, resurufin, indigotrisulfonate, indigocarmine, anthroquinone-2-sulfonic acid, and neutral red. EPR spectra were recorded using a Bruker ESP300E spectrometer equipped with a

Bruker liquid nitrogen-evaporating cryostat at 150 K, 20-milliwatt microwave power at 9.43 GHz, and a modulation amplitude of $2G_{pp}$. All spectra reported are the average of five scans.

2.3 Results

Mutagenesis of Q-site Residues—Site-directed mutants of several conserved residues within the membrane intrinsic domain of *E. coli* SQR were generated. Based upon the x-ray structure, the chosen residues are all located around the Q_p-site. SdhC[S27] was mutated to an Ala residue; SdhC[R31] and SdhD[D82] were both mutated to Leu. SdhD[Y83] was mutated to Phe, Ala, and Lys. All mutants and wild-type enzymes were expressed in *E. coli* DW35, which contains a deletion in the *frdABCD* operon and an inactivated *sdhCDAB* operon to eliminate any chromosomally encoded enzyme contributing to the activity. The chosen residues are located directly within hydrogen bonding distance of the bound quinone molecule. SdhC[S27] is a candidate for hydrogen bonding to the O4 atom of UQ, while SdhD[Y83] lies on the opposite side, acts as a ligand for the O1 atom, and has been postulated to act as a proton donor during quinone reduction. SdhD[D82] lies in close proximity to UQ as well and could potentially interact directly with the quinone or act through its interaction with SdhD[Y83]. SdhC[R31] is also a major structural component of the quinone binding site as it lies equidistant between the heme and the UQ; additionally, this residue has been proposed to act as a modulator of the pK_a of the side chain OH of SdhD[Y83] (*21*).

*Characterization of Enzyme Activities Is Shown in **Table 2.1***—To ensure that loss of activity was not a result of breakdown of the enzyme, SDS-PAGE was performed on all membrane preparations (data not shown). This indicated that the wild-type as well as all the mutant enzymes were equally overexpressed to very high levels, whereas assembly and membrane targeting were unaffected. These results were verified by use of a covalently bound flavin assay to determine the exact concentration of SQR within the bacterial membrane. PMS-MTT (phenazine methosulfate-3-(4,5-dimethylthiazolyl-2-)2,5,diphenyltetrazolium bromide) assay results, which measure the functionality of the SdhAB dimer, were unchanged between the wild-type and mutant enzymes (data not shown). The succinate/Q_0 reductase assay monitors the physiological activity of SQR, and all of the mutants showed drastically reduced activity compared with the wild-type. As mutants of residues SdhC^{S27}, SdhC^{R31}, and SdhD^{D82} were unable to reduce the UQ analog Q_0, measurement of the enzyme K_m for Q_0 was not possible. Mutants of SdhD^{Y83} were also defective in their ability to reduce Q_0, although there was retention of 15–28% of wild-type activity. When SdhD^{Y83} was mutated to an Ala or Lys, the K_m for Q_0 was elevated as well, whereas a Phe substitution showed a K_m similar to wild-type. SQR is capable of operating in the reverse direction as a fumarate reductase, and this can be monitored by the plumbagin/fumarate assay. These mutations had different effects on the ability of the enzyme to oxidize reduced plumbagin, a menaquinol analog. The SdhC^{S27A} mutant only reduced plumbagin oxidation by 33% in contrast to its severe effect on Q_0 reduction (**Table 2.1**). Mutation of SdhD^{Y83} resulted in an elevated K_m for plumbagin, and the loss of

the ability to oxidize reduced plumbagin was similar to the effect seen on Q_0 reduction. The SdhC^{R31L} and SdhD^{D82L} mutants were severely affected in their ability to oxidize reduced plumbagin, similar to the effect seen with succinate/Q_0 activity. These results confirm that SdhC^{R31} and SdhD^{D82} are integral to the quinone chemistry of the enzyme in both the forward and reverse direction, whereas SdhC^{S27} is more essential for quinone reduction than for menaquinol oxidation and SdhD^{Y83} probably is more essential for quinone binding rather than being a direct participant in the chemistry of the Q_P-site.

The ability to complement growth of *E. coli* DW35 on aerobic minimal medium supplemented with succinate as the sole carbon source is a simple measure of *in vivo* functionality of the enzyme. **Figure 2.2** shows aerobic growth curves for cultures complemented with plasmids expressing each of the mutants. Cells harboring the wild-type enzyme on pFAS plasmid grew with a doubling time of 2.0 h. Mirroring the physiological activity of succinate oxidation, cells harboring plasmids expressing SdhC^{S27A}, SdhC^{R31L}, and SdhD^{D82L} mutants failed to grow. Despite the significant loss of physiological activity *in vitro*, the SdhD^{Y83F}, SdhD^{Y83A}, and SdhD^{Y83K} mutants were still able to grow on succinate-supplemented minimal medium with doubling times of 2.7, 2.0, and 2.2 h, respectively. That we did not observe a more significant difference in growth rates given the wide range of enzymatic activities can be attributed to the high degree of enzyme expression from the pFAS plasmid.

The ability of the mutant SQR to complement growth in *E. coli* DW35 in anaerobic glycerol-fumarate minimal medium was also examined. None of the

mutants was able to support growth, whereas *E. coli* DW35 harboring the wild-type plasmid could (**Figure 2.3**). *E. coli* SQR is a very poor fumarate reductase, and when this activity is impaired the enzyme can no longer support growth on glycerol-fumarate medium despite the high expression levels.

Impairment of the Q Binding Site Disrupts Heme Reduction—The redox state of the heme can be measured spectrophotometrically at 560 nm. In this way, it is possible to observe whether the *b*-type heme sandwiched between the membrane subunits participates in the electron transfer relay. Heme reduction was monitored following the addition of 10 mM succinate. The rate of reduced heme appearance as well as the amount of reduced heme were compared between the mutants and the wild-type. In **Figure 2.4**, heme reduction curves are shown for the wild-type and the mutants. Experiments were also performed in the presence of 0.35 mM pentachlorophenol, a potent Q-site inhibitor (*22*). To compare the different spectra, traces are normalized to the total amount of dithionite-reducible heme in each sample.

In the wild-type enzyme, the addition of succinate results in an immediate, rapid increase in reduced heme, whereas this rate is reduced in the mutants. The SdhC^{S27A}, SdhC^{R31L}, and SdhD^{D82L} mutants had greatly reduced rates of heme reduction compared with the wild-type. Mutations of SdhD^{Y83} also had a significant effect on heme reduction rates, although the effect was not as large as for the other mutations. Not only did these mutations in the Q-site perturb the rate at which electrons reach the heme, they also had an effect on the extent of heme reduction

once equilibrium was reached. There was a slight decrease in total heme reduction when SdhD^{D82} and SdhD^{Y83} were mutated, but a very noticeable decrease was observed in the SdhC^{S27} and SdhC^{R31} mutants. When comparing heme reduction in the Q-site mutants to heme reduction in the presence of pentachlorophenol, the results are strikingly similar. Traces in the presence of inhibitor are nearly identical in shape to those of the Q-site mutants and indicate a reduced rate and extent of heme reduction. These data suggest that impairment of the Q-site is directly responsible for the impediment to heme reduction.

EPR Spectroscopy of Mutant SQR—To determine whether the effects on heme reduction could be related to defective quinone reduction, we examined membranes enriched for wild-type or mutant enzyme using EPR and focused on the SQ radical intermediate. An SQ radical signal has been previously identified in *E. coli* fumarate reductase as well as preparations of submitochondrial particles (*23*). An SQ intermediate has yet to be confirmed in *E. coli* SQR, although an SQ has been detected by EPR in eukaryotic membrane preparations (*24*) as well as in *Paracoccus denitrificans* (*25*).

We were able to visualize a radical signal at g = 2.005 in the membranes expressing wild-type SdhCDAB in both "as is" air-oxidized membranes as well as a significantly larger signal under turnover conditions (**Figure 2.5**). Neither signal was present in the background *E. coli* DW35 membranes. Under turnover conditions, the EPR line shape is slightly altered with wings characteristic of a FAD radical (*26*). A conventional potentiometric redox titration on *E. coli* DW35 membranes expressing

wild-type SdhCDAB identifies two radical species within the sample (**Figure 2.6**). These species can be effectively resolved along the potential domain into a high potential species, which we identify as the SQ signal, and a low potential species, due to a radical at the FAD cofactor in SdhA. The low potential signal was highly attenuated in membranes not activated with malonate or membranes containing oxaloacetate, which when bound to the active site can interact directly with the FAD (data not shown). Curve fitting of this FAD signal reveals a midpoint potential of -148 mV at pH 8.0 for the two-electron reduction of FAD to $FADH_2$. This is in reasonable agreement with the parameters previously reported by us (*26*). The higher potential SQ signal has a midpoint potential of 60 mV at pH 8.0. Both the E_{m1}(SQ/Q) and E_{m2}(QH$_2$/SQ) transitions had equivalent values, which equates to 33% of the quinone being EPR visible ($K_{STAB} \sim 1.0$). That the SQ signal has a smaller amplitude than the flavin signal is likely due to a lower occupancy at the Q_p-site (UQ concentration dependent) compared with the FAD site (covalently bound flavin). It is likely that the growth conditions used resulted in a larger concentration of menaquinone compared with UQ in the membrane preparations used.

In contrast to the wild-type enzyme, when redox titrations were performed on the Q-site mutants by EPR, each of these mutants retained the FAD radical signal whereas they all lacked the SQ signal (**Table 2.1**). The FAD signal appears at the same midpoint potential as that seen in the wild-type, yet no other signal is observed at any other potential. Representative redox titrations for the SdhC[S27A] and SdhD[Y83F] mutants are shown in **Figure 2.7**.

2.4 Discussion

$E.\ coli$ SQR shares significant sequence and structural similarity with its mitochondrial ortholog. Although most of the similarity is found within the two membrane-extrinsic subunits, there are significant portions within the membrane domain that contain a number of very highly conserved residues, mainly surrounding the heme moiety and the Q_p-site. In this study, we mutated several conserved residues within the Q-site that are poised in prime positions for a direct interaction with the bound substrate according to the high-resolution crystal structure (*21*).

We investigated the possible roles of residues SdhC[S27], SdhC[R31], SdhD[D82], and SdhD[Y83]. We found that each mutant, although expressed to equivalent levels compared with wild-type enzyme, had a serious defect in the ability to reduce UQ. Mutations in the three former residues resulted in enzymes inactive in quinone reduction, whereas mutations of SdhD[Y83] led to active enzymes although with significantly reduced physiological activities. This highlights the critical importance of these residues in defining the binding pocket and/or the mechanism of quinone reduction. SdhC[S27], SdhC[R31], and SdhD[D82] have structural significance within the Q_p-site as their side chains are in positions able to hydrogen bond to the UQ. The loss of physiological activity associated with these mutants may be caused by loss of quinone binding. SdhC[S27] and SdhC[R31] have previously been identified as key residues within the Q-site (*27*), and SdhD[Y83] has been suggested to play an active role in reduction of the quinone as a possible proton donor due to its close proximity to the O1 oxygen of UQ (*21*). The results in this communication, however,

suggest that SdhD[Y83] plays a more important role in binding of the quinone and is not essential for protonation of the quinone. Removal of the OH side chain in the SdhD[Y83F] mutant resulted in an 85% loss in activity but the K_m for Q_0 was not altered. Mutation of SdhD[Y83] to either Ala or Lys reduced activity ~75% and additionally had an effect on quinone binding as evidenced by the increase in K_m for Q_0. This would suggest that SdhD[Y83] plays a role in defining the proper architecture and orientation of the quinone in the binding site but is not essential for protonation of the quinone. Rather, another amino acid residue and/or water molecule may be the direct proton donor (*28*).

The mutations in these residues also had an effect on activity when the enzyme acted as a fumarate reductase. Mutants defective in Q_0 reduction also had corresponding decreases in their plumbagin/fumarate activities, suggesting that both quinone reduction and oxidation occur at the same site within the enzyme. SdhC[S27] did not have as great an effect on plumbagin oxidation as was seen on Q_0 reduction. The differences in structure between UQ and menaquinol may cause the molecules to bind and interact with different residues within the Q-site, so differences in activity in either direction can be expected. This result is consistent with recent observations with *E. coli* fumarate reductase where a slightly different orientation for menaquinone and UQ have been shown for the Q_P-site in that SQR paralog (*29*).

It was not anticipated that mutations made to the Q-site would have effects on electron transfer to the heme. Electrons at the [3Fe-4S] cluster face a bifurcating pathway to either the heme or the Q-site and would be expected to tunnel to both

sites given the distances involved. Indeed, it has been proposed that the heme serves as an electron sink such that electrons are donated to the heme first, and when both the [3Fe-4S] and the heme are reduced, this would allow for the concomitant two-electron reduction of the bound quinone (*28*). In this mechanism, the heme would hold an electron until the [3Fe-4S] cluster was reduced, thus preventing formation of an SQ radical that could interact with oxidants in the native, aerobic environment in which the enzyme operates *in vivo*, in such a way as to prevent production of high amounts of reactive oxygen species resulting in oxidative stress that has been shown to be harmful to cells (*30*). Although such a hypothesis may be appealing, the results here do not indicate that this is the preferred mechanism.

The results presented here indicate that the quinone, not the heme, likely receives the first electron from the [3Fe-4S] cluster, although rapid electron equilibration between the heme and quinone cannot be ruled out (*3*). When we disrupt the Q-site through mutation, we observe that the rate of electron transfer to the heme is decreased. We conclude that a functional Q-site is required for optimal heme reduction. Electron tunneling rates can be affected by distances between, as well as midpoint potentials of, each cofactor, although the effect of the latter may be minimal (*1*). In the case of *E. coli* SQR, the heme is only slightly closer, edge-to-edge, to the [3Fe-4S] compared with the bound quinone. However, the midpoint potential of the UQ pair is significantly higher than the midpoint potential of the heme ($E_{m,8}$ = −15 mV), suggesting that the quinone may be the preferred receptor of the electron from the [3Fe-4S]. Our results show that in the absence of a functional Q-site, there

is still a slow leakage of electrons to the heme but compared with the wild-type enzyme the rate is radically slower. This low rate of electron transfer is surprising considering the close distance between these two centers. This distance between the [3Fe-4S] and the heme should lend itself to fast redox equilibrium regardless of the state of the Q-site, but given that the opposite is observed, perhaps a gating mechanism may be in place to prevent the electrons from tunneling directly to the heme from the [3Fe-4S] cluster. A potential candidate here is residue SdhB[H207], which lies directly between the cluster and the heme. Its electron density in the crystal structure suggests a mobile side chain that could modulate electron flow between these redox centers (*28*). SdhB[H207] is in direct proximity to the [3Fe-4S] cluster, the bound UQ, and a heme *b* propionate. Any hydrogen-bonding network in this vicinity would rely heavily on this residue, and an empty Q-site may disrupt this network.

Using potentiometric methods in combination with EPR spectroscopy, we have demonstrated for the first time the presence of a ubisemiquinone intermediate bound to the Q_p-site of *E. coli* SQR. This SQ signal can be convincingly separated from any interfering FAD radical along the potential domain. Given the stability of the SQ, it is likely that regular turnover of the enzyme occurs through this radical intermediate. A ubisemiquinone has also been demonstrated in *E. coli* menaquinol:fumarate oxidoreductase, but only in a site-specific mutant (FrdC-E29L) (*29*). It is perhaps notable that it is the wild-type form of *E. coli* SQR in which the SQ is observed. Moreover, all the mutants studied here lacked the SQ signal as only the FAD radical was observed in the EPR experiments. There is a correlation

between loss of enzyme activity and lack of a ubisemiquinone intermediate. This effect may be due to either the inability to bind quinone or a decrease in the stability of the radical. The latter may be the case in the SdhD[Y83] mutants that knock out the radical signal but retain some activity. In this instance, the stability of the quinone may be so reduced that little or no EPR signal may be detected.

We propose a mechanism in which electrons derived from succinate oxidation at the FAD tunnel along the [Fe-S] relay until the [3Fe-4S] cluster. These electrons are subsequently transferred to an awaiting UQ molecule nested within the Q-site, although there is a small possibility that this electron may tunnel to the heme instead. Following the first single electron reduction step, a semiquinone radical species is formed that may be stabilized by any number of the residues that were discussed in this report. The free electron of the SQ may then tunnel back and forth between the heme and the quinone in equilibrium prior to a second electron arriving from the [3Fe-4S] cluster to provide full reduction of the UQ to UQH_2. In this way, the heme cofactor may still behave as an electron sink, but its role is to prevent the interaction of the SQ with molecular oxygen by providing a more suitable oxidizing agent. Mutations that create anomalies in the Q-site or around the heme will surely impair these processes and are likely to result in an increase in the levels of reactive oxygen species generated by the enzyme as well as have functional consequences on enzyme activity. Although the root cause of many of the Complex II-associated diseases remains a mystery, the fact that many of these mutations are found in the same areas as described in this study may again suggest that disruption

of enzymatic activity and possible reactive oxygen species production could be the key to understanding these disease states.

2.5 Addendum

A fact that was never published but is included in Appendix A (**Figure A.1**), is that when exogenous Q_0 is added to succinate-reduced Q-site mutants, the heme is instantly and fully oxidized, and remains in that state. The effect is dependent on Q-binding, as it is not seen in a double Q-site mutant. This is extremely puzzling since under these conditions, the enzyme should be maximally reduced because electrons cannot leave the system through the Q-site; in that case, the redox state of each cofactor should depend on their individual redox potentials relative to the succinate/fumarate couple. A possible explanation for the surprising result is that the binding of UQ to the enzyme elicits a decrease in the midpoint potential of the heme, such that succinate can no longer reduce it. If this were true, Q-site mutants that bind the endogenous UQ weakly, but were unable to reduce it to UQH_2, would demonstrate lower heme reduction rates and reduction levels upon the addition of succinate, as I showed. Once saturating exogenous UQ is added to the system, all available sites would then bind UQ, preventing heme reduction. This might also explain why the pre-steady state MHQ experiments could not detect reduced heme in wild-type SQR until after the initial turnover of the endogenous UQ – the potential is too low. Such a mechanism might be useful under conditions where there is very little UQ available. In such an instance, the heme would be reduced and primed for

the instant that UQ diffuses into the active site. Once UQ enters the Q-site, the drop

in heme potential drives the fast reduction of UQ to the ubisemiquinone form.

2.5 Tables and Figures

Mutant	Succinate/ Q_0 turnover $(\times 10^2 \text{ min}^{-1})$	Km Q_0 (mM)	Plumbagin/fumarate turnover $(\times 10^2 \text{ min}^{-1})$	K_m plumbagin (uM)	SQ signal
DW35	0	n.d	0	n.d	No
SdhCDAB	26 ± 2	0.24 ± 0.01	16 ± 1	80 ± 1	Yes
SdhC^{S27A}DAB	1.1 ± 0.1	n.d	10.6 ± 0.8	80 ± 2	No
SdhCD^{R31L}DAB	0.6 ± 0.1	n.d	1.0 ± 0.1	53 ± 2	No
SdhCD^{D82L}AB	0.5 ± 0.1	n.d	2.3 ± 0.3	81 ± 1	No
SdhCD^{Y83F}AB	3.9 ± 0.3	0.28 ± 0.01	4.9 ± 0.6	260 ± 6	No
SdhCD^{Y83A}AB	7.2 ± 0.6	0.93 ± 0.03	8.8 ± 0.7	283 ± 4	No
SdhCD^{Y83K}AB	6.7 ± 0.5	0.57 ± 0.04	6.8 ± 0.7	134 ± 2	No

Table 1: **Characterization of SdhCDAB activities in the different mutant SQR.**

Catalytic turnover and K_m of Q_0 reduction and plumbagin oxidation were measured in membranes prepared from *E. coli* DW35 harboring plasmid pFAS expressing each of the succinate dehydrogenase mutants. The final column denotes whether an EPR-visible ubisemiquinone radical was observed in the membranes. A loss of the SQ signal indicates the enzyme has lost the ability to bind quinone or the stability of the bound radical intermediate has been greatly diminished. ND – not detectable.
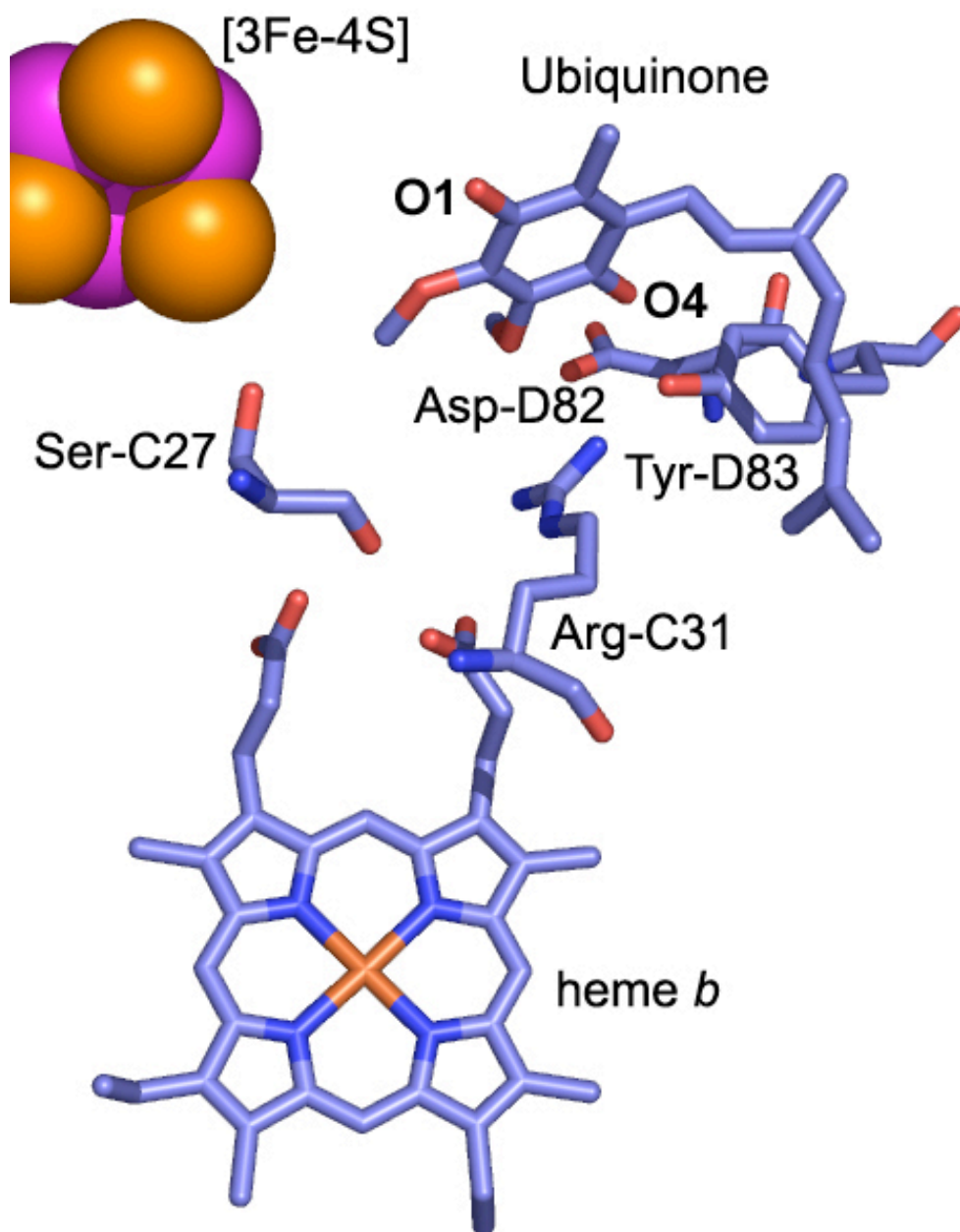
Figure 2.1: Crystal structure of *E. coli* **SQR, centered around the heme**. Several key residues studied around the Q-site and heme are shown. The side chains of these residues are all directed toward the bound ubiquinone and may act as potential ligands (PDB: 1NEK *(21)*).
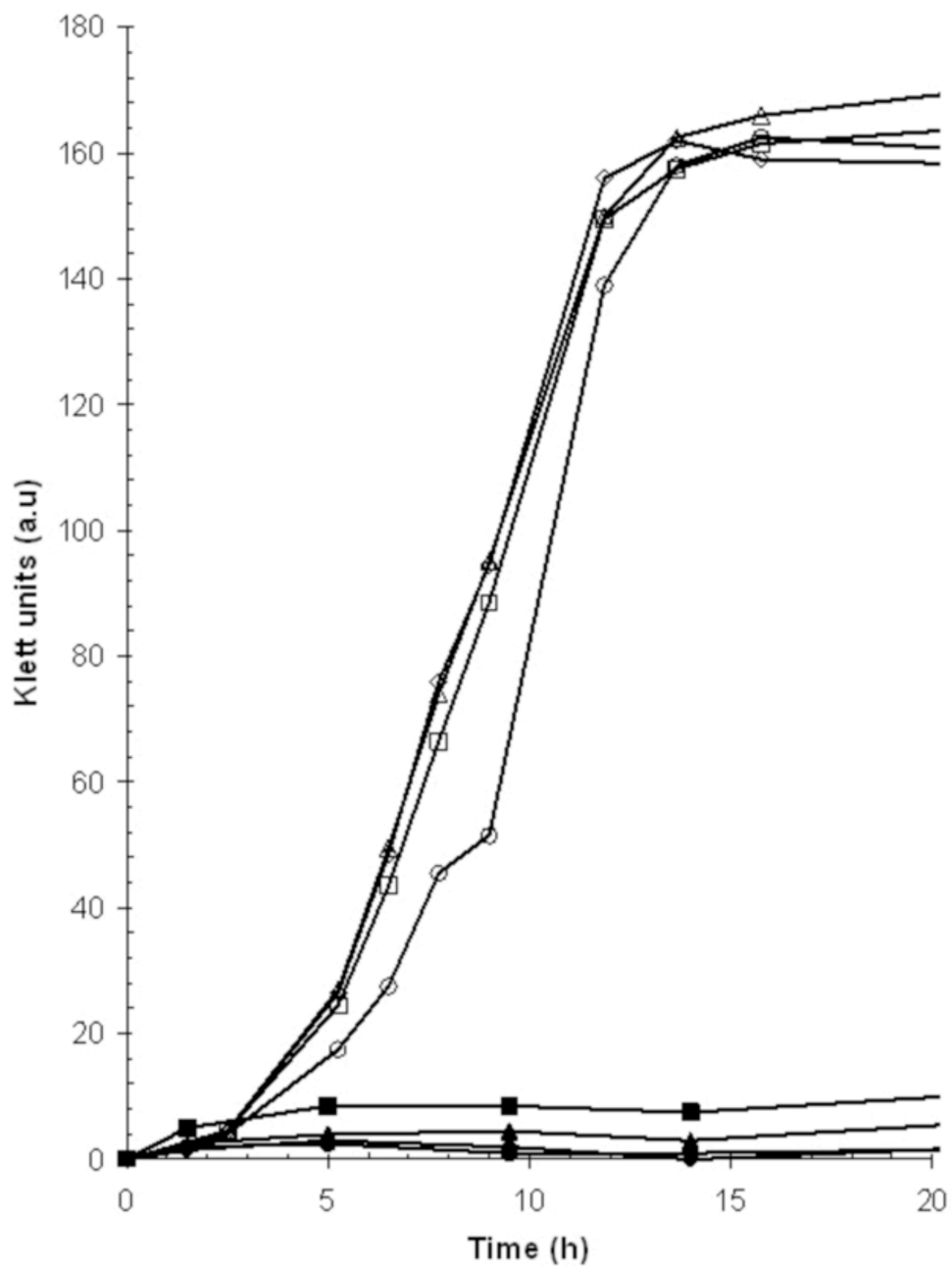
Figure 2.2: Aerobic growth of *E. coli* DW35 cells harboring plasmids expressing wild-type and mutant SQR on minimal medium supplemented with succinate. (•) DW35 host; (◊) SdhCDAB; (▪) SdhC^{S27A};

(♦), SdhC^{R31L}; (▲) SdhD^{D82L}; (○) SdhD^{Y83F}; (△), SdhD^{Y83A}; (□) SdhD^{Y83K}.
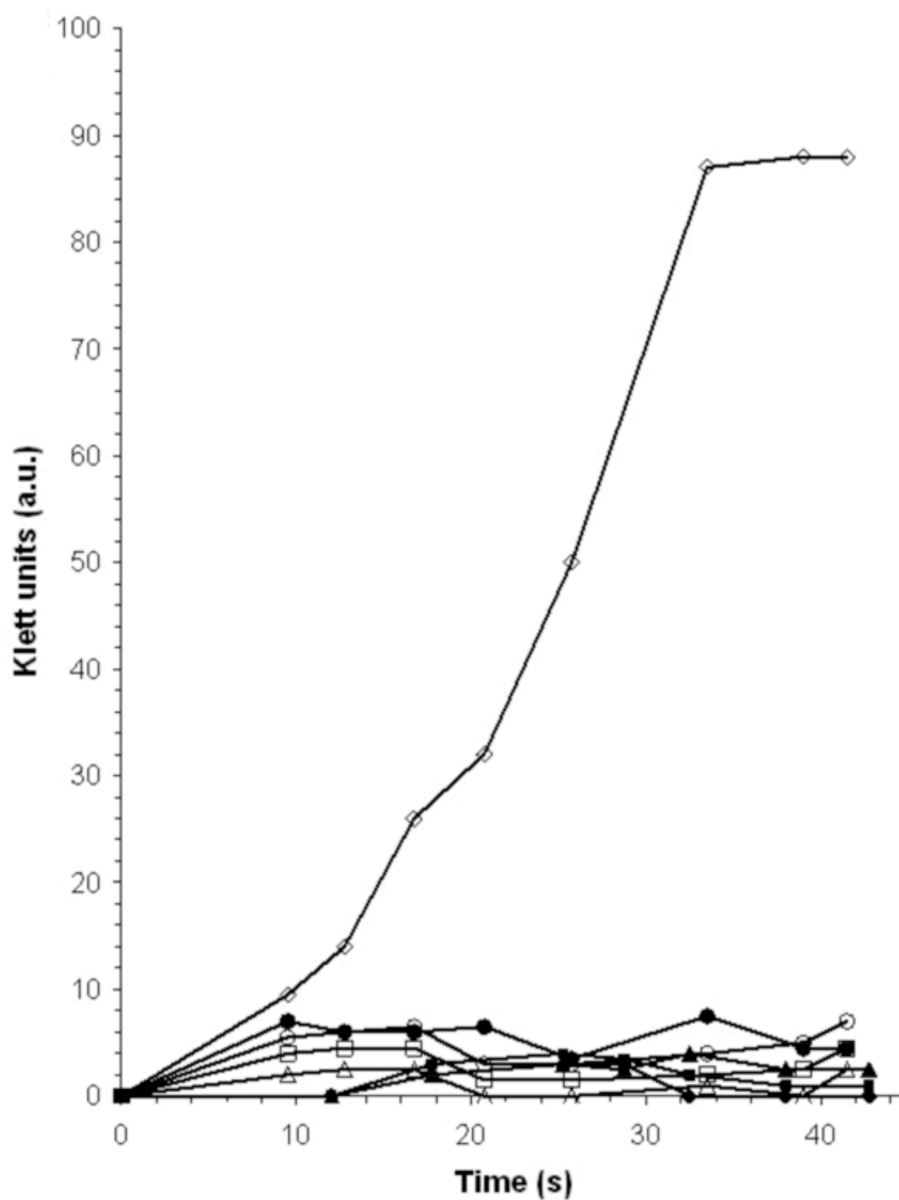
Figure 2.3: Anaerobic growth of *E. coli* DW35 cells harboring plasmids expressing wild-type and mutant SQR on minimal medium supplemented with glycerol-fumarate. ($\bullet$) DW35 host; ($\diamond$) SdhCDAB; ($\blacksquare$) SdhC^{S27A}; ($\blacklozenge$), SdhC^{R31L}; ($\blacktriangle$) SdhD^{D82L}; ($\circ$) SdhD^{Y83F}; ($\triangle$), SdhD^{Y83A}; ($\square$) SdhD^{Y83K}.
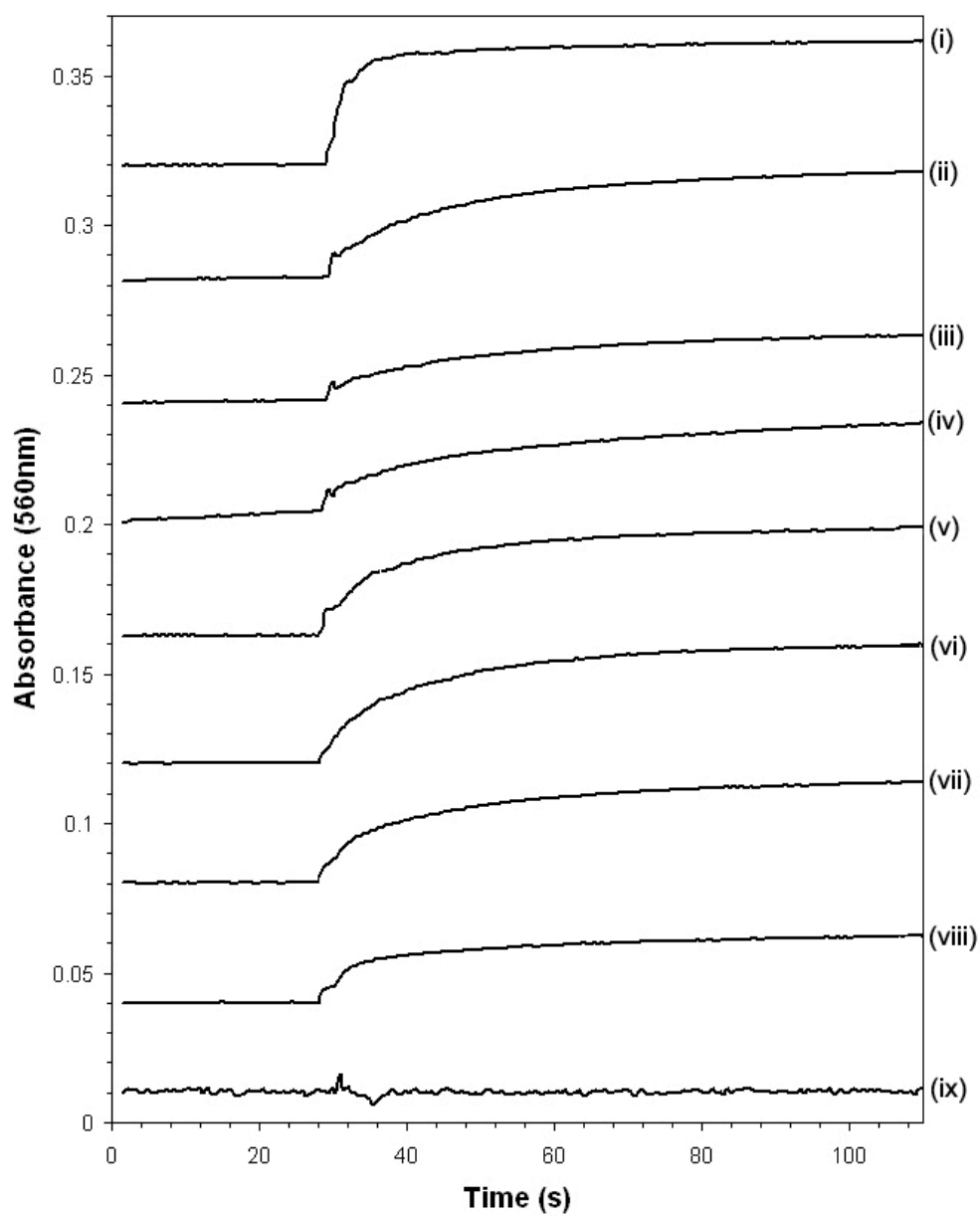
Figure 2.4: Heme reduction assays in the presence of succinate. 8.7 mM succinate was added to membrane vesicles of 0.5 mg ml^{-1} protein at the 30 s time point. An increase in A_{560} denotes reduced heme. Curves are normalized to total amount of dithionite-reducible heme signal. *i*, SdhCDAB, *ii*, SdhC^{S27A}, *iii*, SdhC^{R31L}, *iv*, SdhD^{D82L}, *v*, SdhD^{Y83F}, *vi*, SdhD^{Y83A}, *vii*, SdhD^{Y83K}, *viii*, SdhCDAB + 0.35 mM pentachlorophenol, *ix*, DW35 host.
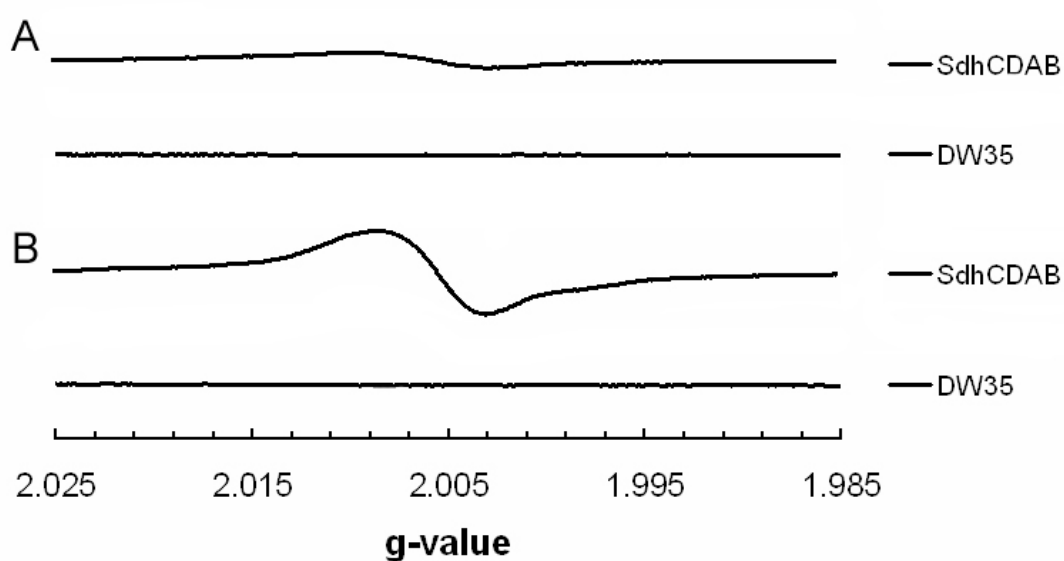
Figure 2.5: EPR spectra of wild-type SdhCDAB and background in air-oxidized membranes (*A*) and under turnover conditions (*B*) in the presence of 25 mM succinate. The g = 2.005 radical signal is only observed in membranes containing wild-type SQR. The amplitude of the signal is greatly increased in the presence of succinate.
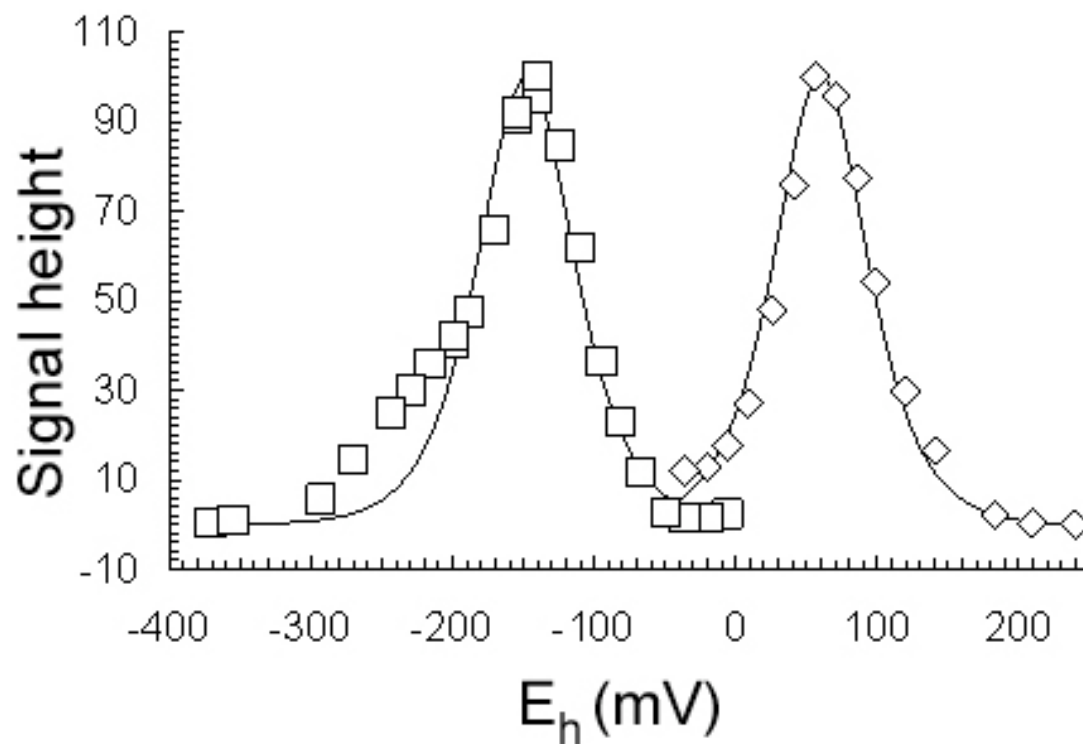
Figure 2.6: Potentiometric titration curves of the g = 2.005 radical signal in wild-type SdhCDAB membrane vesicles at pH 8.0. Two different radical species are observed. The FAD radical signal appears at lower potentials ($E_{m,8}$ = −148 mV), and the ubisemiquinone radical signal appears at higher potentials ($E_{m,8}$ = 60 mV). Peak-trough differentials were plotted as a function of E_h. Signal heights are normalized to 100%.
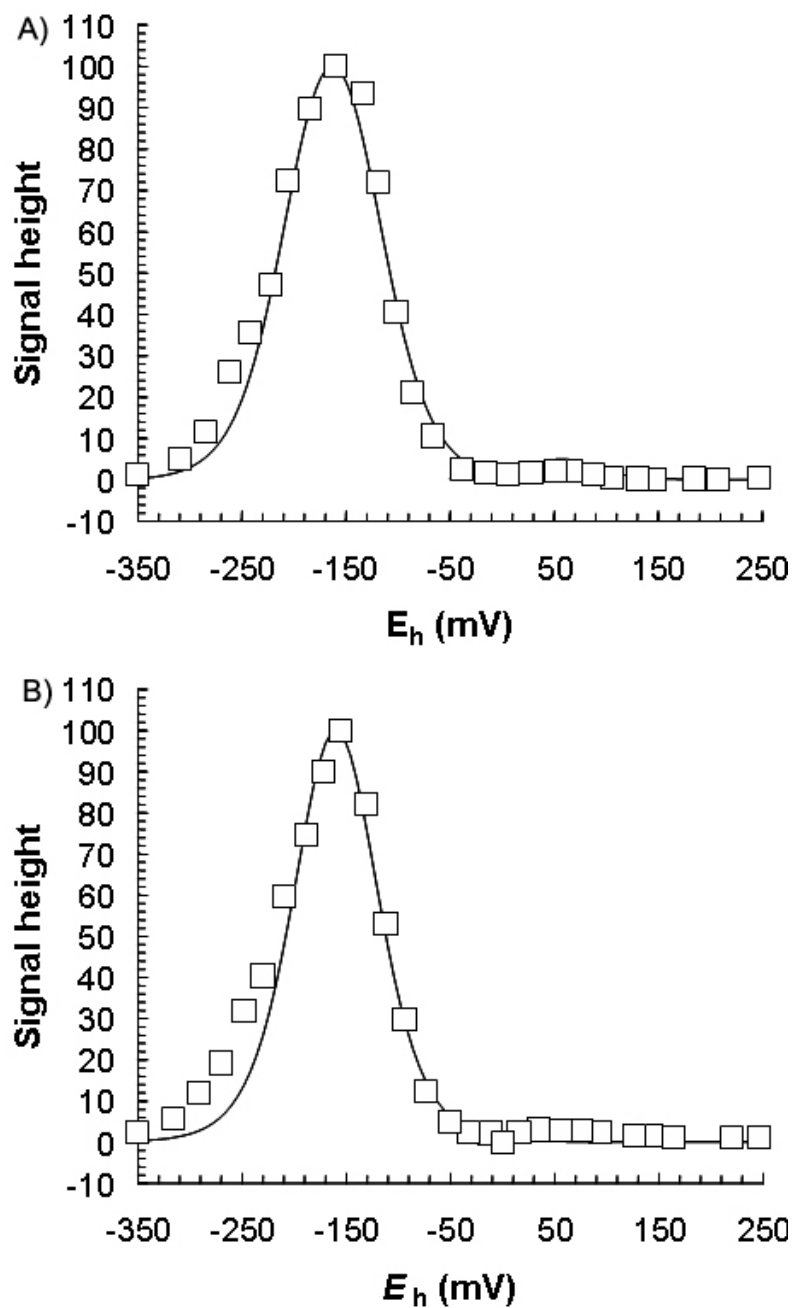
Figure 2.7: Potentiometric titrations of the g = 2.005 signal as a function of E_h in mutant SdhCDAB membrane vesicles at pH 8.0. *A*, redox titration of SdhC[S27A] membranes. *B*, redox titration of SdhD[Y83F] membranes. The low potential FAD radical signal is maintained, but the ubisemiquinone signal is abolished.

2.7 References

1. Page, C. C., Moser, C. C., Chen, X., and Dutton, P. L. (1999) Natural engineering principles of electron tunnelling in biological oxidation-reduction, *Nature 402*, 47-52.

2. Nakamura, K., Yamaki, M., Sarada, M., Nakayama, S., Vibat, C. R., Gennis, R. B., Nakayashiki, T., Inokuchi, H., Kojima, S., and Kita, K. (1996) Two hydrophobic subunits are essential for the heme *b* ligation and functional assembly of complex II (succinate-ubiquinone oxidoreductase) from *Escherichia coli*, *J Biol Chem 271*, 521-527.

3. Anderson, R. F., Hille, R., Shinde, S. S., and Cecchini, G. (2005) Electron transfer within complex II. Succinate:ubiquinone oxidoreductase of *Escherichia coli*, *J Biol Chem 280*, 33331-33337.

4. Hagerhall, C., and Hederstedt, L. (1996) A structural model for the membrane-integral domain of succinate: quinone oxidoreductases, *FEBS Lett 389*, 25-31.

5. Matsson, M., Tolstoy, D., Aasa, R., and Hederstedt, L. (2000) The distal heme center in *Bacillus subtilis* succinate:quinone reductase is crucial for electron transfer to menaquinone, *Biochemistry 39*, 8617-8624.

6. Hartman, P. S., Ishii, N., Kayser, E. B., Morgan, P. G., and Sedensky, M. M. (2001) Mitochondrial mutations differentially affect aging, mutability and anesthetic sensitivity in *Caenorhabditis elegans*, *Mech Ageing Dev 122*, 1187-1201.

7. Ishii, N., Fujii, M., Hartman, P. S., Tsuda, M., Yasuda, K., Senoo-Matsuda, N., Yanase, S., Ayusawa, D., and Suzuki, K. (1998) A mutation in succinate dehydrogenase cytochrome *b* causes oxidative stress and ageing in nematodes, *Nature 394*, 694-697.

8. Senoo-Matsuda, N., Yasuda, K., Tsuda, M., Ohkubo, T., Yoshimura, S., Nakazawa, H., Hartman, P. S., and Ishii, N. (2001) A defect in the cytochrome *b* large subunit in complex II causes both superoxide anion overproduction and abnormal energy metabolism in *Caenorhabditis elegans, J Biol Chem 276*, 41553-41558.

9. Baysal, B. E., Ferrell, R. E., Willett-Brozick, J. E., Lawrence, E. C., Myssiorek, D., Bosch, A., van der Mey, A., Taschner, P. E., Rubinstein, W. S., Myers, E. N., Richard, C. W. r., Cornelisse, C. J., Devilee, P., and Devlin, B. (2000) Mutations in *SDHD*, a mitochondrial complex II gene, in hereditary paraganglioma, *Science 287*, 848-851.

10. Niemann, S., and Muller, U. (2000) Mutations in *SDHC* cause autosomal dominant paraganglioma, type 3, *Nat Genet 26*, 268-270.

11. Westenberg, D. J., Gunsalus, R. P., Ackrell, B. A., Sices, H., and Cecchini, G. (1993) *Escherichia coli* fumarate reductase frdC and frdD mutants. Identification of amino acid residues involved in catalytic activity with quinones, *J Biol Chem 268*, 815-822.

12. Maklashina, E., Berthold, D. A., and Cecchini, G. (1998) Anaerobic expression of *Escherichia coli* succinate dehydrogenase: functional replacement of fumarate reductase in the respiratory chain during anaerobic growth, *J Bacteriol 180*, 5989-5996.

13. Sambrook, J., and Russell, D. W. (2001) Molecular Cloning: A Laboratory Manual, 3rd Edition, 1.32-1.170, A8.40-A8.51.

14. Rothery, R. A., and Weiner, J. H. (1996) Interaction of an engineered [3Fe-4S] cluster with a menaquinol binding site of *Escherichia coli* DMSO reductase, *Biochemistry 35*, 3247-3257.

15. Rothery, R. A., Blasco, F., and Weiner, J. H. (2001) Electron transfer from heme b_L to the [3Fe-4S] cluster of *Escherichia coli* nitrate reductase A (NarGHI), *Biochemistry 40*, 5260-5268.

16. Ackrell, B. A., Kearney, E. B., and Mayr, M. (1974) Role 3f oxalacetate in the regulation of mammalian succinate dehydrogenase, *J Biol Chem 249*, 2021-2027.

17. Markwell, M. A., Haas, S. M., Bieber, L. L., and Tolbert, N. E. (1978) A modification of the Lowry procedure to simplify protein determination in membrane and lipoprotein samples, *Anal Biochem 87*, 206-210.

18. Singer, T. P., Salach, J., Hemmerich, P., and Ehrenberg, A. (1971) Flavin peptides, *Methods Enzymol 18*, 416-427.

19. Rothery, R. A., and Weiner, J. H. (1998) Interaction of a menaquinol binding site with the [3Fe-4S] cluster of *Escherichia coli* fumarate reductase, *Eur J Biochem 254*, 588-595.

20. Kita, K., Vibat, C. R., Meinhardt, S., Guest, J. R., and Gennis, R. B. (1989) One-step purification from *Escherichia coli* of complex II (succinate: ubiquinone oxidoreductase) associated with succinate-reducible cytochrome b_{556}, *J Biol Chem 264*, 2672-2677.

21. Yankovskaya, V., Horsefield, R., Tornroth, S., Luna-Chavez, C., Miyoshi, H., Leger, C., Byrne, B., Cecchini, G., and Iwata, S. (2003) Architecture of succinate dehydrogenase and reactive oxygen species generation, *Science 299*, 700-704.

22. Maklashina, E., and Cecchini, G. (1999) Comparison of catalytic activity and inhibitors of quinone reactions of succinate dehydrogenase (Succinate-ubiquinone oxidoreductase) and fumarate reductase (Menaquinol-fumarate oxidoreductase) from *Escherichia coli*, *Arch Biochem Biophys 369*, 223-232.

23. Hagerhall, C., Magnitsky, S., Sled, V. D., Schroder, I., Gunsalus, R. P., Cecchini, G., and Ohnishi, T. (1999) An *Escherichia coli* mutant quinol:fumarate reductase contains an EPR-detectable semiquinone stabilized at the proximal quinone-binding site, *J Biol Chem 274*, 26157-26164.

24. Ruzicka, F. J., Beinert, H., Schepler, K. L., Dunham, W. R., and Sands, R. H. (1975) Interaction of ubisemiquinone with a paramagnetic component in heart tissue, *Proc Natl Acad Sci U S A 72*, 2886-2890.

25. Hung, S. C., Grant, C. V., Peloquin, J. M., Waldeck, A. R., Brit, R. D., and Chan, S. I. (2000) ESEEM studies of succinate:ubiquinone reductase from *Paracoccus denitrificans*, *J Biol Inorg Chem 5*, 593-602.

26. Maklashina, E., Iverson, T. M., Sher, Y., Kotlyar, V., Andrell, J., Mirza, O., Hudson, J. M., Armstrong, F. A., Rothery, R. A., Weiner, J. H., and Cecchini, G. (2006) Fumarate reductase and succinate oxidase activity of *Escherichia coli* complex II homologs are perturbed differently by mutation of the flavin binding domain, *J Biol Chem 281*, 11357-11365.

27. Yang, X., Yu, L., He, D., and Yu, C. A. (1998) The quinone-binding site in succinate-ubiquinone reductase from *Escherichia coli*. Quinone-binding

domain and amino acid residues involved in quinone binding, *J Biol Chem 273*, 31916-31923.

28. Horsefield, R., Yankovskaya, V., Sexton, G., Whittingham, W., Shiomi, K., Omura, S., Byrne, B., Cecchini, G., and Iwata, S. (2006) Structural and computational analysis of the quinone-binding site of complex II (succinate-ubiquinone oxidoreductase): a mechanism of electron transfer and proton conduction during ubiquinone reduction, *J Biol Chem 281*, 7309-7316.

29. Maklashina, E., Hellwig, P., Rothery, R. A., Kotlyar, V., Sher, Y., Weiner, J. H., and Cecchini, G. (2006) Differences in protonation of ubiquinone and menaquinone in fumarate reductase from *Escherichia coli, J Biol Chem 281*, 26655-26664.

30. Finkel, T., and Holbrook, N. J. (2000) Oxidants, oxidative stress and the biology of ageing, *Nature 408*, 239-247.

Chapter 3: *Escherichia coli* Succinate Dehydrogenase Variants Lacking the Heme *b**

3.1 Introduction

E. coli SQR has a b-type heme within the membrane domain that is essentially identical to that found in the eukaryotic enzyme. The role of this heme has been the focus of great debate. Although it is redox-active (1), it is not known whether it is essential for enzyme catalysis. This ambiguity stems from the fact that the heme does not lie on the FAD-[Fe-S] relay connecting succinate oxidation with the site of ubiquinone binding (the Q-site) within the membrane-intrinsic domain of the enzyme. Inspection of the structure (**Figure 3.1**), however, reveals that the heme lies 13.1 Å (edge to edge) from the [3Fe-4S] cluster and 6.5 Å from the ubiquinone that cocrystallized with the enzyme (2). These distances are short enough for rapid electron transfer among the [3Fe-4S] cluster, the bound ubiquinone, and the heme. Interestingly, the E. coli QFR and SQR share much of the same catalytic and structural properties (3-5), but QFR lacks heme. Thus, determining the role of the heme of SQR would be an important step in gaining a complete understanding of its structure and function.

Previous experiments to create a heme-free SQR by expressing the enzyme in a *hemA E. coli*-deletion strain, which is unable to synthesize heme, failed as a result of improper enzyme assembly, prompting the hypothesis that the heme is necessary for proper subunit formation and integration (6). In addition, further attempts to remove the heme by site-directed mutagenesis proved to be ineffective (7, 8). Here we successfully created a heme-free mutant of E. coli SQR, which retains catalytic activity and many wild-type properties.

3.2 Materials and Methods

Bacterial strains and plasmids – *E. coli* strains DW35 (Δ*frdABCD*, *sdhC*::*kan*) (*9*) and SASX41B (*HfrP02A hemA41 metB1 relA1*) (*10*) were used for overexpression of SdhCDAB from the plasmid pFAS (p$_{FRD}$*sdh*C$^+$D$^+$A$^+$B$^+$) as described in ref. (*11*). *E. coli* TG1 cells (K12, Δ(*lac-proAB*), *supE*, *thi*, *hsd* Δ5 F′[*traD*36 *proA*$^+$B$^+$*lacI*^{q} *lacZ* ΔM15]) (Amersham Biosciences) were used for all cloning protocols. Site-directed mutagenesis methods were performed as described in ref. (*1*).

Cell growth and preparation of membrane vesicles – DW35 cells expressing the appropriate enzymes were grown in batch cultures in Terrific Broth under microaerobic conditions and harvested as described in ref. (*1*). SASX41B cells were grown anaerobically in glycerol-fumarate minimal medium (*12*) in 19-liter carboys (from a 250 mL Luria-Bertani broth innoculum supplemented with 50 μg mL^{-1} 5-aminolevulinic acid) (*13*) at 37 °C for 30 h. Further, 100 μg mL^{-1} ampicillin was routinely used in all cell cultures. Additionally, 100 μg mL^{-1} streptomycin and 50 μg mL^{-1} kanamycin were added to all DW35 cultures. Growth studies were performed in Klett flasks containing minimal medium supplemented with 20 mM succinate (*1*).

PMSF was added to a final concentration of 0.2 mM before cell lysis by French Press. Membranes were isolated by differential centrifugation (*1*). Activation of the SQR enzyme required a 20-min incubation at 30 °C with 1 mM malonate, and 100 mM Mops/ 5 mM EDTA was used ubiquitously as the buffer system. A modified

Lowry assay (*14*) was used to determine the protein concentration in the membrane vesicles.

SDS-PAGE – Protein samples were run on a 12.5% polyacrylamide gel. After a 5-min incubation at 70 °C, 45 µg of protein were loaded onto each lane. Low-molecular-mass markers were obtained from Bio-Rad and Invitrogen. All gels were stained with Coomassie brilliant blue.

Enzyme activity, quantitation, and ROS generation – Both the succinate:Q_0 and plumbagin (5-hydroxy-methyl-napthalene-1,4-dione):fumarate assays have been described before (*1*). SQR-enriched membranes were added to an oxygen-depleted cuvette containing the appropriate substrates to initiate the reaction. The Q_1-reductase and PES assays also have been described (*5*). All membranes were incubated with 1 mM malonate to remove the oxaloacetate inhibitor bound to the active-site FAD.

The measurement of superoxide production was performed with a standard cytochrome *c* reduction assay (*15*).

The protoheme IX content of cytochrome *b* was determined by the pyridine hemochromogen difference spectra (dithionite-reduced minus ferricyanide-oxidized) ($\varepsilon^{558-540} = 23.98$ mM^{-1}·cm^{-1}) as described in ref. (*16*). Quantitation of covalently-bound flavin in Sdh-enriched membranes was performed as described previously (*17*).

Purification of SQR – Membranes were solubilized with 1% Thesit ($C_{12}E_9$; Anatrace), and the extract was bound to a DEAE fast-flow anion exchange resin as described in ref. (*18*), with the exception that the initial buffer was 10 mM K-P_i (pH 7.5). The anion exchange resin containing the bound enzyme was collected on a small filter, washed with 75 mM NaCl, and eluted with 300 mM NaCl.

UV-VIS and EPR spectroscopy – Reduced minus oxidized spectra of the membranes were performed at a protein concentration of 0.5 mg mL^{-1}. Excess dithionite was added to the cuvette to reduce the sample before obtaining a sample spectrum. A Hewlett Packard 8453 UV-VIS diode array spectrophotometer was used to perform all spectral readings.

To generate oxidized samples for EPR analysis, 170 μL of membranes were placed into a standard EPR tube, to which DCPIP was added to a final concentration of 0.8 mM before freezing. Potentiometric titrations were performed as reported (*1*). [Fe-S] cluster and heme spectra were recorded by using a Bruker Elexsys E500 EPR spectrophotometer equipped with an Oxford Instruments ESR900 flowing helium cryostat. All EPR experiments were performed at pH 7.0. EPR conditions were 9 K, 20 mW at 9.38 GHz, 10 G_{pp}.

Studies done on the flavosemiquinone and ubisemiquinone radicals were performed by using a Bruker ESP300E spectrometer equipped with a Bruker liquid nitrogen evaporating cryostat at 150 K. EPR conditions were 150 K, 20 mW at 9.47 mW, 2 G_{pp}.

3.3 Results

Mutations of heme ligands result in fully assembled heme-free SQR – The x-ray structure (*2*) of the *E. coli* SQR reveals that the heme *b*, as in the mammalian enzyme, is coordinated by two conserved His residues, one from each of the two membrane-bound subunits (**Figure 3.1**). A previous mutation of one of the heme ligands, SdhC[H84L], does not result in a loss of the heme possibly because of the close proximity of SdhC[H30], which is able to function as a surrogate ligand (*7*). Also, the SdhD[H71Q] mutation results in the conversion of the low-spin hexacoordinated heme into a high-spin pentacoordinated heme, as observed by EPR (*7*). We generated SdhD[H71Y] and SdhC[H84Y] mutants, each of which we hypothesized would eliminate the heme and introduce a hydrogen bond bridging the Tyr side chain and the imidazole of the corresponding histidine on the opposite subunit.

E. coli cells containing overexpressed SdhD[H71Y] or SdhC[H84Y] SQR were dark brown in color, whereas cells containing overexpressed wild-type SQR are brown with a slightly red hue. SDS-PAGE indicates that subunit assembly is unaffected by our mutations to the heme ligands (**Figure 3.2**). After cell lysis, all four subunits of the SdhD[H71Y] and SdhC[H84Y] mutants were clearly visible on SDS-PAGE. The concentration of SQR in membrane samples can be assayed by estimating the amount of covalent-linked flavin (*18*). Membranes containing overexpressed wild-type, SdhD[H71Y], and SdhC[H84Y] SQR contain 3.1, 1.0, and 2.4 nmol of SQR per mg of membrane protein, respectively. Based on the amounts of SQR assembled into the cytoplasmic membrane and our SDS-PAGE analyses (**Figure 3.2**), it is clear that these mutations do not significantly alter the structural characteristics of the SdhCD

membrane domain, although mutating the SdhD^{H71} ligand has a more pronounced effect on the stability of the enzyme. Although the loss of the heme cofactor leads to increased instability of the enzyme, both mutant membrane subunits are still capable of properly anchoring the soluble SdhAB dimer to the membrane.

UV-VIS and EPR spectroscopies confirm the loss of the heme cofactor – Dithionite-reduced minus "as is" air-oxidized absorbance spectra of membranes enriched in mutant SQR indicate a substantial lack of heme absorbance (**Figure 3.3A**). Spectra of membranes enriched in wild-type SQR exhibit a strong Soret absorbance at 427 nm, a broad β-absorbance with maximum at 530 nm, and considerable α-absorbance at 559 nm. In the DW35 host membranes, the observed absorbances arise from the hemes of the *bo$_3$*- and *bd*-oxidases (*19*), and there is a noticeable shift in the absorbance maxima in these membranes. The heme absorption spectra of both the SdhD^{H71Y} and SdhC^{H84Y} mutants are greatly diminished in the amplitude of the Soret absorbance as well as α-absorbance, compared with the wild-type SQR. In fact, the amplitudes of these absorbances are lower than those found in spectra of the DW35 host strain. The likely explanation for this finding is that the contribution from the spectrum of the heme from the oxidase is diluted out of the membranes by the overexpression of the heme-free SQR. Further confirmation of the loss of the *b* heme through measurement of the protoheme IX content was determined by the pyridine hemochromogen difference spectra (**Table 3.1**). Both SQR Tyr mutants contained only background amounts of *b* heme produced by the *bo$_3$*- and *bd*-oxidases present in the host strain DW35.

EPR spectroscopy was used to verify the cofactor composition in the mutant enzymes (**Figure 3.3**). For the EPR experiments, membranes enriched in SQR were fully oxidized with 0.8 mM 2,6-dichlorophenolindophenol (DCPIP) to conditions where only the [3Fe-4S] cluster and heme are EPR-visible. The signal arising from the [3Fe-4S] cluster in the SdhB subunit appears as a peak at g = 2.02 (**Figure 3.3B**), with a broad trough immediately upfield. This signal is easily detected in membranes enriched in wild-type SQR, but is lacking in the DW35 host membranes. EPR spectra of membranes containing SdhD[H71Y] or SdhC[H84Y] SQR exhibited a [3Fe-4S] cluster spectrum identical to that of wild-type membranes. The amount of enzyme assembled in the mutants' membranes reflected by the [3Fe-4S] cluster and FAD levels was, however, reduced by approximately one third, compared with wild-type enzyme. These results affirm the conclusion that enzyme assembly has been largely unaffected by the mutation.

The heme in *E. coli* SQR is EPR-detectable and has a characteristically high anisotropic low-spin spectrum with a g_z of 3.66 (**Figure 3.3C**) (*20*). This signal is obviously absent in membranes enriched in the mutant SQR, as well as in membranes of the DW35 host strain. The signal at g = 3.36 is found in all of the membrane preparations and can be assigned to the heme b_{558} of cytochrome *bd* (*21*).

Another EPR signal detectable in DW35 membranes is contributed by the pentacoordinated high-spin hemes of *bo$_3$*- (*22*) and *bd*-oxidase (*21*). Previous studies of an SdhD[H71Q] mutant indicated that a high-spin pentacoordinate heme can be incorporated into SQR (*7*), and it was necessary to eliminate this possibility for

our SdhC^{H84Y} and SdhD^{H71Y} mutants. A sharp peak is observed at g = 6.01 in DW35 membranes, corresponding to the presence of high-spin hemes (**Figure 3.3D**). In wild-type SQR-enriched membranes, this signal is diminished because the cytochrome oxidase concentration is diluted by SQR overexpression. A similar pattern was recorded in both of the mutants. Any conversion from low- to high-spin heme is easily detected by EPR (*7*), but here such a conversion is clearly absent. Taken together the optical and EPR data unambiguously indicate that both of our mutations have eliminated the heme from its regular position within the membrane domain.

Evidence of a competent Q-site is provided by the presence of a ubisemiquinone (USQ) radical observed by EPR. Wild-type SQR cycles through a semiquinone intermediate ($E_{m,7}$ = +100 mV) at the Q-site, which is detectable by potentiometric titration of the g= 2.005 signal in SQR-containing membranes (*1*). As the redox titration of SdhD^{H71Y} membranes indicates (**Figure 3.4**), both the flavosemiquinone (FSQ) and USQ radicals, which are found in the wild-type SQR, are preserved in the mutant SQR at the appropriate midpoint potentials. Titrations of SdhC^{H84Y}-enriched membranes are similar (data not shown). The K_{STAB} of the USQ radical in wild-type SQR has a value of ≈1 (*1*), and this value is unperturbed in either of the mutants.

Heme-free SQR variants retain physiological activity – The physiological activities of the mutant SQR were characterized by a spectrophotometric assay (**Table 3.1**). When using Q$_0$ as a substrate, the turnover rates for the heme-free SQR decreased to

$\approx$50–60% of that of the wild type, but the K_m for Q_0 in the mutants was within the range of that found with wild-type SQR. By using Q_1 as a substrate, the mutant enzymes show an even better retention of activity compared with wild type (**Table 3.1**). The succinate:Q_1-reductase activity, when described as a ratio to the nonphysiological succinate:phenazine ethosulfate (PES) activity, is unity in the wild-type enzyme, whereas there is only a 6% and 30% loss in activity in the SdhD^{H71Y} and SdhC^{H84Y} samples, respectively. The K_m values for Q_1 were only slightly elevated. During catalysis of the reverse reaction by using reduced plumbagin as a menaquinol analog, the heme-free mutants lost $\approx$50% of wild-type turnover, similar to the effect observed on succinate:Q_0 reductase activity, which suggests that the absence of heme affects both processes similarly. The similarities in K_m for both ubiquinone and menaquinol in the wild-type and mutant enzymes suggest that the loss of the heme does not result in major changes in the structural components of the Q-site.

The *in vivo* functionality of the enzyme was determined by monitoring aerobic growth of *E. coli* DW35 harboring plasmids expressing SQR in succinate-supplemented minimal medium. Either the SdhC^{H84Y} or SdhD^{H71Y} mutant was competent in sustaining growth under these conditions because it had a similar doubling time ($\approx$2 h) as the wild-type SQR-expressing cells (data not shown).

Heme-free SQR enzymes are highly sensitive to detergent – Although the lack of heme cofactor does not appear to have serious effects on catalytic activity in the native membrane, the same cannot be said for the enzyme in the presence of detergent.

Normally, wild-type SQR can tolerate detergent extraction and ion exchange chromatography while remaining highly active (*2*). However, in the case of the SdhC^{H84Y}DAB or SdhCD^{H71Y}AB mutant, incubation of these SQR-enriched membranes with low Thesit (C$_{12}$E$_9$) concentrations, below the critical micellar concentration of 0.1 mM, results in a dramatic loss of succinate:Q$_1$-reductase activity (IC$_{50}$ of 0.0005% or ≈20 μM) (**Figure 3.5**). Moreover, after the addition of other detergents commonly used for extraction (Triton X-100 or dodecylmaltoside) at concentrations of 0.01%, the wild-type SQR is unaffected, whereas both heme-free SQR lose nearly all physiological activity (data not shown). The sensitivity of the mutant enzymes to low levels of detergent (**Figure 3.5**) is consistent with some disruption of the structural integrity of the enzyme because there also is a time-dependent loss of succinate oxidase activity in the PES reaction as well as the Q$_1$-reductase activity (data not shown). This finding is consistent with the known sensitivity of the SdhAB enzyme to air or temperature when removed from the SdhCD subunits (*7*). Standard purification of detergent-solubilized mutant SQR (*17*) was attempted by anion exchange chromatography, but was unsuccessful. In contrast to wild type, the mutant SQR eluted with a significant depletion of SdhCD (data not shown), indicative of dissociation of SdhAB from the membrane anchor. Unfortunately, the detergent sensitivity of the mutant SQR precludes any isolation of the intact complex. Indeed, the effect of detergent confirms the role of the heme in providing structural stability for the enzyme.

Loss of the heme does not affect reactive oxygen species (ROS) production – It has been proposed that the heme acts as an electron sink during enzyme turnover to prevent prolonged exposure of the USQ or FSQ radicals to oxidants in the cellular environment (*2*). In support of this hypothesis, the *E. coli* paralog, QFR, which lacks heme, generates 20-fold more ROS than SQR during aerobic succinate oxidation (*15*). Therefore, we assayed the production of superoxide radicals by our heme-free SQR mutants during catalytic turnover (**Figure 3.6**). The rate of ROS production by both the SdhC^{H84Y} and SdhD^{H71Y} mutants were reduced by 60%, compared with the wild-type enzyme. This finding correlates well with the physiological rate of succinate/Q$_0$ turnover, which also was halved in the mutants. As such, it does not appear that the heme is acting to suppress ROS production in the wild-type SQR.

Expression of the heme-free mutants in a heme-deficient E. coli strain – It may be possible that a minute amount of heme, below our detection limits, may have been inserted into some of the heme-free mutant SQR, and this small subset of heme-containing enzyme was responsible for some of the wild-type characteristics observed herein. To ensure that this notion was not the case, the SdhD^{H71Y} mutant was expressed in the *E. coli* strain, SASX41B, which is incapable of heme biosynthesis in the absence of the heme precursor, 5-aminolevulinic acid. Wild-type or heme-containing mutants of SQR do not assemble in this strain (*7*). Conversely, expression of the SdhD^{H71Y} mutant was capable in the SASX41B strain (**Figure 3.2**), and enzyme assembly did not appear to be affected. However, when expressed in the SASX41B strain, the SdhD^{H71Y} enzyme appeared to have a non-stoichiometric

ratio of the SdhA and SdhB subunits, which was not observed in the DW35 strain. Nevertheless, the SdhD[H71Y] from both *E. coli* strains had similar kinetic properties with respect to the ubiquinone activity (**Table 3.1**).

3.4 Discussion

Oyedotun *et al.* (*23*) reported that mutation of the axial ligands of the heme in *Saccharomyces cerevisiae* complex II had minimal consequences on enzyme activity and quinone function. The results of these studies, however, showed that some fumarate-oxidizable heme was still retained in all of their mutants. In contrast, the two mutant SQR we have presented here unmistakably lack the heme as verified by convincing spectroscopic and EPR techniques. Considering that a large cofactor was removed from the interior of the protein, the removal of the heme from the *E. coli* SQR did not have a substantial effect on the enzyme's function. In addition to the heme ligands, the heme in the native enzyme must undoubtedly contact the protein component of the enzyme at multiple points within the membrane core. It will be interesting to see whether the loss of the heme has left a void in the intersubunit space or the membrane domain has shifted to compensate. The presence of a functional Q-site and the stability of the USQ would suggest that the protein backbone has not been greatly impacted. Because the heme propionates are positioned ≈7 Å from the Q-site, changes in the protein structure around the heme should manifest as disruptions in Q-binding, and this effect is not observed in the membrane-bound enzyme.

The instability of the heme-free SQR in the presence of detergents emphasizes a structural role of the heme in the enzyme. Also, the disparity in the stoichiometry of SdhA and SdhB in the SdhD^{H71Y} mutant when expressed in the heme-deficient *E. coli* strain SASX41B suggests that the enzyme may be more susceptible to proteolysis when the enzyme assembles in an environment completely devoid of heme. In DW35 cells, the heme may transiently associate with the hydrophobic SdhCD dimer in the mutant SQR during the initial stages of assembly and membrane integration before it is eventually lost, thereby stabilizing the membrane-intrinsic components before assembly of the final complex. In the absence of heme in the SASX41B cells, abnormal assembly or a loose association between subunits may increase the sensitivity of SdhA to proteolytic cleavage, and thus we may be observing some partially assembled enzyme within the membrane. This finding indicates a structural role for the heme not only in the holoenzyme, but also during the early phases of assembly, consistent with previous notions (*6*). The presence of a significant quantity of intact, fully functional SdhD^{H71Y} enzyme, even in the SASX41B cells, suggests that insertion of the heme into the membrane domain of the wild-type protein may not necessarily precede formation of the fully folded apoenzyme, but the presence of heme may enhance the efficacy of folding.

We have shown that the heme is not an essential component of the catalytic mechanism, which is extraordinary given that the heme cofactor is conserved from prokaryotes to eukaryotes. However, *E. coli* QFR can carry out the same reaction in the absence of the heme. In addition, the heme *b* in mitochondrial complex II has been shown to be resistant to reduction by succinate (*24*), which is likely a

consequence of its low midpoint potential ($E_{m,7}$ = −185 mV in the mammalian, compared with $E_{m,7}$ = +35 mV in the bacterial enzyme). In light of our results, it is entirely plausible that mammalian complex II may not rely on electron transfer through the heme at all.

Despite our observation that heme-free SQR is catalytically functional both *in vitro* and *in vivo*, the heme is clearly redox-active in the wild-type enzyme (*1*). The heme does not seem to have a role in reducing ROS production either. The lack of heme cofactor does not have an impact on the midpoint potential of nearby redox centers ([3Fe-4S] or quinone) (data not shown), and this notion can be rejected as the cause for the modest drop in activity observed here. It has been previously determined that the rate of electron transfer between the Q-site and the heme can be considered very fast (*25*). In a model where the electrons from the [3Fe-4S] cluster reduce the bound ubiquinone directly, the heme may act to lower the thermodynamic barrier of electron transfer from the [3Fe-4S] by delocalizing the negative charge on the USQ, thus increasing the transfer rate of the second electron, which is likely coupled to the protonation of the quinone. It is difficult to surmise whether such a rate increase could result in the magnitude of changes observed herein because the kinetics of quinone reduction occur on a millisecond timescale, whereas electron transfer rates through the enzyme occur on a microsecond timescale (*26*). However, when electron transfer rates are lowered by modulating the midpoint potential of the [Fe-S] clusters, a significant effect is seen on the quinone-reduction kinetics (*27*).

In summary, the results reported here propose a function for the heme in *E. coli* SQR in maintaining a high rate of catalysis, in addition to its structural purpose, while excluding its absolute requirement in the catalytic mechanism, as well as its role in ROS suppression.

3.5 Tables and Figures

Host/Enzyme	Succinate/ Q_0 turnover, s^{-1}	K_m Q_0, mM	Q_1/PES	K_m Q_1, uM	Plumbagin/ fumarate turnover, s^{-1}	K_m Plumbagin, mM	heme b protein, nmol mg^{-1}
DW35/SdhCDAB	37	0.20	1.01	2.5	30	0.13	4.1
DW35/SdhC^{H84Y}DAB	22	0.71	0.7	8	16	0.10	0.5
DW35/SdhCD^{H71Y}AB	18	0.31	0.94	10	16	0.11	0.6
SASX41B/SdhCD^{H71Y}AB	18	0.27	n.d.	n.d.	n.d.	n.d.	n.d.
DW35/pBR322*	n.d.	n.d.	n.d.	n.d.	n.d.	n.d.	0.6

Table 3.1: Physiological activity and K_m determinations of ubiquinol reduction and menaquinol oxidation in membranes enriched in SQR.

*DW35/pBR322 is the host strain, which does not contain either SdhCDAB or FrdABCD so that it shows no activity for either succinate–ubiquinone reductase activity or menaquinol–fumarate oxidase activity. It has normal levels for *bo*- and *bd*-oxidases.

n.d., not determined.
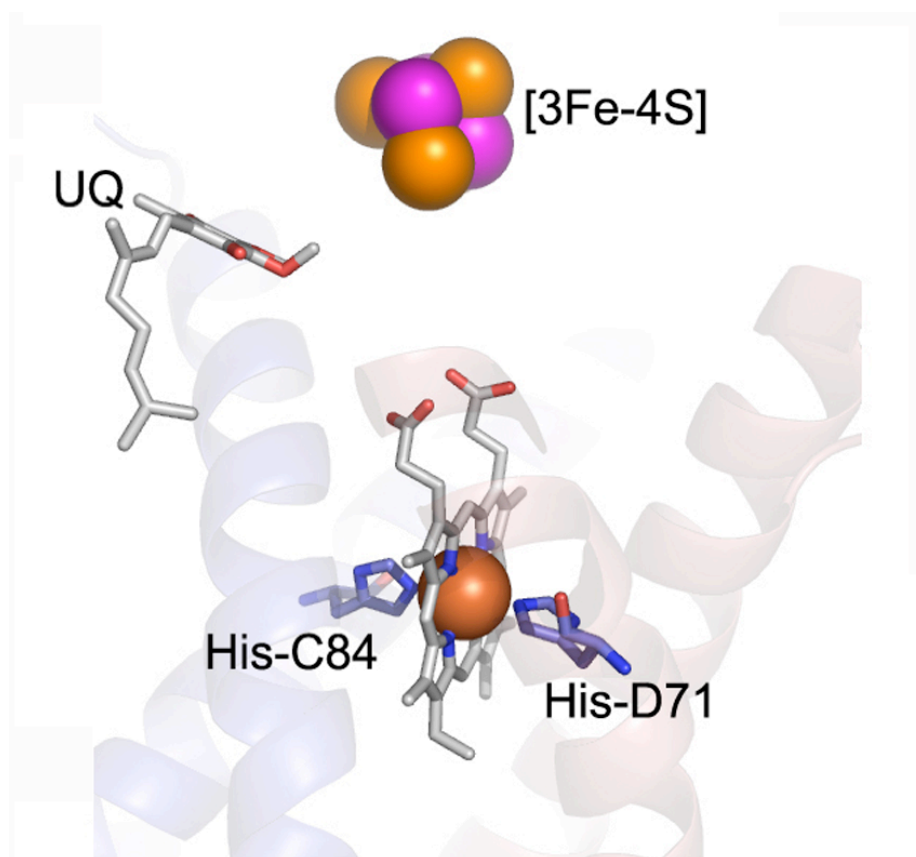
Figure 3.1: Close-up view of the membrane domain of SdhCDAB. The two His axial heme ligands are indicated (PDB: 1NEK *(2)*).
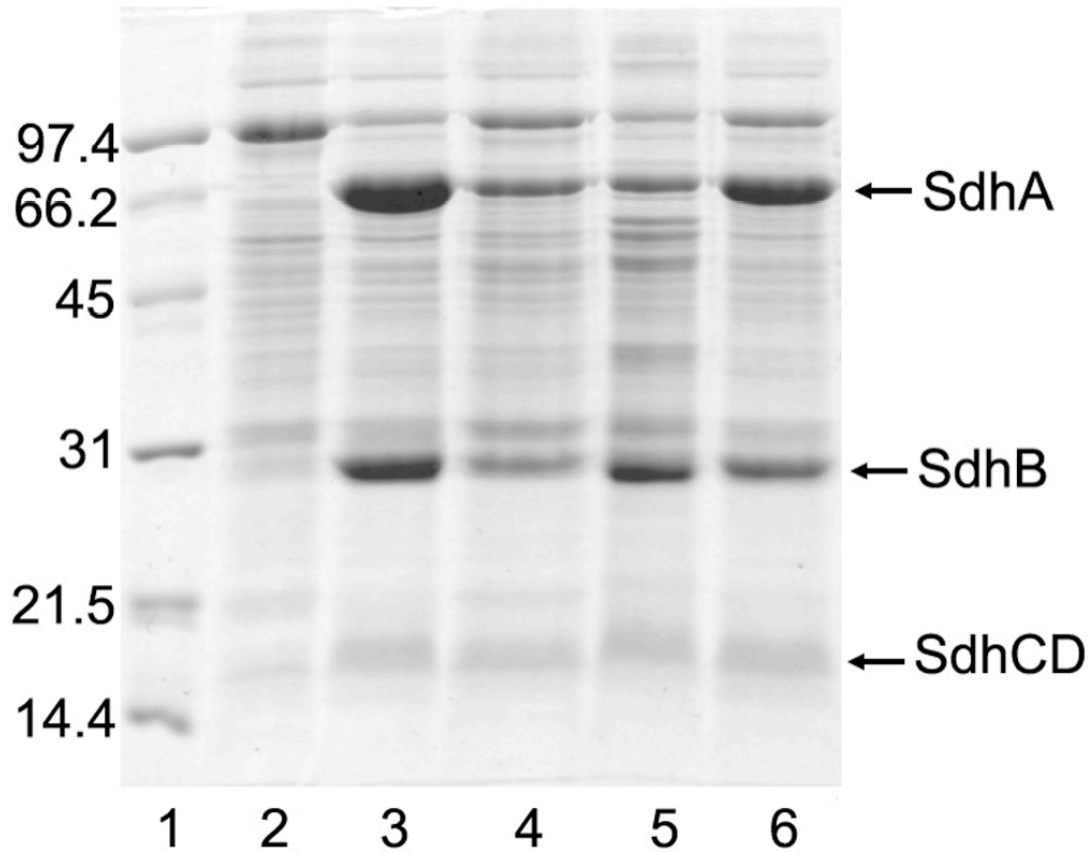
Figure 3.2: Expression of wild-type and *E. coli* SQR mutants. SDS-PAGE analysis of SQR-enriched membranes. Lane 1, low-molecular-mass markers (Bio-Rad); lane 2, DW35 membranes; lane 3, DW35/SdhCDAB membranes; lane 4, DW35/SdhD^{H71Y} membranes; lane 5, SASX41B/SdhD^{H71Y} membranes; lane 6, DW35/SdhC^{H84Y} membranes. Finally, 45 μg of protein were loaded in each lane.
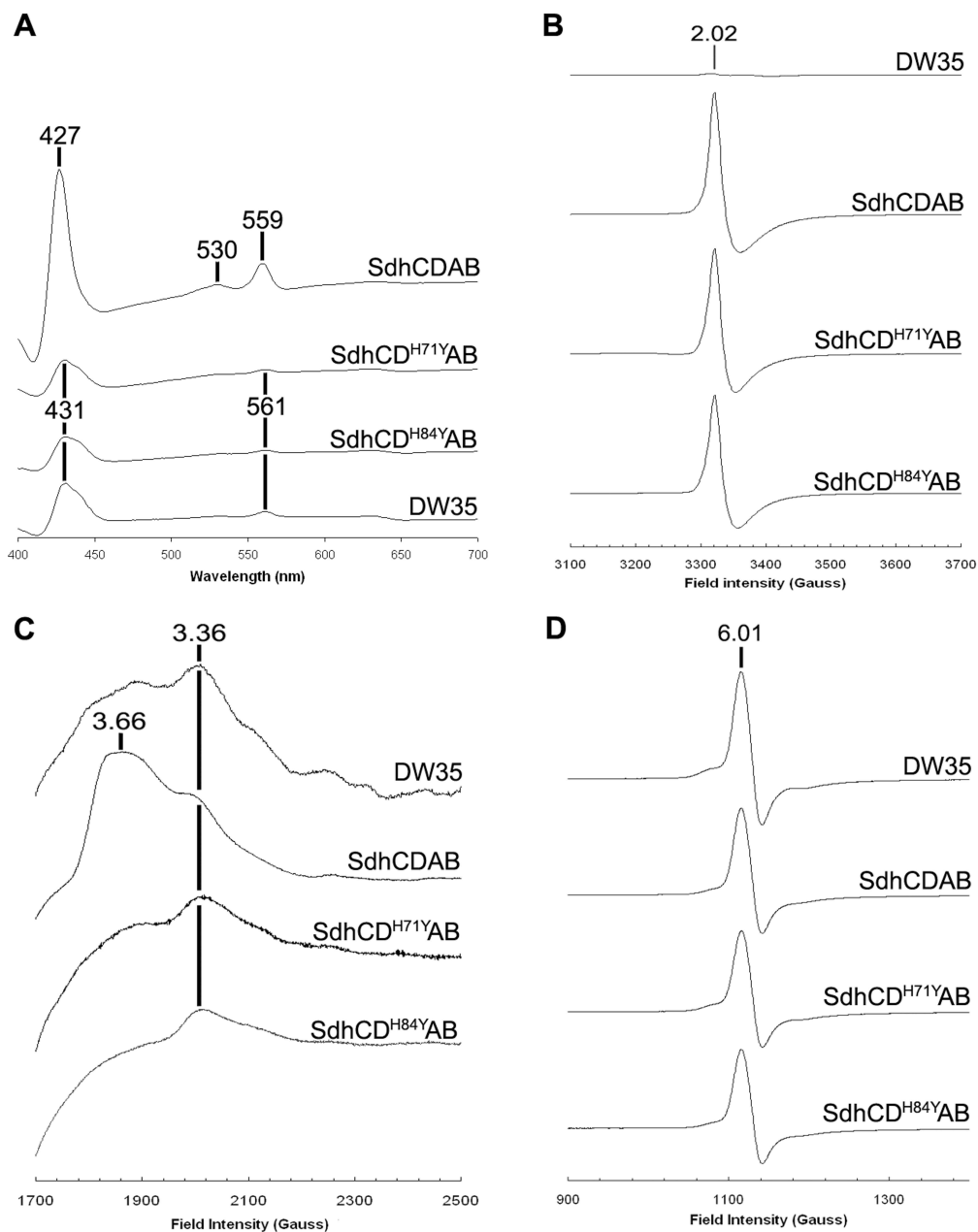
Figure 3.3: Biophysical analysis of SQR-enriched DW35 membranes. (*A*) Dithionite reduced minus air-oxidized absorbance spectra. (*B*) [Fe-S] cluster EPR spectra. (*C*) Low-spin heme EPR spectra. (*D*) High-spin heme EPR spectra. Spectra in *B* are normalized for FAD content, and spectra in *C* and *D* are normalized to a protein concentration of 30 mg ml^{-1}.
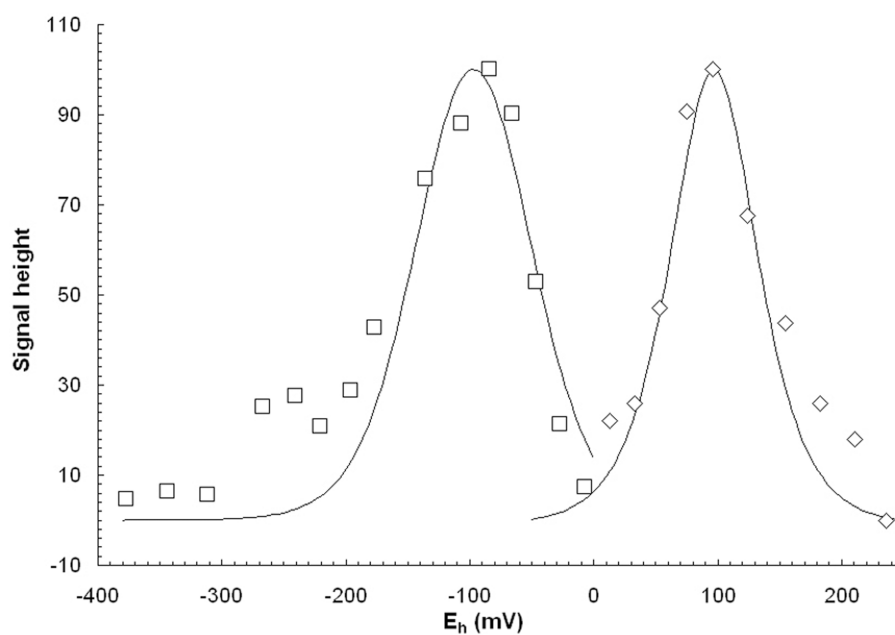
Figure 3.4: Potentiometric titration of the g = **2.005 EPR signal in SdhD[H71Y]-enriched DW35 membranes.** Peak troughs are plotted against E_h and were normalized to 100% signal intensity. Both the flavosemiquinone (open squares) and ubisemiquinone (open diamonds) are visible.
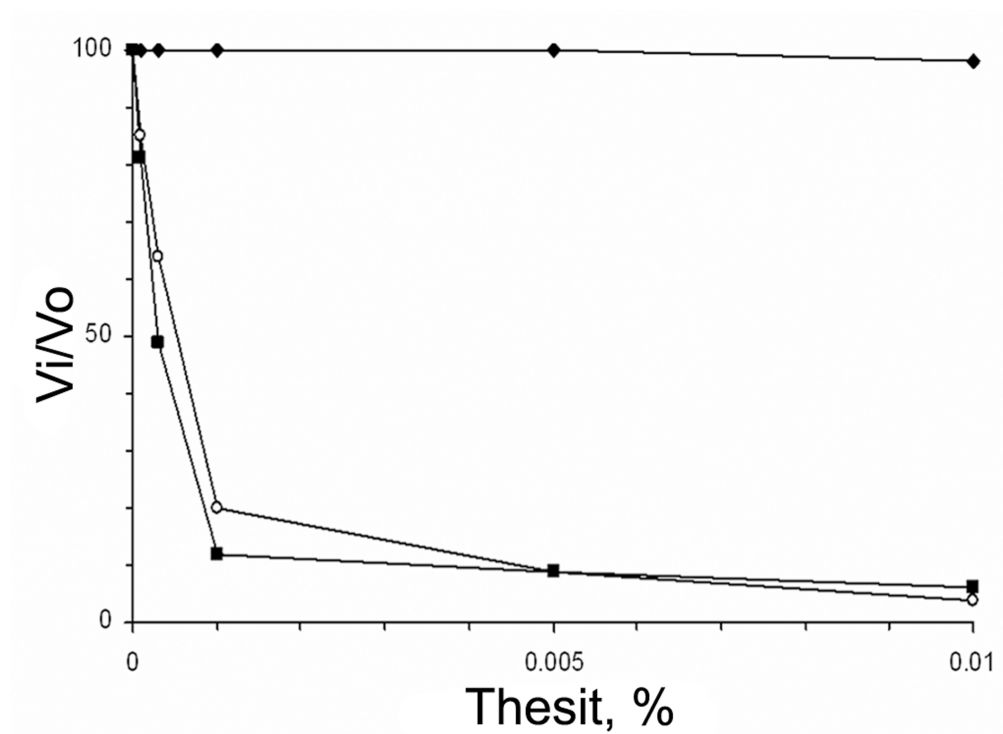
Figure 3.5: Effect of thesit on succinate:Q_1-reductase activity. Membranes were incubated for 5 min at 30 °C in the reaction medium with indicated thesit concentrations before initiation of the reaction. Filled diamonds, SdhCDAB; filled squares, SdhD[H71Y]; open circles, SdhC[H84Y].
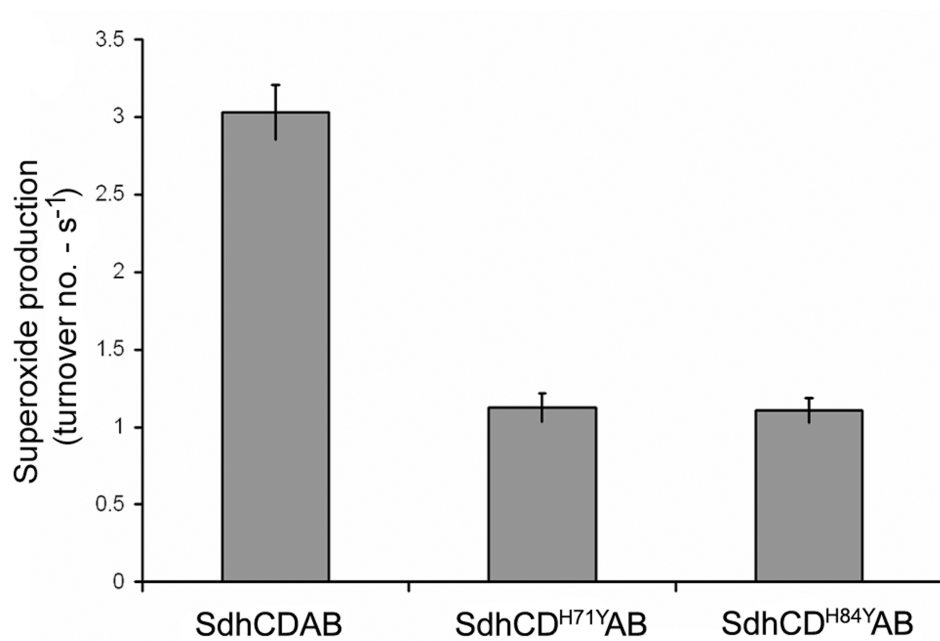
Figure 3.6: Analysis of superoxide radical production rates in DW35 membranes enriched in wild-type or mutant SQR.

3.6 References

1. Tran, Q. M., Rothery, R. A., Maklashina, E., Cecchini, G., and Weiner, J. H. (2006) The quinone binding site in *Escherichia coli* succinate dehydrogenase is required for electron transfer to the heme *b*, *J Biol Chem 281*, 32310-32317.

2. Yankovskaya, V., Horsefield, R., Tornroth, S., Luna-Chavez, C., Miyoshi, H., Leger, C., Byrne, B., Cecchini, G., and Iwata, S. (2003) Architecture of succinate dehydrogenase and reactive oxygen species generation, *Science 299*, 700-704.

3. Iverson, T. M., Luna-Chavez, C., Cecchini, G., and Rees, D. C. (1999) Structure of the *Escherichia coli* fumarate reductase respiratory complex, *Science 284*, 1961-1966.

4. Iverson, T. M., Luna-Chavez, C., Croal, L. R., Cecchini, G., and Rees, D. C. (2002) Crystallographic studies of the *Escherichia coli* quinol-fumarate reductase with inhibitors bound to the quinol-binding site, *J Biol Chem 277*, 16124-16130.

5. Maklashina, E., and Cecchini, G. (1999) Comparison of catalytic activity and inhibitors of quinone reactions of succinate dehydrogenase (Succinate-ubiquinone oxidoreductase) and fumarate reductase (Menaquinol-fumarate oxidoreductase) from *Escherichia coli*, *Arch Biochem Biophys 369*, 223-232.

6. Nihei, C., Nakayashiki, T., Nakamura, K., Inokuchi, H., Gennis, R. B., Kojima, S., and Kita, K. (2001) Abortive assembly of succinate-ubiquinone reductase (complex II) in a ferrochelatase-deficient mutant of *Escherichia coli*, *Mol Genet Genomics 265*, 394-404.

7. Maklashina, E., Rothery, R. A., Weiner, J. H., and Cecchini, G. (2001) Retention of heme in axial ligand mutants of succinate-ubiquinone xxidoreductase (complex II) from *Escherichia coli*, *J Biol Chem 276*, 18968-18976.

8. Vibat, C. R., Cecchini, G., Nakamura, K., Kita, K., and Gennis, R. B. (1998) Localization of histidine residues responsible for heme axial ligation in cytochrome b_{556} of complex II (succinate:ubiquinone oxidoreductase) in *Escherichia coli*, *Biochemistry 37*, 4148-4159.

9. Westenberg, D. J., Gunsalus, R. P., Ackrell, B. A., Sices, H., and Cecchini, G. (1993) *Escherichia coli* fumarate reductase frdC and frdD mutants. Identification of

amino acid residues involved in catalytic activity with quinones, *J Biol Chem 268*, 815-822.

10. Sasarman, A., Surdeanu, M., Szegli, G., Horodniceanu, T., Greceanu, V., and Dumitrescu, A. (1968) Hemin-deficient mutants of *Escherichia coli* K-12, *J Bacteriol 96*, 570-572.

11. Maklashina, E., Berthold, D. A., and Cecchini, G. (1998) Anaerobic expression of *Escherichia coli* succinate dehydrogenase: functional replacement of fumarate reductase in the respiratory chain during anaerobic growth, *J Bacteriol 180*, 5989-5996.

12. Condon, C., and Weiner, J. H. (1988) Fumarate reductase of *Escherichia coli:* an investigation of function and assembly using *in vivo* complementation, *Mol Microbiol 2*, 43-52.

13. Sasarman, A., Surdeanu, M., and Horodniceanu, T. (1968) Locus determining the synthesis of delta-aminolevulinic acid in *Escherichia coli* K-12, *J Bacteriol 96*, 1882-1884.

14. Markwell, M. A., Haas, S. M., Bieber, L. L., and Tolbert, N. E. (1978) A modification of the Lowry procedure to simplify protein determination in membrane and lipoprotein samples, *Anal Biochem 87*, 206-210.

15. Messner, K. R., and Imlay, J. A. (2002) Mechanism of superoxide and hydrogen peroxide formation by fumarate reductase, succinate dehydrogenase, and aspartate oxidase, *J Biol Chem 277*, 42563-42571.

16. Berry, E. A., and Trumpower, B. L. (1987) Simultaneous determination of hemes *a, b*, and *c* from pyridine hemochrome spectra, *Anal Biochem 161*, 1-15.

17. Singer, T. P., Salach, J., Hemmerich, P., and Ehrenberg, A. (1971) Flavin peptides, *Methods Enzymol 18*, 416-427.

18. Horsefield, R., Yankovskaya, V., Tornroth, S., Luna-Chavez, C., Stambouli, E., Barber, J., Byrne, B., Cecchini, G., and Iwata, S. (2003) Using rational screening and electron microscopy to optimize the crystallization of succinate:ubiquinone oxidoreductase from *Escherichia coli*, *Acta Crystallogr D Biol Crystallogr 59*, 600-602.

19. Salerno, J. C., Bolgiano, B., Poole, R. K., Gennis, R. B., and Ingledew, W. J. (1990) Heme-copper and heme-heme interactions in the cytochrome *bo*-containing quinol oxidase of *Escherichia coli*, *J Biol Chem 265*, 4364-4368.

20. Yang, X., Yu, L., and Yu, C. A. (1997) Resolution and reconstitution of succinate-ubiquinone reductase from *Escherichia coli*, *J Biol Chem 272*, 9683-9689.

21. Rothery, R. A., and Ingledew, W. J. (1989) The cytochromes of anaerobically grown *Escherichia coli*. An electron-paramagnetic-resonance study of the cytochrome *bd* complex *in situ*, *Biochem J 261*, 437-443.

22. Cotter, P. A., Chepuri, V., Gennis, R. B., and Gunsalus, R. P. (1990) Cytochrome *o* (*cyoABCDE*) and *d* (*cydAB*) oxidase gene expression in *Escherichia coli* is regulated by oxygen, pH, and the *fnr* gene product, *J Bacteriol 172*, 6333-6338.

23. Oyedotun, K. S., Yau, P. F., and Lemire, B. D. (2004) Identification of the heme axial ligands in the cytochrome b_{562} of the *Saccharomyces cerevisiae* succinate dehydrogenase, *J Biol Chem 279*, 9432-9439.

24. Yu, L., Xu, J. X., Haley, P. E., and Yu, C. A. (1987) Properties of bovine heart mitochondrial cytochrome b_{560}, *J Biol Chem 262*, 1137-1143.

25. Anderson, R. F., Hille, R., Shinde, S. S., and Cecchini, G. (2005) Electron transfer within complex II. Succinate:ubiquinone oxidoreductase of *Escherichia coli*, *J Biol Chem 280*, 33331-33337.

26. Moser, C. C., Farid, T. A., Chobot, S. E., and Dutton, P. L. (2006) Electron tunneling chains of mitochondria, *Biochim Biophys Acta 1757*, 1096-1109.

27. Cheng, V. W., Ma, E., Zhao, Z., Rothery, R. A., and Weiner, J. H. (2006) The iron-sulfur clusters in *Escherichia coli* succinate dehydrogenase direct electron flow, *J Biol Chem 281*, 27662-27668.

Chapter 4: The Heme Binding Pocket of *Escherichia coli* Succinate Dehydrogenase Enables Out of Plane Distortions of the Heme b^*

4.1 Introduction

During aerobic metabolism, *Escherichia coli* SQR catalyzes the oxidation of succinate to fumarate and ultimately transfers the chemical energy to the ubiquinone pool to be used in the terminal reduction of oxygen by cytochrome oxidase. Located within the membrane, sandwiched between the SdhC and SdhD subunits is a bis-histidine-coordinated *b*-type heme. The heme is evolutionarily conserved in all eukaryotic Complex II enzymes but it does not lie in the direct pathway of the electron transfer relay between the FAD and Q-site.

While the heme undergoes redox cycling in the presence of succinate and quinones, this redox activity does not appear to be essential for enzyme function as in the last chapter, a heme-free mutant retains a significant amount of catalytic activity and is capable of supporting the growth of *E. coli* on succinate (*1*). Although it is clear that the heme is necessary to stabilize the structure of the isolated SQR enzyme (*1, 2*) the exact function of this heme cofactor in electron transfer remains to be determined.

The mitochondrial respiratory chain is a significant source of free radicals but the contribution of Complex II to the overall generation of reactive oxygen species (ROS) is relatively minor. Through an auto-oxidative process, *E. coli* SQR normally produces low quantities of ROS in the form of superoxide (*3*), however, mutations around the Q-site in *E. coli* SQR (and also *Saccharomyces cerevisiae* complex II) can lead to an increased rate of superoxide production (*4, 5*). It has been suggested that the heme is

behaving as an electron buffer to prevent the production of ROS from a Q-site-stabilized ubisemiquinone (*6*) but experimental evidence for this is lacking.

The redox potential ($E_{m,7}$) of the heme in *E. coli* SQR is +20 mV. This is in stark contrast to published values for the heme in bovine Complex II, which has an $E_{m,7}$ of -185 mV (*7*). It is for this reason that the heme in mammalian Complex II cannot be reduced in the presence of succinate (*7*) but the heme of *E. coli* SQR can be reduced by succinate and oxidized by ubiquinone (*8, 9*).

Given the apparent non-essential role of the heme on the succinate:ubiquinone oxidoreductase activity of *E. coli* SQR, coupled with its absolute conservation in all related succinate dehydrogenases, we have tested the hypothesis that the heme redox state may regulate enzyme activity. In order to examine possible effects of a changing redox state of the heme, we used a directed mutagenesis approach to modulate heme midpoint potential and evaluated the consequences on enzyme function.

4.2 Materials and methods

Site-directed mutagenesis – The EcoRI/BamHI fragment of the pFAS plasmid (*9*) containing the *sdhCDAB* operon was subcloned into the cloning vector pTZ18R ((Amp^R, *lacZ'*), GE Healthcare). This plasmid was used as a template for site-directed mutagenesis to introduce the required single mutations according to the QuikChange procedure (Stratagene). The mutagenic

oligonucleotides (Integrated DNA Technologies) used in the PCR reactions are listed in Appendix B (**Table B.1**). All mutations were confirmed by DNA sequencing (DNA Core Facility, Department of Biochemistry, University of Alberta). In order to create the double mutants, the KpnI-BamHI fragment of the plasmid bearing the SdhC^{V87D} mutation was cut out and reinserted into the plasmid containing the appropriate second mutation. Once all mutagenesis was complete, the EcoRI-SphI fragment was then subcloned back into pFAS and transformed into *E. coli* strain DW35 (Δ*frdABCD, sdhC*::*kan*), a strain that does not synthesize any wild type SQR or QFR (*10*). All genetic manipulations were done in the *E. coli* strain TG1 ((*hsd*Δ5 *thi* Δ(*lac-proAB*) *F'*[*traD*36 *proAB+lacI*q *lacZ*ΔM15]), Amersham Biosciences)).

Isolation of crude membranes – E. coli DW35 expressing SQR mutant proteins was grown in terrific broth media overnight for 16-18 hours using a 1:100 starter inoculum as reported previously (*8*). After harvesting, cells were lysed by multiple passes through an Avestin Emulsiflex in the presence of 20 μM PMSF. The bacterial inner membrane fraction was isolated using differential centrifugation as previously described (*8*). During the procedure, membranes were incubated at 30 ºC for 15 minutes with 1 mM malonate to remove oxaloacetate bound at the FAD site of SQR. All cells and membrane isolations were maintained in 100 mM MOPS/5 mM EDTA buffers.

Protein quantitation – To assess the overall expression and assembly of SdhCDAB, all membrane samples were examined after electrophoresis on a 12.5% SDS-PAGE gel (*1*). 45 µg of membranes were loaded alongside a low molecular weight ladder (Bio-Rad) and stained with Coomassie blue. Protein was quantitated using the Lowry assay (*11*) and SQR levels quantitated by measuring covalent-flavin (*12*).

Enzyme activity assays – The succinate/Q_0 and plumbagin/fumarate assays were performed as described previously (*8*). In order to calculate k_{cat} and K_m values, the Q_0 or plumbagin concentration was varied from 0.07 mM to 0.3 mM and data was plotted to an Eadie-Hofstee graph. The succinate PMS-MTT assay was performed as before (*13*).

UV-VIS and electron paramagnetic resonance (EPR) spectroscopy – Reduced *minus* oxidized absorbance spectra were recorded on a Hewlett Packard 8453 UV-VIS diode array spectrophotometer. Membranes were diluted to a protein concentration of 0.5 mg mL^{-1} in degassed 100 mM MOPS/5 mM EDTA buffer (pH 7.0). Samples were reduced with either excess sodium dithionite, or 9 mM sodium succinate.

Potentiometric titrations were performed as previously described (*8*). Protein concentrations within the EPR samples varied from 20-30 mg mL^{-1}. Oxidized membrane samples were made by adding DCPIP to a final concentration of 0.8 mM (*1*). All samples were made using standard 3 mm

diameter quartz EPR tubes and stored in liquid nitrogen until analyzed. EPR spectroscopy was performed on either a Bruker Elexsys E500 or Bruker ESP300E EPR Spectrophotometer, each equipped with an Oxford Instruments ESR900 flowing helium cryostat. Both [3Fe-4S] and heme b EPR spectra were recorded at 12 K, 20 mW at 9.47 GHz, 10 G_{pp}.

Measurement of reactive oxygen species – A cytochrome c reduction assay was used to quantitate the production of superoxide during enzyme turnover (*3*). A disc assay was used to measure the susceptibility of *E. coli* to oxidative stress. Agar overlays of the appropriate *E. coli* culture were made. 0.7 cm-wide discs of Whatman no.1 filter paper were placed atop the overlays and 3 μl of a 0.5 mM or 0.25 mM solution of methyl viologen were added to the center of each disc. The plates were incubated overnight at 37°C and the diameter of the resulting zone of inhibition was measured along two orthogonal axes.

4.3 Results and Discussion

Selection of residues to mutate – Using site-directed mutagenesis, we attempted to modulate the redox potential of the heme by changing residues within its second coordination sphere. We selected residues in the immediate vicinity of the heme (within 5 Å of the heme edge) using the x-ray structure (PDB code: 1NEK) (*6*) as a guide, and focused mainly on residues with sidechains pointed directly at the heme **(Figure 4.1)**. When measuring

effects on catalytic activity, we concentrated on mutations to non-conserved amino acids located away from the propionates and the Q-site, in order to avoid effects unrelated to the heme potential (**Table 4.1**).

Expression and membrane assembly of mutant enzymes **–** The mutations introduced into the SdhCD membrane domain chosen for study did not have a detrimental effect on the expression and assembly of the enzyme as determined by SDS-PAGE analysis of crude membranes over-expressing each of the mutant proteins (Appendix B – **Figure B.1**). The covalent-flavin assay was used to quantify the amount of SdhA in each sample; levels of FAD varied between 1.5-2.5 nmol FAD mg^{-1} total protein and correlated well with SdhA levels seen on the SDS-PAGE gel. All of the mutant SQR proteins were expressed at similar levels to wild-type SQR.

A PMS-MTT assay was performed which measures non-physiological succinate oxidation activity of the enzyme. This assay requires only a functional SdhAB dimer and thus it is a measure of overall expression and insertion into the membrane. As shown in **Table 4.1**, the PMS-MTT activity of the mutant enzymes was similar to that of wild-type SQR, although the SdhD^{A23S}, SdhC^{V87D}, and SdhC^{H30G} mutant proteins had somewhat lower activity. Thus, mutations in the membrane domain did not significantly alter the ability of the enzyme to oxidize succinate to fumarate.

Determination of the midpoint potential of heme b in mutant SQR **-** Using a combination of redox potentiometry and EPR spectroscopy, we determined the midpoint potential of the heme in all SQR mutant enzymes (**Table 4.1**). We also measured the midpoint potential of the [3Fe-4S] (FS3) cluster, which should be unaffected by mutations in the transmembrane domain. The midpoint potential of the [3Fe-4S] cluster was not significantly altered in any of the SQR mutants ($E_{m,7}$ = +60 mV). In wild-type *E. coli* SQR, the midpoint potential of the heme is +20 mV. Using only site-directed mutagenesis, we were successful in generating mutant enzymes with a wide range of heme potentials, from +20 mV down to -80 mV. All the mutant enzymes exhibited a low spin EPR spectrum and therefore remained hexa-coordinate. The location of the mutated residue relative to the heme did not appear to be a relevant factor as sites on either face of the heme, top or bottom, were all capable of eliciting a change in redox potential. In some cases, a single amino acid residue difference was enough to drop the redox potential of the heme by as much as 75 mV and a combination of the SdhC^{F38D} and SdhC^{V87D} mutations had a cumulative effect, resulting in a 100 mV change.

As expected, the introduction of an Asp residue into the low dielectric environment of the heme resulted in drops of 20-60 mV in the heme potential depending on the position of the mutation. Negatively charged amino acids are expected to stabilize the oxidized form of the heme, which is cationic. This is consistent with results in synthetic heme protein maquettes in which the addition or subtraction of a single charged amino acid in the

vicinity of a bis-His coordinated heme yielded a change in heme redox chemistry of approximately ±50 mV (*14*).

Interestingly, none of the mutations resulted in an increase in heme potential, which might be expected when the heme microenvironment is more hydrophobic (as in the SdhC^{T37I} or SdhC^{H30A} mutants). In these cases, the lower dielectric within the protein milieu might be expected to raise the E_m of the heme through stabilization of the electronically neutral ferrous heme state. Instead, the redox potential of the heme dropped 40-70 mV in these mutants. This highlights the inherent unpredictability in these types of experiments. In these cases, the counterintuitive result may be due to increased solvent exposure of the heme (in the x-ray structures, SdhC^{H30} appears to shield the heme cofactor from nearby water molecules) or differential packing against the hydrophobic core, which may instead stabilize the oxidized form of the heme (*14*).

In contrast to the soluble domains of *E. coli* SQR and eukaryotic Complex II, the membrane domains share very low sequence identity, and the few conserved sequences are confined to key areas of the enzyme near the Q-site and heme propionates. Despite the fact that both share the same core 4-helix bundle-type structure, the individual residues along those helices are quite varied. However, the locations in three-dimensional space of key backbone α–carbons are well conserved even though the overall membrane domains have slight structural differences (*15*). Due to the bis-histidine coordination and common architecture conserved in both *E. coli*

and eukaryotic enzymes, the amino acids and their side chains immediately near the heme align quite well when comparing the structures of *E. coli* SQR to avian (*16*) or porcine Complex II (*15*) (PDB codes 1ZOY and 2H88, respectively).

A comparison of residues immediately next to the heme cofactor indicate that the heme binding pocket in the eukaryotic Complex II is much more polar than in *E. coli* SQR (*15*). Many of the nonpolar residues that we chose to mutate have a polar counterpart in pig Complex II (**Table 4.1**). As we have shown, individual amino acid mutations in *E. coli* SQR can drop the redox potential of the heme by up to 70 mV. Given the cumulative nature of these amino acid replacements, the increased dielectric environment is likely a major cause of the large 200 mV difference between the midpoint potential of the heme in mitochondrial Complex II and *E. coli* SQR.

Considering the unusually high midpoint potential of the heme in *E. coli* compared to the eukaryotic counterpart, it may simply be a case that in the *E. coli* enzyme, the heme-binding pocket has evolved to maximize the E_m of the heme. If the enzyme has actively selected for a high potential heme this may indicate some as yet unknown function. If the role of the heme is purely to maintain structure then the redox potential of the heme is a meaningless quality. In the mitochondrial Complex II, the redox potential of the heme may have been selected to be very low, but alternatively, the absence of selection may have caused the potential to drift down to the current value ($E_{m,7}$ = -185 mV) which is not much higher than the potential of bis-imidazole-ligated

heme *b* in solution ($E_{m8.5}$ = -235 mV) (*17*). Since the heme in mitochondrial complex II is not reducible by succinate, whereas it is in *E. coli* SQR, this implies that if a function exists for the heme in the *E. coli* enzyme, this function has been lost in the mitochondrial enzymes.

Visible spectroscopy of heme b in mutant SQR enzymes – An analysis of each of our mutants using room temperature visible absorption spectroscopy shows that all the membrane samples exhibit typical heme absorption spectra with Soret maxima at 410 nm and 427 nm in the oxidized and reduced states, respectively (data not shown). Normal β- and α- band absorbance maxima at 542 nm and 560 nm were also observed. This suggests that the heme environment is not dramatically altered as a result of the mutations. When succinate instead of dithionite was used to reduce the heme, the levels of reduced heme reflected the EPR-determined midpoint potential. In the SdhC[F38D]/SdhC[V87D] double mutant with the lowest redox potential, succinate-reducible heme is only approximately 10% of wild-type SQR levels (Appendix B – **Figure B.2**).

Catalytic characterization of mutant enzymes – In order to assess the effect of heme potential on catalytic turnover, we measured the ability of the mutants to reduce the ubiquinone analogue, Q_0, in the presence of excess succinate. As shown in **Table 4.1**, all of the mutants were catalytically active. Wild-type SQR reduces Q_0 with a k_{cat} of 43 s^{-1}. Given the non-essential role of heme *b* in

catalysis, we did not see a correlation between the midpoint potential of the heme and Q-reductase activity, although most of the mutant proteins had a reduced capacity to reduce quinol. In most cases, we measured a 10-40% decrease in the catalytic activity of the enzyme. A complete loss of the heme only attenuates activity by roughly 50% (*1*), so the range we observed here is reasonable. Surprisingly, the SdhC[V85T] mutant enzyme, which has a heme $E_{m,7}$ of -45 mV (65 mV lower than wild-type SQR), was able to reduce Q_0 as well, if not slightly better than wild-type SQR. As well, none of the mutations had a significant effect on the K_m for Q_0. This suggests that quinol binding is not affected by any of the mutations, as expected from their substantial distance from the Q-site. Additionally, there was no correlation between the catalytic efficiency of the quinol reduction (k_{cat}/K_m) and the midpoint potential of the heme (**Table 4.1**). Mutant enzymes that had the lowest midpoint potentials tended to have the lowest catalytic efficiencies but this relationship was not absolute.

Fumarate reductase activity of mutant SQR enzymes – E. coli SQR is able to catalyze the reverse reaction, fumarate reduction, when supplied with a source of reducing equivalents. We measured the ability of the mutant enzymes to catalyze the reduction of fumarate with the quinone analogue plumbagin, and similar to the forward reaction, little correlation was observed between E_m and activity (**Table 4.1**). In all mutant enzymes that we tested, plumbagin oxidation rates were directly proportional to Q_0 reduction

rates. Thus, we have shown that *in vitro*, the midpoint potential of the *E. coli* SQR heme does not have a definitive effect on the ability of the enzyme to reduce quinol or oxidize quinone substrates, although most of our mutations had some minor negative effects on enzyme turnover and catalytic efficiency. This may suggest that the high midpoint potential of the heme could be optimal for the function of the *E. coli* enzyme.

Reactive oxygen production in vitro – We examined the effect of lower heme midpoint potential on the production of ROS. *E. coli* SQR is known to produce ROS in the form of superoxide primarily from the FAD binding site (*3*) and we measured the production of superoxide during enzyme turnover using a cytochrome c reduction assay (**Table 1**). Wild-type SQR produces superoxide at a rate of approximately 2 s^{-1}. All of the mutant enzymes tested produced superoxide at a rate equivalent to wild-type SQR when normalized to catalytic turnover and this amounts to approximately 5% the rate of Q_0 reduction. Thus, lowering the redox potential of the heme has no appreciable effect on the production of ROS in this enzyme.

Reactive oxygen production in vivo – We determined whether these mutants could be producing increased levels of superoxide *in vivo* by examining the sensitivity to paraquat, which redox cycles within the cell to generate ROS. *E. coli* expressing SQR mutants that produce enhanced levels of ROS should be especially vulnerable to paraquat-induced oxidative stress. Disc assays were

performed on DW35 cells expressing wild-type as well as mutant SQR (**Table 4.1**). When 1.5 μmol of paraquat were added to the 0.6 cm filter discs, the zone of inhibition around the cells expressing wild-type SQR was 1.7 cm^2. The corresponding zones of inhibition surrounding the DW35 cells expressing the mutant SQR enzymes were in every case smaller when compared to those cells expressing wild-type SQR. Paraquat sensitivity was not enhanced in any of the mutants tested and similar results were obtained when 0.75 μmol of paraquat were used (not shown). These results mirror the *in vitro* results: superoxide production was not increased as the redox potential of the heme was decreased.

It has been suggested that the FAD is the major site of superoxide production in SQR (*3*). The high potential of the heme may allow it to draw electrons away from the FAD. By lowering the potential of the heme, this would cause electrons to linger at the FAD, increasing ROS production. Alternatively, the heme may act as an electron sink to prevent the formation of ROS via the stable ubisemiquinone intermediate. In this case, we should expect that a reduced capacity for electrons would increase the lifetime of the ubisemiquinone intermediate and thus increase the production of superoxide from the Q-site. However, we have yet to find any evidence that changes to the physical properties of the heme can lead to an increased production of superoxide, either *in vivo* or *in vitro.* At this point, we can effectively rule out the possibility that the heme is actively involved in ROS suppression in this enzyme.

EPR characterization of heme b in mutant SQR enzymes – The *b* heme of *E. coli* SQR is a highly anisotropic low spin (HALS)-type characterized by an EPR signal with a large g_z feature ($g_z > 3$) (*18*). The HALS signal is a result of strain on the heme iron, due to the near perpendicular orientation of the imidazole sidechains belonging to the two histidine ligands (*19, 20*). In wild-type SQR, the EPR lineshape of the ferric heme consists of two components that likely arise from two distinct conformations of the heme (**Figure 4.2**). The heterogeneous signal observed is a combination of a sharp peak at $g_z = 3.66$ and a broad signal centered at $g_z = 3.55$. Due to the high g anisotropy of these HALS-type hemes, g_x and g_y values are difficult to measure.

The SdhD[V19D] mutation resulted in the most dramatic change in the EPR lineshape of the heme. Here, we observed the appearance of a new rhombic species at g=3.00 in addition to the regular signal in the g=3.5-3.6 range (**Figure 4.3**) and these two signals both titrate to the same midpoint potential (**Table 4.1**). Given the low g anisotropy of this new species, this signal likely arises from a subpopulation of the enzyme in which the two histidine ligands are coplanar. The addition of an Asp residue in this position likely disrupts the normal orientation of the nearby SdhD[H71] ligand during assembly of the heme, leading to the incorporation of other rotamers of the imidazole sidechain.

In these experiments and others (*21*), we observed mutant SQR enzymes that appear to shift the equilibrium towards one of the two

conformational states that exist in wild-type SQR (**Figure 4.3**). Our results suggest that the different EPR signals are a likely consequence of out-of-plane distortions of the porphyrin ring. The ferrous form of the heme cofactor tends to adopt a more planar conformation but in the ferric form, the pyrrole (Fe-N) bonds are shorter due to the smaller Fe(III) ionic radius (*22, 23*), and it is common for the porphyrin ring to distort out of plane (*24*). Distortion of the heme away from planarity is energetically unfavorable in Fe-porphyrins, and is heavily influenced by the surrounding protein milieu (*25, 26*).

Out-of-plane distortions of the porphyrin ring are normally dependent on hydrogen bonding with the heme propionates and van der Waals contacts with the porphyrin ring. In model heme systems, possible distortions include saddled, ruffled, domed, waved, and propellering conformations (*27, 28*), although it is the two former configurations that are most commonly observed. Our data suggest that a saddled porphyrin ring is the origin of one of the observed EPR lineshapes, while the other is due to a more planar orientation of the porphyrin. This is consistent with more recent crystal structures of the *E. coli* SQR, which modeled the heme in a more saddled conformation (*29*). This is in contrast to the initial 1NEK structure which modeled the heme in a near planar conformation (*6*). Thus, there is evidence that the heme in *E. coli* SQR can exist in both states. The differences in conformation amongst the various SQR structures may represent varying oxidation states of the protein crystal.

An examination of the hydrogen-bonding network around the heme propionates reveals some interesting results. SdhC[H91], SdhB[H207], and SdhD[R20] form a hydrogen bonding network with the propionate distal to the Q-site. SdhD[Q78] and SdhC[R31] are hydrogen bonded to the proximal propionate (**Figure 4.4**). In the 2WDV x-ray structure containing the saddled heme, the pyrrole ring associated with the distal propionate is shifted towards SdhD[R20] while the proximal pyrrole ring contorts in the opposite direction, towards SdhD[R31]. Along the pseudo two-fold axis of the heme, SdhD[R20] and SdhC[R31] are in equivalent positions, as are SdhC[H91] and SdhD[Q78]. These residues surrounding the heme propionates are generally well conserved among different Complex II homologs.

Mutations around the heme propionates show an interesting pattern. The SdhD[R20L] and SdhC[R31L] mutations result in a shift towards the broad EPR spectrum at g_z=3.55 ($E_{m,7}$ = -25 mV and +15 mV, respectively), although the effect is not as pronounced in the SdhD[R20L] mutant. Conversely, the SdhC[H91L] and SdhD[Q78L] mutations ($E_{m,7}$ = -30 mV and +8 mV (*21*), respectively) both cause a shift towards the sharp species at g_z=3.66 (**Figure 4.3**). The mutation of any one of these "girder" residues is likely to cause the heme propionate to shift towards the remaining residue, resulting in the equilibrium shift towards planarity or distortion. For example, in the case of the SdhC[H91L] mutation, the distal propionate will shift towards SdhD[R20], and vice versa. The pattern of symmetry in mutations to the hydrogen bonding network of the propionates strongly suggests that one of the species seen by EPR is the

heme in a saddled conformation, as this distortion is characterized by the same two-fold symmetry. The crystal structure of the SdhB[H207T] was recently elucidated (*30*) and shows the distal propionate shifted towards SdhD[R20]. This is the same configuration that is expected in the SdhC[H91L] mutation and consistently, both the SdhC[H91L] mutant and SdhB[H207T] mutant ($E_{m,7}$ = +20mV (*30*)) exhibit the same sharp EPR spectra. Additionally, in the SdhB[H207T] mutant, the heme in that crystal structure has been modeled as less distorted than in the 2WDV structure, which shows the most heme distortion. This suggests that the sharp EPR species may represent a relatively more planar conformation.

Mutations to amino acids packed against the face of the porphyrin ring can also shift the equilibrium between the saddled and planar conformations (**Figure 4.5**). SdhC[H30] is in close van der Waals distance (~3.5 Å) to the top, distal pyrrole ring of the heme (we refer to the propionate end as the top of the heme). In all the crystal structures, this pyrrole ring appears to be most distorted from planarity, and the position of SdhC[H30] suggests that this residue strongly contributes to the out-of-plane distortion of that ring. We expect the loss of this residue will relieve the protein influence and cause a more planar orientation of the porphyrin molecule. When we mutated SdhC[H30] we noted a shift in equilibrium towards the sharp EPR species. The SdhC[V87D] mutation also results in the observation of the sharp species. This residue is located at a farther distance from the heme (9 Å) but the Asp residue here likely interacts with the nearby SdhC[H30] residue, pulling it away

from the heme, and leading to increased planarity in the porphyrin ring. Considering these results and the SdhB^{H207T} crystallographic data, we can confidently assign the sharp EPR species as originating from a more planar conformation of the heme, whereas the broad component of the lineshape is derived from a more saddled distortion.

Interestingly, mutations along the bottom edge of the heme are also able to elicit the same spectroscopic shifts as those along the top edge of the heme (**Figure 4.5**). Here, the SdhD^{A23S} mutation gives rise to a broad signal, however, the g$_z$ value is shifted upfield to g=3.40. This shift is likely a result of interactions between the serine hydroxyl and the nearby heme ligand, SdhD^{H71}, which may reduce the angle of the two histidine ligands away from perpendicularity. SdhC^{V85} lies at an equidistant position on the opposing side of the bottom, distal pyrrole ring as SdhD^{A23} and we can observe a similar symmetry in the EPR spectra as with the mutations around the heme propionates. In a saddled conformation, the distal, bottom pyrrole ring would be displaced away from planarity towards Sdh^{CV85}. The introduction of a polar Ser or Thr juxtaposed with the relatively hydrophobic pyrrole ring should displace the ring away from the hydroxyl. Thus, the SdhC^{V85T} mutation should increase planarity (sharp EPR species) while the SdhD^{A23S} mutation should decrease planarity (broad EPR species). Our results are consistent with this. Unexpectedly, when an Asp residue is mutated into either of the two positions, we did not see a change in the EPR spectroscopic

characteristics of the heme. Here, the increased length of the Asp sidechain may leave the carboxyl in a position too far to interact with the pyrrole ring.

SdhC^{T37} is situated next to the proximal, bottom pyrrole ring, but its hydroxyl group is pointed away from the heme and as such the dipole here may not be interacting directly with the porphyrin ring. The SdhC^{T37I} mutation introduces a much bulkier sidechain at this position, which would force the proximal, bottom pyrrole ring away for steric reasons, favoring a more saddled porphyrin conformation. Hence, we observe the broad EPR species in this mutant (g_z=3.55).

Of note, mutations associated with increased planarity of the porphyrin molecule are also associated with lower midpoint potentials. This trend does not hold when considering mutations around the propionates but this is likely due to unpredictable changes in the hydrogen-bonding network. Distorted porphyrin systems result in decreased electron density at the heme iron and an increase in redox potential (*31*). Taken together, there is strong, consistent support for saddled distortions in the *E. coli* SQR heme.

4.4 Summary

We made mutations in *E. coli* SQR that modulated the midpoint potential of the heme by nearly 100 mV and assessed the effect on the catalytic ability of the enzyme. We could not observe a correlation between heme E_m and catalytic activity, although many of our mutants had 10-40% reduced activity compared to wild-type SQR. In addition, we did not find

evidence that the heme is involved in the suppression of ROS, either *in vitro* or *in vivo*.

Studies have shown that in the c-type cytochromes, out-of-plane distortions can be conserved among protein homologs across different organisms (*28*). The conservation of what is an energetically unfavorable process suggests some purpose for such higher order structures. Here, an examination of the biophysical data may indicate that in the ferric state, the heme cofactor in wild-type SQR exists in a heterogenous population of saddled and planar conformations. The relevance of this is unclear as yet, but the saddling of the heme likely contributes to its high midpoint potential in this particular Complex II homolog.

A shift in conformation between the oxidized and reduced heme implies that redox-linked conformational changes may be a possible mechanism to regulate enzyme activity. Already, it has been demonstrated that other cytochromes are capable of large scale, conformational changes associated with the redox state of their heme cofactors (*32, 33*). Assuming that the ferrous heme adopts a nearly planar conformation, the shift between a saddled and planar state during redox cycling could be communicated throughout the structure of the membrane domain, given the face of the heme is in van der Waals contact with a large portion of the transmembrane helices. As well, the heme propionates are hydrogen bonded to key residues that constitute the Q-site and minor changes here could impact the enzyme affinity for the ubiquinone pool. The subtle effects on enzyme activity that we

observed when we reduced the capacity of the heme to be accept electrons could indicate a fine-tuning of enzyme activity as a function of heme redox potential. If the heme is acting as a molecular sensor of the redox state of the quinone pool, a redox-induced conformational change could provide a possible mechanism.

4.5 Tables and Figures

Mutant	$E_{m,7}$ heme b	$E_{m,7}$ [3Fe-4S]	k_{cat} Q_0 (s^{-1})	k_{cat}/K_m Q_0 (x10^6 M^{-1} s^{-1})	PMS-MTT(s^{-1})	k_{cat} PB (s^{-1})	Disc Assays (cm^2)	ROS production (s^{-1})
SdhCDAB	20	60	42.9 ± 0.4	0.29 ± 0.06	19.9 ± 0.2	39.6 ± 1.5	1.73	2.0 ± 0.4
D-V19D	2	55	30.0 ± 3.3	0.23 ± 0.03	23.2 ± 0.8	n.d.	n.d.	n.d.
D-A23D	-5	40	35.7 ± 1.3	0.26 ± 0.01	20.9 ± 0.7	n.d.	n.d.	n.d.
C-F38D	-10	50	38.1 ± 2.6	0.28 ± 0.04	20.9 ± 0.6	35.7 ± 1.1	1.19	1.2 ± 0.4
C-V85D	-13	55	14.8 ± 0.4	0.29 ± 0.05	11.4 ± 0.4	n.d.	n.d.	n.d.
C-T37I	-22	50	30.3 ± 2.2	0.22 ± 0.02	16.5 ± 0.7	29.2 ± 1.5	n.d.	n.d.
C-F38S	-25	40	37.3 ± 4.7	0.24 ± 0.06	20.4 ± 0.8	n.d.	1.31	1.6 ± 0.1
C-H30A/C-V87D	-30	45	29.7 ± 3.1	0.17 ± 0.03	21.2 ± 0.4	n.d.	n.d.	n.d.
D-A23S	-40	60	27.1 ± 2.0	0.16 ± 0.02	11.0 ± 0.3	27.9 ± 1.1	n.d.	n.d.
C-V87D	-43	35	34.1 ± 1.8	0.20 ± 0.03	22.9 ± 0.8	n.d.	n.d.	n.d.
C-V85T	-45	60	48.4 ± 1.1	0.36 ± 0.02	26.2 ± 1.5	54.2 ± 1.8	n.d.	2.8 ± 0.3
C-H30G	-50	45	27.9 ± 2.0	0.22 ± 0.03	12.9 ± 0.2	n.d.	1.17	0.8 ± 0.1
C-H30A	-54	53	32.4 ± 3.3	0.21 ± 0.03	17.6 ± 0.4	29.8 ± 1.2	n.d.	n.d.
C-H30S	-62	40	35.3 ± 2.0	0.21 ± 0.04	21.5 ± 0.9	n.d.	n.d.	n.d.
C-F38D/C-V87D	-80	60	13.3 ± 1.7	0.05 ± 0.01	15.9 ± 0.2	21.6 ± 1.0	1.61	0.8 ± 0.1

Table 4.1: Redox characteristics, physiological and non-physiological activities and ROS assays of wild-type and mutant SQR. Turnover numbers have all been normalized to FAD content. Activity data were averaged from at least three independent measurements.

n.d. – not determined
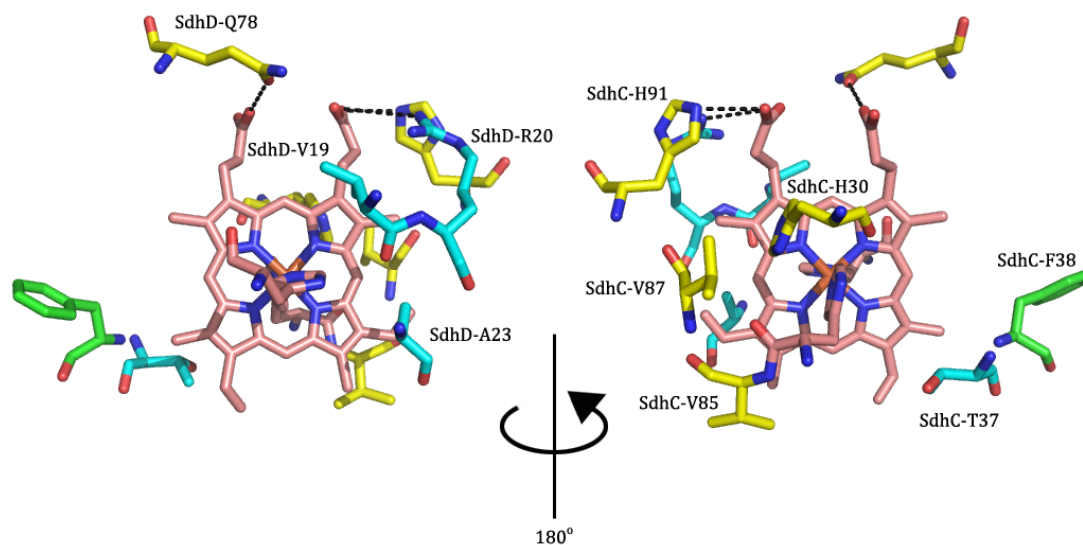
Figure 4.1: Residues selected for mutation. Residues which result in the shift towards the "sharp" EPR spectrum when mutated are colored in yellow while positions causing a shift towards the the "broad" EPR spectrum are colored in blue. Residues which, when mutated, did not result in an altered EPR spectrum are shown in green (PDB: 1NEK *(6)*).

Figure 4.2: Ferric heme EPR lineshapes of the two heme conformations.

The signal in wild-type SQR is a mixture of a sharp and broad species, exemplified in the SdhC[H30A] and SdhC[T37I] mutant SQR, respectively.

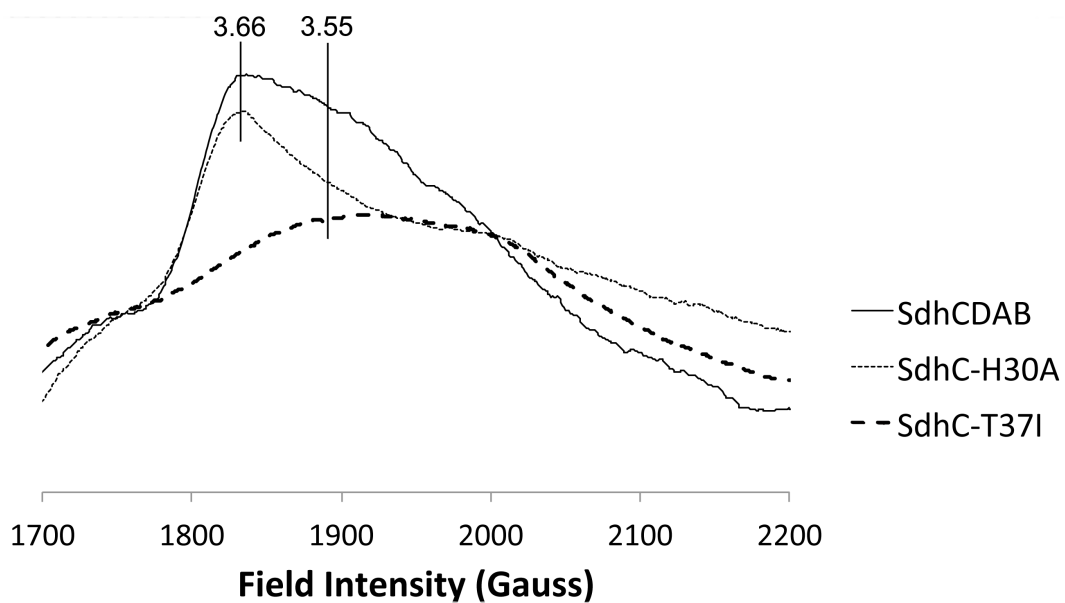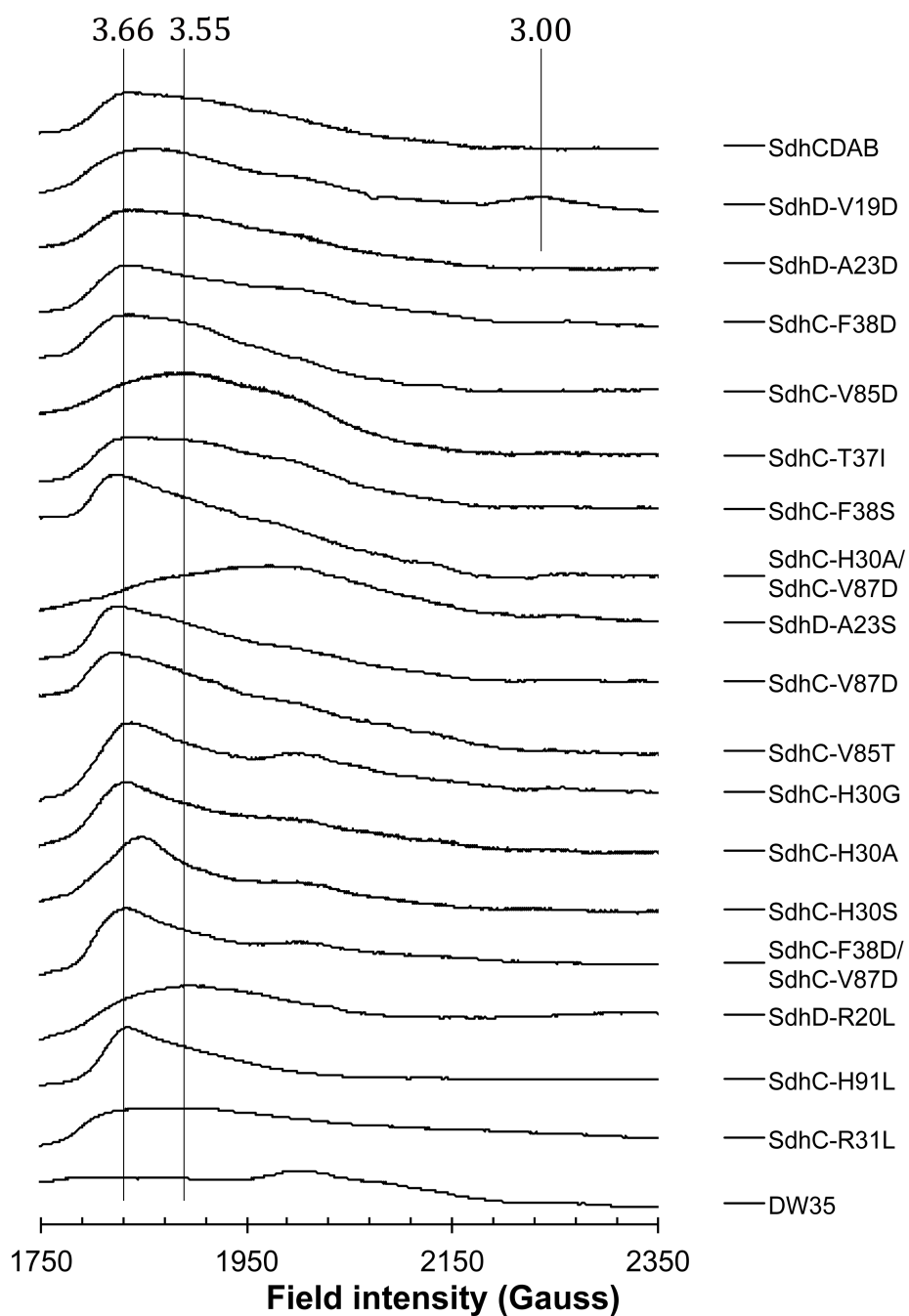**Figure 4.3: EPR Spectra of low-spin heme** Crude membranes enriched in

wild-type and mutant SQR were oxidized with 0.8 mM DCPIP. Spectra were

recorded at 20 mW at 12 K.
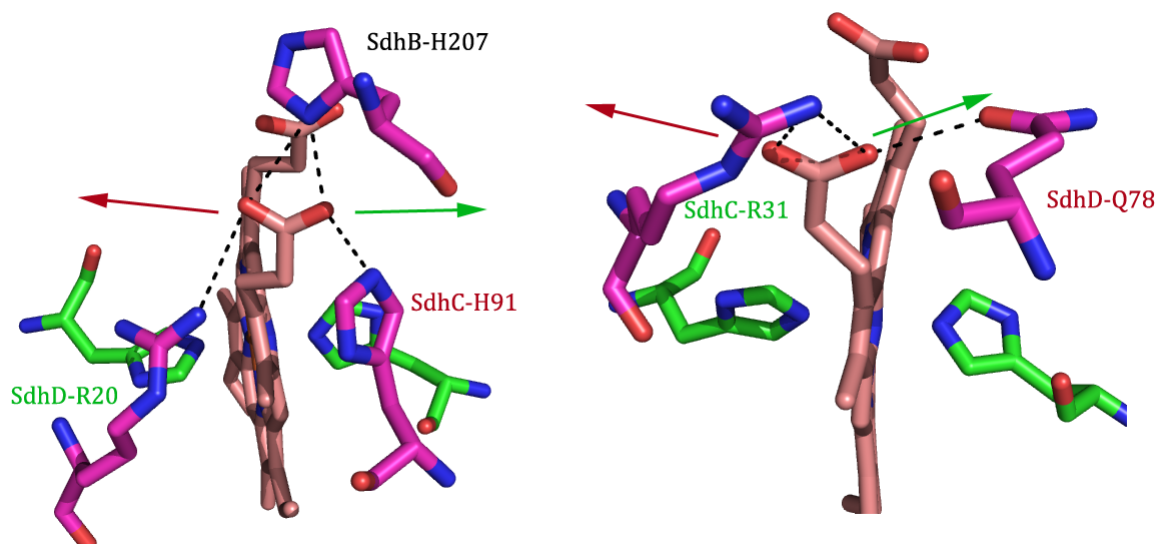
Figure 4.4: The hydrogen-bonding network around the heme propionates. The distal propionate is shown on the left while the proximal propionate is shown on the right. Each propionate is held in position by residues on either side. Mutation of SdhD[R20] and SdhC[R31] to a Leu results in the propionate shifting towards the other "girder" (green arrows). Mutation of SdhC[H91] and SdhD[Q78] to a Leu causes a shift in the propionate in the other direction (red arrows).
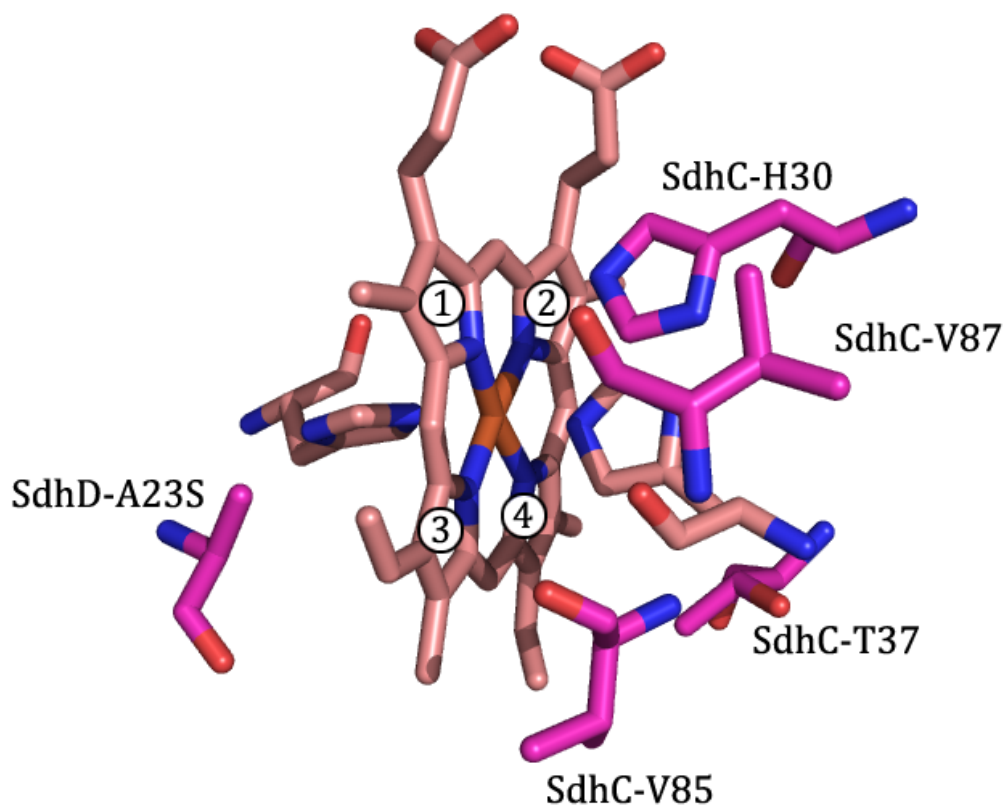
Figure 4.5: Interactions between the heme face and surrounding residues. Mutations to the residues depicted are able to affect the planarity of the porphyrin ring. Pyrrole rings are denoted as (1) top, distal (2) top, proximal (3) bottom, distal (4) bottom, proximal.

4.6 References

1. Tran, Q. M., Rothery, R. A., Maklashina, E., Cecchini, G., and Weiner, J. H. (2007) *Escherichia coli* succinate dehydrogenase variant lacking the heme *b*, *Proc Natl Acad Sci U S A 104*, 18007-18012.

2. Maklashina, E., Rothery, R. A., Weiner, J. H., and Cecchini, G. (2001) Retention of heme in axial ligand mutants of succinate-ubiquinone xxidoreductase (complex II) from *Escherichia coli*, *J Biol Chem 276*, 18968-18976.

3. Messner, K. R., and Imlay, J. A. (2002) Mechanism of superoxide and hydrogen peroxide formation by fumarate reductase, succinate dehydrogenase, and aspartate oxidase, *J Biol Chem 277*, 42563-42571.

4. Zhao, Z., Rothery, R. A., and Weiner, J. H. (2006) Effects of site-directed mutations in *Escherichia coli* succinate dehydrogenase on the enzyme activity and production of superoxide radicals, *Biochem Cell Biol 84*, 1013-1021.

5. Szeto, S. S., Reinke, S. N., Sykes, B. D., and Lemire, B. D. (2007) Ubiquinone-binding site mutations in the *Saccharomyces cerevisiae* succinate dehydrogenase generate superoxide and lead to the accumulation of succinate, *J Biol Chem 282*, 27518-27526.

6. Yankovskaya, V., Horsefield, R., Tornroth, S., Luna-Chavez, C., Miyoshi, H., Leger, C., Byrne, B., Cecchini, G., and Iwata, S. (2003) Architecture of succinate dehydrogenase and reactive oxygen species generation, *Science 299*, 700-704.

7. Yang, X., Yu, L., and Yu, C. A. (1997) Resolution and reconstitution of succinate-ubiquinone reductase from *Escherichia coli*, *J Biol Chem 272*, 9683-9689.

8. Tran, Q. M., Rothery, R. A., Maklashina, E., Cecchini, G., and Weiner, J. H. (2006) The quinone binding site in *Escherichia coli* succinate dehydrogenase is required for electron transfer to the heme *b*, *J Biol Chem 281*, 32310-32317.

9. Kita, K., Vibat, C. R., Meinhardt, S., Guest, J. R., and Gennis, R. B. (1989) One-step purification from *Escherichia coli* of complex II (succinate: ubiquinone oxidoreductase) associated with succinate-reducible cytochrome b556, *J Biol Chem 264*, 2672-2677.

10. Maklashina, E., Berthold, D. A., and Cecchini, G. (1998) Anaerobic expression of *Escherichia coli* succinate dehydrogenase: functional replacement of fumarate reductase in the respiratory chain during anaerobic growth, *J Bacteriol 180*, 5989-5996.

11. Westenberg, D. J., Gunsalus, R. P., Ackrell, B. A., Sices, H., and Cecchini, G. (1993) *Escherichia coli* fumarate reductase frdC and frdD mutants. Identification of amino acid residues involved in catalytic activity with quinones, *J Biol Chem 268*, 815-822.

12. Markwell, M. A., Haas, S. M., Tolbert, N. E., and Bieber, L. L. (1981) Protein determination in membrane and lipoprotein samples: manual and automated procedures, *Methods Enzymol 72*, 296-303.

13. Singer, T. P., Salach, J., Hemmerich, P., and Ehrenberg, A. (1971) Flavin peptides, *Methods Enzymol 18*, 416-427.

14. Shifman, J. M., Gibney, B. R., Sharp, R. E., and Dutton, P. L. (2000) Heme redox potential control in *de novo* designed four-alpha-helix bundle proteins, *Biochemistry 39*, 14813-14821.

15. Sun, F., Huo, X., Zhai, Y., Wang, A., Xu, J., Su, D., Bartlam, M., and Rao, Z. (2005) Crystal structure of mitochondrial respiratory membrane protein complex II, *Cell 121*, 1043-1057.

16. Huang, L. S., Sun, G., Cobessi, D., Wang, A. C., Shen, J. T., Tung, E. Y., Anderson, V. E., and Berry, E. A. (2006) 3-nitropropionic acid is a suicide inhibitor of mitochondrial respiration that, upon oxidation by complex II, forms a covalent adduct with a catalytic base arginine in the active site of the enzyme, *J Biol Chem 281*, 5965-5972.

17. Shifman, J. M., Moser, C. C., Kalsbeck, W. A., Bocian, D. F., and Dutton, P. L. (1998) Functionalized *de novo* designed proteins: mechanism of proton

coupling to oxidation/reduction in heme protein maquettes, *Biochemistry 37*, 16815-16827.

18. Peterson, J., Vibat, C., and Gennis, R. B. (1994) Identification of the axial heme ligands of cytochrome b_{556} in succinate: ubiquinone oxidoreductase from *Escherichia coli*, *FEBS Lett 355*, 155-156.

19. Migita, C. T., and Iwaizumi, M. (1981) Low-temperature EPR studies of highly anisotropic low-spin (protoporphyrinato) iron (III) complexes, *Journal of the American Chemical Society 103*, 4378-4381.

20. Berry, E. A., and Walker, F. A. (2008) Bis-histidine-coordinated hemes in four-helix bundles: how the geometry of the bundle controls the axial imidazole plane orientations in transmembrane cytochromes of mitochondrial complexes II and III and related proteins, *J Biol Inorg Chem 13*, 481-498.

21. Cheng, V. W., Johnson, A., Rothery, R. A., and Weiner, J. H. (2008) Alternative sites for proton entry from the cytoplasm to the quinone binding site in *Escherichia coli* succinate dehydrogenase, *Biochemistry 47*, 9107-9116.

22. Korszun, Z. R., Bunker, G., Khalid, S., Scheidt, W. R., Cusanovich, M. A., and Meyer, T. E. (1989) Extended X-ray absorption fine structure study of *Rhodospirillum rubrum* and *Rhodospirillum molischianum* cytochromes *c*': relationship between heme stereochemistry and spin state, *Biochemistry 28*, 1513-1517.

23. Collins, D. M., Countryman, R., and Hoard, J. L. (1972) Stereochemistry of low-spin iron porphyrins. I. Bis(imidazole)-α,β,γ,δ-tetraphenylporphinatoiron(III) chloride, *J Am Chem Soc 94*, 2066-2072.

24. Le Moigne, C., Picaud, T., Boussac, A., Loock, B., Momenteau, M., and Desbois, A. (2009) Redox effects on the coordination geometry and heme conformation of bis(N-methylimidazole) complexes of superstructured Fe-porphyrins. A spectroscopic study, *Inorg Chem 48*, 10084-10092.

25. Anderson, K. K., Hobbs, J. D., Luo, L., Stanley, K. D., Quirke, J. M. E., and Shelnutt, J. A. (1993) Planar-nonplanar conformational equilibrium in metal derivatives of octaethylporphyrin and meso-nitrooctaethylporphyrin, *Journal of the American Chemical Society 115*, 12346-12352.

26. Hobbs, J. D., and Shelnutt, J. A. (1995) Conserved nonplanar heme distortions in cytochromes *c, J Protein Chem 14*, 19-25.

27. Yatsunyk, L. A., Carducci, M. D., and Walker, F. A. (2003) Low-spin ferriheme models of the cytochromes: correlation of molecular structure with EPR spectral type, *J Am Chem Soc 125*, 15986-16005.

28. Jentzen, W., Ma, J. G., and Shelnutt, J. A. (1998) Conservation of the conformation of the porphyrin macrocycle in hemoproteins, *Biophys J 74*, 753-763.

29. Ruprecht, J., Yankovskaya, V., Maklashina, E., Iwata, S., and Cecchini, G. (2009) Structure of *Escherichia coli* succinate:quinone oxidoreductase with an occupied and empty quinone-binding site, *J Biol Chem 284*, 29836-29846.

30. Ruprecht, J., Iwata, S., Rothery, R. A., Weiner, J. H., Maklashina, E., and Cecchini, G. (2011) Perturbation of the quinone binding site of complex II alters the electronic properties of the proximal [3Fe-4S] iron-sulfur cluster, *J Biol Chem*

31. Olea, C. J., Kuriyan, J., and Marletta, M. A. (2010) Modulating heme redox potential through protein-induced porphyrin distortion, *J Am Chem Soc 132*, 12794-12795.

32. Furlan, S., Penna, G. L., Banci, L., and Mealli, C. (2007) *Ab initio* molecular dynamics of heme in cytochrome *c*, *J Phys Chem B 111*, 1157-1164.

33. Morgado, L., Bruix, M., Londer, Y. Y., Pokkuluri, P. R., Schiffer, M., and Salgueiro, C. A. (2007) Redox-linked conformational changes of a multiheme cytochrome from *Geobacter sulfurreducens*, *Biochem Biophys Res Commun 360*, 194-198.

Chapter 5: Empirical Electron Transfer Rates Through the Electron Transport Relay of *Escherichia coli* Succinate Dehydrogenase*

---

*This work was a collarboration with Victor Cheng, Sarah Chobot, Marc Strampraad, Richard A. Rothery, Leslie Dutton, Simon de Vries, and Joel H. Weiner.

5.1 Introduction

The electron transport chains in all living organisms rely on the fundamental ability of electrons to tunnel through various respiratory complexes, from one prosthetic group to the next, before reducing a terminal electron acceptor. Each complex contains a simple electron transfer relay comprised of a series of nodes, insulated from the aqueous phase by the surrounding protein milieu. Successful electron transfer allows the organism to harness the reducing power of various metabolic intermediates, converting that energy into a proton gradient for subsequent use in oxidative phosphorylation, small molecule transport, or motility in bacteria. However, the distances between the sequential metal cofactors present a physical barrier that must be overcome by outer sphere electron transfer (*1*).

Marcus theory was first proposed in 1953 as a theoretical solution for electron tunneling in oxidation-reduction reactions (*1*). Since then, the model has been refined numerous times (*2-5*) and the working Duttonian model has shown itself to be a reasonable estimation of many biologically relevant electron transfer reactions while considering only four key variables (*6-8*). These are the distance between cofactors, the packing density of the surround protein milieu, the thermodynamic driving force, and the reorganization energy associated with the electron transfer reaction.

From a technical perspective, *Escherichia coli* succinate:quinone oxidoreductase (SQR, succinate dehydrogenase, SdhCDAB) is a very

appealing model system for the study of electron transfer rates *in situ*. The active site flavin adenine dinucleotide (FAD) in SdhA; the three [Fe-S] clusters in SdhB (FS1, a [2Fe-2S cluster, FS2, a [4Fe-4S] cluster, and FS3, a [3Fe-4S] cluster); and the *b* heme sandwiched between SdhC and SdhD in the membrane, are all spectroscopically distinct in an electron paramagnetic resonance (EPR) spectrometer and thus, the redox state of each can be unambiguously determined (*9*). Very high protein expression levels, which are a necessity in these types of experiments, are easily achieved (*10*).

In addition to measuring the kinetics of electron transfer in wild-type SQR, we seek to compare the wild-type electron tunneling rates to those in the SdhB^{I150H} mutant SQR, where the midpoint potential (E_m) of FS2 has decreased from -213 mV to -338 mV (*9*). Compared to FS1 and FS3, which have potentials of +15 mV and +55 mV, respectively, the midpoint potential of FS2 is very low, typical of the "low potential" cluster that is commonly found in the center of [Fe-S] chains of various redox enzymes (*11*). Electrons must tunnel through FS2 on the way from FAD to the Q-site, and the presence of a highly endergonic electron tunneling reaction may serve as a rate-limiting step in the electron transfer relay. A "check" in the rate of electron transfer may reduce the accumulation of electrons at the end of the chain. A saturation of electrons at the Q-site increases the likelihood of extraneous electron transfer reactions and short circuits, such as the auto-oxidative formation of reactive oxygen species (*12*).

In this study, a multi-institutional collaboration with Dr. Leslie Dutton's laboratory at the University of Pennsylvania as well as Dr. Simon de Vries' laboratory at TU Delft in the Netherlands, we sought to use the technology of microsecond freeze-hyper quenching (MHQ) (*13*) to empirically measure electron transfer rates through *E. coli* SQR.

5.2 Materials and Methods

Bacterial strains and plasmids– Wild-type and mutant SQR proteins were expressed in *E. coli* strain DW35 (Δ*frdABCD, sdhC*::*kan*), and transformed with plasmid pFAS (*10*), which contains the full length *sdhCDAB* operon. The SdhB[I150H] mutant was created by site-directed mutagenesis as described in previous work (*9*).

Enzyme preparation and purification – *E. coli* DW35 cells were grown overnight in TB media as before (*14*). Upon harvesting, an Avestin Emulsiflex was used to lyse the cells in the presence of 20 μM PMSF. The protein enriched inner membrane was isolated by differential centrifugation (*14*). All SQR preparations were subjected to an activation step in 1 mM malonate at 30 °C for 20 minutes and 1 mM malonate was kept in the buffer for all subsequent centrifugation steps. During preparation of the membranes, all samples were maintained in a 100 mM MOPS/ 5 mM EDTA buffer, pH 7.0.

Prior to the MHQ experiments, the malonate present in the membrane solutions had to be removed. Two wash steps were performed. Membranes

were pelleted by ultracentrifugation and resuspended in 200 mM sodium phosphate buffer, pH 8.0.

Electron transfer simulations – The rates of electron transfer were calculated from the following equations:

$\log_{10} k_{et}^{ex} = 13-(1.2-0.8\rho)(R-3.6)-3.1(\Delta G° + \lambda)^2 / \lambda$

$\log_{10} k_{et}^{en} = 13-(1.2-0.8\rho)(R-3.6)-3.1(\Delta G° + \lambda)^2 / \lambda - \Delta G° / 0.06$

In these equations, R is the edge to edge distance between the two prosthetic groups. ρ is the packing density, which we set to 0.76, the typical value in proteins. $\Delta G°$ is the thermodynamic driving force, and λ is the reorganization energy, which we set as 0.7 eV (*11*).

The following midpoint potentials (pH 7.0) were used in the calculations for wild-type SQR, based on values derived by Cheng *et al.* (*9*): FAD: E_1=-79 mV, E_2=-295 mV; [2Fe-2S]: +15 mV; [4Fe-4S]: -213 mV; [3Fe-4S]: +55 mV; Q: E_1=+332 mV, E_2=-152 mV; *b* heme: +35 mV. The same values were used in the calculations for the SdhB[I150H] mutant except the value of FS2, which was -338 mV.

Microsecond freeze hyper-quench kinetics – The rapid kinetics experiments were performed on the unique MHQ machine at TU Delft (*13*). 250 µL of the crude membranes (~20 mg mL^{-1}) were reacted with 200 mM succinate or buffer. All samples were filtered through a 20 µm pore size filter to remove all solid precipitates. HPLC pumps were used to inject each solution into the

mixing chamber where the final solution is forced through an orifice. A 20 µm orifice was used for samples at timepoints less than 0.8 ms. For longer timepoints, a 100 µm orifice was used. The resulting jetstream from the mixer is sprayed onto the inner surface of a 77 K tungsten-coated rotor spinning at 6000 rpm where the reaction is quenched. The resulting powder residue was scraped off and analyzed by EPR or low-temperature UV-VIS spectroscopy. After spraying, all MHQ samples were maintained in a liquid nitrogen environment to prevent further reactivity.

UV-VIS Spectroscopy – MHQ samples were diluted in 140 K isopentane and heme spectra were obtained in an SLM-Aminco DW2000 scanning spectrophotometer, equipped with a liquid nitrogen cryogenic system, as described in ref (*15*).

Electron Paramagnetic Resonance – To analyze the MHQ samples, the powder was packed into quartz EPR tubes. Among different samples, the density of the flakes was kept constant as much as possible. [Fe-S] reduction levels were measured on a Varian E-9 spectrometer equipped with a helium boil-off cryostat system, consisting of a home-made glass transfer line and quartz sample holder.

In order to define the redox potentials of the cofactors, redox potentiometry was performed on membranes suspended in 100 mM HEPES/ 5 mM EDTA, pH 8.0, using protocols previously described (*9*). These samples

were analyzed in a Bruker Elexsys E500 EPR spectrometer equipped with an Oxford Instruments ESR900 flowing helium cryostat.

EPR measurements were made at 12 K for FS1, FS3, and heme measurements; and 40 K for FS2 and FAD measurements. FS1, FS3, heme, and FAD spectra were acquired at 20 mW microwave power while FS2 measurements were determined at 2 mW. All EPR experiments were performed using a microwave frequency of 9.38 GHz and 100 kHz modulation amplitude.

Stopped-flow kinetics – Stopped-flow was performed on a Sequential Bio SX-17MV stopped flow spectrometer, operated in single-mixing absorbance mode. The unit was equipped with a 2 mm optical pathlength unit cell with an associated dead time < 2 ms. SQR-enriched membranes were diluted to 1 mg mL^{-1} in 100 mM HEPES/ 5 mM EDTA/ 20 mM glucose, pH 8.0. 5 U mL^{-1} of glucose oxidase (Sigma) were added during the experiments to achieve anaerobiosis. The membranes were mixed with either the buffer above, or a buffer solution containing 200 mM succinate. All experiments were carried out at room temperature.

Curve fitting – The MHQ data were fit to either a single (1) or double (2) exponential equation:

1) $y = Ae^{-kt} + y_0$

2) $y = A_1e^{-k_1t} + A_2e^{-k_2t} + y_0$

The stopped-flow data were fit to either the single exponential equation (1) above or a zero-order rate equation (3):

$$3)\ y = -kt + y_0$$

For first-order kinetics, $t_{1/2} = k(\ln(2))$.

For zero-order kinetics, $t_{1/2} = y_{max}/2k$.

5.3 Results

Electron transfer simulations – Sarah Chobot, in Dr. Leslie Dutton's lab, carried out electron transfer simulations for both wild-type SQR and the SdhB^{I150H} mutant, using midpoint potentials determined at pH 7.0 (*9*). The simulation presented in **Figure 5.1***A* follows the path of the two electrons following succinate oxidation in wild-type SQR as they are passed from the reduced FADH$_2$ to the quinone. According to the simulation, we should expect sub-microsecond reduction of both FS1 and FS3. Due to the extremely low midpoint potential of the FS2, it remains oxidized throughout the timecourse. The heme and FS3 get reduced on a similar timescale. However, neither FS3 nor the heme gets fully reduced as electrons are shared between the two prior to reduction of the Q.

   Figure 5.1*B* shows the results of the simulation of electron flow through the SdhB^{I150H} mutant. Assuming an edge to edge distance of 9.2 Å, measured in the 1NEK x-ray crystal structure (*16*), the estimated rate of tunneling from FS1 to FS2 in wild-type SQR is calculated to be 7.1 x 10^4 s^{-1} ($t_{1/2}$ = 10 µs). In the mutant, that rate decreases to 1.7 x 10^3 s^{-1} ($t_{1/2}$ = 402 µs)

a 40-fold difference. This difference is reflected in the simulation. Electron transfer upstream of FS1 is unaffected by the mutation, as indicated by the similar, fast reduction of FS1 in both traces. However, due to the lag in tunneling through FS2 caused by the mutation, all subsequent electron transfer steps downstream of FS2 suffer a delay in the mutant.

Sample optimization for microsecond freeze hyper-quench experiments – In order to empirically compare the rates of electron transfer through wild-type SQR and the SdhB[I150H] mutant, SQR-enriched membranes were subjected to MHQ experiments. Steady state kinetic experiments are typically performed on "activated" enzyme samples. The usual method for activating the enzyme involves a fifteen minute incubation with 1 mM malonate at 30 ℃ followed by a series of washes with malonate-containing buffer which removes the tightly-bound oxaloacetate inhibitor at the SdhA active site (*14*). Although a weaker inhibitor of SQR, the malonate is nonetheless still bound to the active site and we discovered in our initial MHQ experiments that the dissociation of malonate and ensuing binding of succinate was fairly slow and interfered with a proper analysis of the kinetics. Thus, it was useful to perform the MHQ experiments on membrane samples in the absence of malonate. To solve the issue, we opted to replace the 100 mM MOPS buffer containing 1 mM malonate with a 100 mM phosphate buffer. Small negatively charged anions such as phosphate are also capable of activating SQR (*17*).

All MHQ experiments were performed at pH 8.0 to enable accurate measurement of the true rates of electron transfer through the enzyme. The driving force for succinate oxidation is greater at higher pH ($E_{m,8}$ = -60 mV) and SQR catalytic activity is optimal at pH 8.0 (*18*). Potentiometric titrations indicated the midpoint potentials of FS2 and FS3 did not change between pH 7.0 and pH 8.0. However, the potential of FS1 was pH-dependent, decreasing from +15 mV at pH 7.0 to -40 mV at pH 8.0. Thus, the reduction of FS1 is coupled to a protonation event. The ionizable group responsible for this redox-Bohr effect is unknown but could potentially be SdhB[E57] which is the nearest charged residue to FS1. The lower $E_{m,8}$ of FS1 increases the rate of the limiting step of electron tunneling from FS1 to FS2 as the driving force ΔG is less endergonic; at pH 8.0, the rate is calculated as 3.4 x 10^5 s^{-1} ($t_{1/2}$ = 2 μs) in wild-type SQR and 9.1 x 10^3 s^{-1} ($t_{1/2}$ = 76 μs) in the SdhB[I150H] mutant, which is still a 40-fold difference between the two.

Determining electron transfer rates through the [Fe-S] relay – In the MHQ experiments, SQR-enriched membranes were reacted with saturating levels of succinate. Samples were generated at timepoints ranging from 140 μs to 200 ms. Each MHQ sample was analyzed by EPR spectroscopy to determine the redox state of each of the three [Fe-S] clusters. The 0% reduction control was taken as the reduction level in SQR membranes reacted against buffer alone and 100% reduction controls were made as succinate-reduced SQR reacted against succinate. The kinetics of electron transfer through FS1 and

FS3 in wild-type SQR and the SdhB[I150H] mutant are shown in **Figure 5.2**. In both cases, very little reduction of either center was observed in the sub-millisecond samples. It was not until the 800 µs sample when we began to see evidence of reduction of FS1. This seems slower than expected and we attributed this to the requisite dissociation of phosphate from the active site before succinate can bind and donate electrons into the chain. The solutions for the best-fit equations are shown in **Table 5.1**. FS2 reduction was never observed in any of the MHQ samples.

In both wild-type and the SdhB[I150H] mutant, we can observe approximately 50% reduction of FS1 at steady state, since the midpoint potential of FS1 and the succinate/fumarate couple ($E_{m,8}$ = -29 mV) are similar at pH 8.0. The kinetics of FS1 reduction in wild-type SQR fit well to a double exponential rate equation (**Figure 5.2*A***). The two phases likely derive from the initial fast reduction of FS1 by succinate ($t_{1/2}$ = 3.4 ms), followed by a slower second phase of reduction as electrons tunnel to FS3 ($t_{1/2}$ = 81.4 ms). Roughly half of the succinate-reducible population of FS1 is reduced in each phase.

In contrast, the SdhB[I150H] mutant has a different kinetic profile with respect to FS1 reduction (**Figure 5.2*B***). The data still conform to a double exponential fit and both the initial fast reduction phase ($t_{1/2}$ = 2.6 ms) and the slower second phase ($t_{1/2}$ = 226 ms) proceed at similar rates, given the spread in the data. This is expected since the mutation does not affect the physical properties of the electron transfer relay upstream of the FS1 cluster.

The difference in the electron transfer kinetics between wild-type and mutant SQR are even more pronounced when we consider FS3 reduction. In wild-type SQR, FS3 reduction is best fit to a double exponential equation (**Figure 5.2*A***). An initial fast reduction of FS3 ($t_{1/2}$ = 0.28 ms) is expected as electrons arrive from FS1. At later timepoints, the slow oxidation of FS3 by ubiquinone becomes an issue and the rate of FS3 reduction ($t_{1/2}$ = 28.9 ms) reflects equilibrium with the Q-pool. The apparent $t_{1/2}$ of FS3 reduction is approximately 20-30 ms, but the initial, very fast phase of reduction suggests that in wild-type SQR, electron transfer from FS1 to FS3 is likely to be much faster than that.

Compared to wild-type SQR, the SdhB[I150H] mutation results in a very noticeable decrease in the rate of FS3 reduction (**Figure 5.2*B***). In the mutant, a quick initial phase of reduction is not observed. Instead, only a single phase is seen. The rate of electron transfer to FS3 in the mutant is closer to the rate of quinone oxidation, thus FS3 reduction levels are in greater equilibrium with the Q-pool. The apparent $t_{1/2}$ of FS3 reduction here is about 88 ms, or about 4-fold slower than in wild-type SQR.

The MHQ samples were also analyzed for the presence of a radical signal, arising from the flavosemiquinone intermediate. However, the flavin radical EPR signal, which is typically observed around g=2.0 (*14*), could not be defined with any certainty.

Stopped-flow was utilized to measure heme reduction rates – During our preliminary MHQ experiments, we found that the heme was not reduced on the same timescale as the [Fe-S] clusters. We saw very little reduction of the heme on the sub-millisecond timescale. Rather, even in samples as late as 25 ms, only very little heme reduction could be observed by low-temperature UV-VIS spectroscopy (data not shown). Given the relatively slow kinetics of heme reduction, stopped-flow experiments were more suitable than MHQ to compare the reduction rates of wild-type SQR to the SdhB[I150H] mutant.

Stopped-flow experiments indicated that heme reduction in wild-type SQR began about 5 ms post-reaction with succinate (**Figure 5.3*A***) while in the SdhB[I150H] mutant heme reduction could only be seen after 15-20 ms (**Figure 5.3*B***). The first evidence of heme reduction in the stopped-flow experiments is observed much sooner than in the MHQ experiments. The origin for this difference here may be twofold. First, the stopped flow experiments were performed in HEPES buffer, not phosphate buffer. Although less of the enzyme may be in the "activated" state when in HEPES buffer, there is no lag caused by the requisite dissociation of inhibitory molecules from the FAD active site. The difference in kinetics may also stem from the temperature differential between the two methods. Stopped-flow is performed at 20 °C, whereas the reaction at the head of the MHQ mixer occurs at 10 °C. Succinate binding and oxidation rates should exhibit an Arrhenius-like dependence on temperature; furthermore, the electron

tunneling rates between prosthetic groups has been shown to be temperature-dependent above 150 K (*2*),

Other considerable differences are seen in the heme reduction rates of wild-type SQR and the SdhB[I150H] mutant. The solutions to the best-fit equations for heme reduction are shown in **Table 5.2**. In wild-type SQR, heme reduction can only be fit to a linear, zero-order reaction rate with $t_{1/2}$ = 12 ms. Heme reduction in the SdhB[I150H] mutant was fit to a first-order, single exponential equation with $t_{1/2}$ = 44 ms.

5.4 Discussion

The SdhB[I150H] mutation results in a significant drop in the midpoint potential of the [4Fe-4S] FS2 cluster and an associated decrease in catalytic activity (*9*). The aim of this study was to empirically compare the electron transfer rate in wild-type SQR and the SdhB[I150H] mutant. The Duttonian model makes several predictions about the pre-steady state reduction kinetics:

1)   No accumulation of reduced FS2.

2)   The presence of a flavosemiquinone intermediate.

3)   Sub-millisecond kinetics of electron transfer through the [Fe-S] clusters in wild-type SQR.

4)   An approximate 40-fold decrease in the rate of FS3 reduction in the SdhB[I150H] mutant.

5)   Reduction of the *b* heme on a similar timescale as FS3 reduction.

There are certainly some discrepancies between the predicted, theoretical behavior and our experimental results.

As the simulations predicted, a reduced FS2 EPR signal could not be detected in either wild-type SQR or the SdhB[I150H] mutant. Given the low potential of the FS2 cluster relative to the succinate/fumarate couple, its final reduction level is expected to be very low, and reduced FS2 cannot accumulate due to the very fast rate of the FS2 to FS3 electron transition.

As well, the model predicts the accumulation of a flavosemiquinone intermediate as the first electron tunnels to FS1. While there is some activity in that area of the EPR spectrum in many of the MHQ samples, the signal-to-noise ratio was not sufficient for unambiguous assignment of a flavin radical. This suggests that if the flavosemiquinone is present, its concentration is quite low. As the potential of the flavosemiquinone is much lower than either FS1 or FS3, the two electrons from the oxidation of succinate are much more likely to accumulate further down the chain.

The model also deviates from our experiments when we consider the kinetics of [Fe-S] cluster reduction. The reduction of FS1 occurs on a much slower timescale than predicted as its reduction may occur with a $t_{1/2}$ as high as 5 ms. This difference may have two possible causes: slow dissociation of the phosphate molecule in the active site; and succinate binding, oxidation, and hydride transfer to the FAD requires time. As well, large conformational

changes within SdhA may be associated with catalysis (*19, 20*). However, the MHQ data do indicate that FS1 reduction occurs at the same rate in both wild-type SQR and the SdhB[I150H] mutant, as predicted by the model. In the mutant, evidence of the slower rate of electron transfer through FS2 is seen in the higher percentage of FS1 reduced in the first phase of reduction. The block between FS1 and FS3 results in a higher proportion of FS1 reaching its final reduction level, sooner.

The apparent reduction rate of FS3 shows only a ~4-fold decrease in the mutant (from $t_{1/2} \sim 25$ ms to $t_{1/2} = 88$ ms), rather than 40-fold decrease predicted in the model. However, this does not necessarily suggest an error in the model. Since the MHQ experiments were performed on crude membranes, the presence of endogenous quinone obscures the true kinetics of FS3 reduction. The true rates are likely to be faster than the apparent rates we report here. The initial fast phase of FS3 reduction in wild-type SQR is not seen in the SdhB[I150H] mutant. This phase ($t_{1/2} = 0.28$ ms) is likely closer to the true rate of FS3 reduction before electrons are lost to the Q-site. This rate of this phase is significantly faster than the apparent rate of FS3 reduction in wild-type SQR, and is nearly 100 times faster than the apparent rate measured in the SdhB[I150H] mutant. The absence of the quick phase in FS3 reduction is the most direct evidence of the block in electron tunneling caused by the drop in FS2 potential in the SdhB[I150H] mutant.

The results of the stopped-flow experiments are similar to the MHQ data. The rates of heme reduction are similar to the apparent rates of FS3

reduction as measured by MHQ. Heme reduction in the SdhB[I150H] mutant is approximately 4-fold slower when compared to wild-type SQR. The difference in reaction order may be due to the accumulation of reduced FS3, which acts as the electron donor for the heme (either directly, or indirectly, via the Q-site (*14*)). In wild-type SQR, the rapid reduction of FS3 and its accumulation results in zero-order reduction of the heme. In contrast, the lower accumulation of reduced FS3 results in heme reduction that is dependent on the concentration of reduced FS3, hence the first-order kinetics.

However, the model fails when it predicts that reduction of the heme should begin at roughly the same time as the reduction of FS3. In wild-type SQR, the calculated rate of electron transfer from FS3 to the *b* heme at pH 8.0 (and a edge to edge distance of 13.1 Å) is approximately 8.3×10^4 s^{-1} ($t_{1/2}$ = 8.4 μs). At that rate, heme reduction should occur slightly after FS3 reduction. In wild-type SQR, FS3 reduction was first observed 800 μs after the reaction with succinate, whereas heme reduction could not be seen up to 25 ms post-reaction. Even in the stopped-flow, heme reduction was not seen until 5 ms post-reaction. This delay suggests that there is an impedance on the ability of electrons to tunnel directly from FS3 to the heme.

Our previous work has shown that a non-functional Q-site can affect heme reduction rates (*14*). Also, in the presence of excess succinate and exogenous quinone, the level of reduced heme is directly proportional to the concentration of oxidized Q (unpublished data). Assuming turnover rates of

$\approx$100 s^{-1} in wild-type SQR at pH 8.0 (*18*), we can reasonably expect the first endogenous quinones in our membranes to get reduced on a similar timescale as when we first see heme reduction, which was approximately 5 ms after mixing with succinate. In the SdhB^{I150H} mutant, heme reduction is first seen about 3-fold later compared to wild-type SQR, at 15 ms post-reaction. This happens to correlate with quinone-reductase activity, which is 3-fold lower in this mutant (*9*). As previously asserted by us, electron transfer from FS3 to the quinone is preferable over transfer to the heme (*14*). It is likely that heme reduction only occurs once the Q-pool is partially reduced.

The MHQ experiments performed here provide a glimpse into the kinetics of electron transfer through SQR but an accurate measurement of the kinetics is obscured by the slow dissociation of phosphate and the loss of electrons to the Q-pool. Presently, we are working on a solution to overcome these obstacles and get a sense of the true rates. Instead of performing the MHQ experiments on crude membranes, the better option may be to work with Thesit-solubilized, purified SQR. Similar to the earlier experiments, the enzyme is activated with 1 mM malonate and stored in a 100 mM phosphate buffer until use. However, immediately prior to MHQ, a Bio-Rad spin column is used to exchange the phosphate buffer for a 100 mM HEPES buffer. The buffer exchange should solve the problem of the slow phosphate dissociation, while the purified SQR contains a lower concentration of endogenous quinone. Additionally, performing the MHQ experiments in the presence of

excess pentachlorophenol, a potent Q-site inhibitor may also alleviate interference from the Q-pool. These experiments are currently in progress at TU Delft.

We now have empirical evidence of the changes to electron transfer rates once the midpoint potential of the "low potential cluster" is further decreased. Although the rates we measured by MHQ deviate from the theoretical model, we predict that once we optimize the experimental conditions, we will be able to measure the true rates of electron transfer through the enzyme, which are likely closer to the calculated rates. More importantly, we were able to show direct evidence for the slower rate of electron tunneling through the SdhB[I150H] mutant. As well, the large discrepancy in the timescale of *b* heme reduction between our experiments and the model is further evidence that heme reduction is not a simple case of direct reduction by FS3. Other variables likely play a role in determining electron transfer pathways within the membrane domain of SQR.

5.5 Tables and Figures

		single exponential				double exponential						
		A	k (s^{-1})	$t_{1/2}$ (ms)	y_0	A_1	k_1 (s^{-1})	$t_{1/2,1}$ (ms)	A_2	k_2 (s^{-1})	$t_{1/2,2}$ (ms)	y_0
Wild-type Sdh	FS1	-0.411	57.8	11.9	0.430	-0.241	200	3.4	-0.283	8.5	81.4	0.52
	FS3	0.841	40.0	17.3	0.048	0.289	2500	0.3	0.725	24	28.9	0.017
SdhB^{I150H}	FS1	-0.360	131.6	5.3	0.360	-0.267	303	2.6	-0.243	3	226	0.49
	FS3	1.040	7.9	88.0	0.008	0.338	458	317	0.720	12.1	87.2	-0.004

Table 5.1: Kinetic parameters of FS1 and FS3 reduction determined by MHQ. The reduction of both clusters follows first-order reaction kinetics.

	A	k (s^{-1})	$t_{1/2}$ (ms)	y_0
Wild-type Sdh	n/a	-0.7	12	-0.001
SdhB^{I150H}	-0.043	15.8	44	0.034

Table 5.2: Kinetic parameters of *b* heme reduction determined by stopped-flow. Wild-type SQR data conforms to a zero-order reaction kinetics. The SdhB^{I150H} data fits to a single exponential, first-order equation.
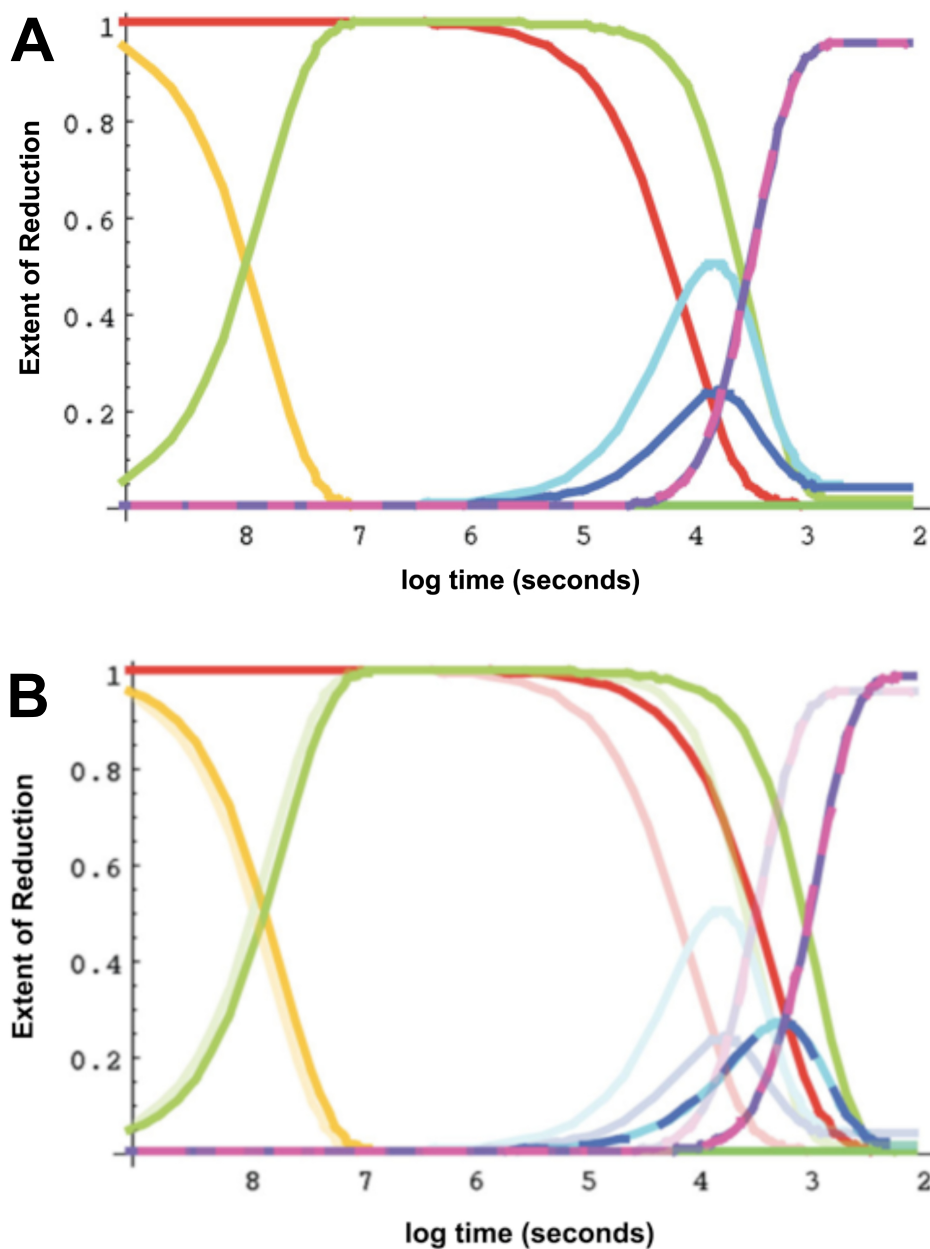
Color scheme: flavosemiquinone, FADH$_2$, FS1, FS2, FS3, heme *b*, ubisemiquinone, ubiquinol

Figure 5.1: Electron transfer simulations. Simulations are shown for *A*) wild-type SQR *B*) SdhB[I150H] mutant. For comparison, the simulations of wild-type SQR are shown in the bottom panel as the transparent traces.
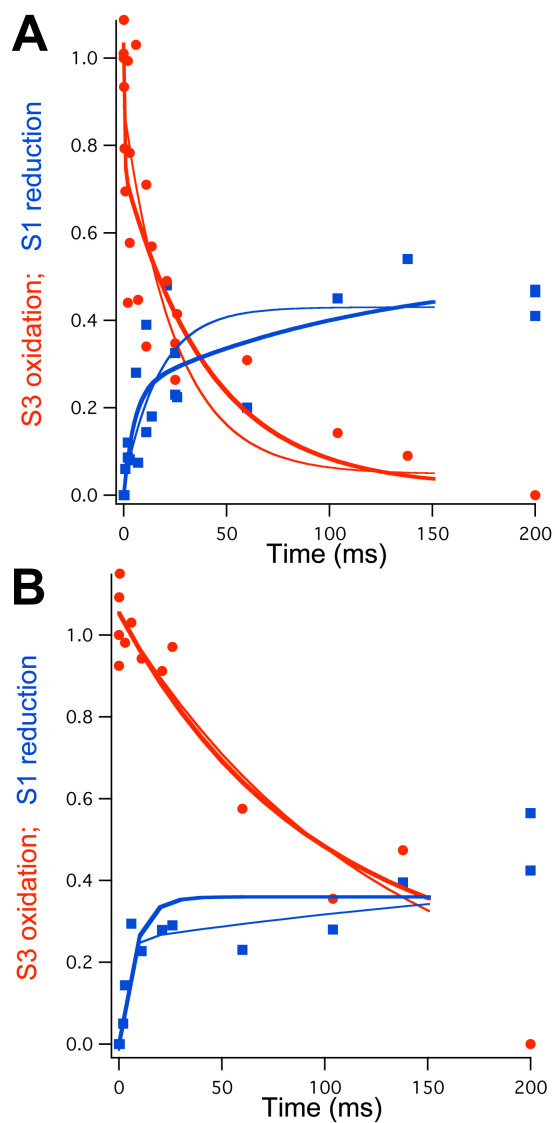
Figure 5.2: MHQ kinetics of FS1 and FS3 reduction. FS1 (blue) and FS3 (red) reduction was tracked in *A*) wild-type SQR *B*) SdhB[I150H] mutant. The redox states of FS1 and FS3 in each MHQ sample were determined by EPR spectroscopy. For FS1, the quantity of the reduced cluster is plotted. For FS3, the amount of oxidized cluster is shown. The data were fit to either a single (thin traces, top; thick traces, bottom) or double (thick traces, top; thin traces, bottom) exponential equation.
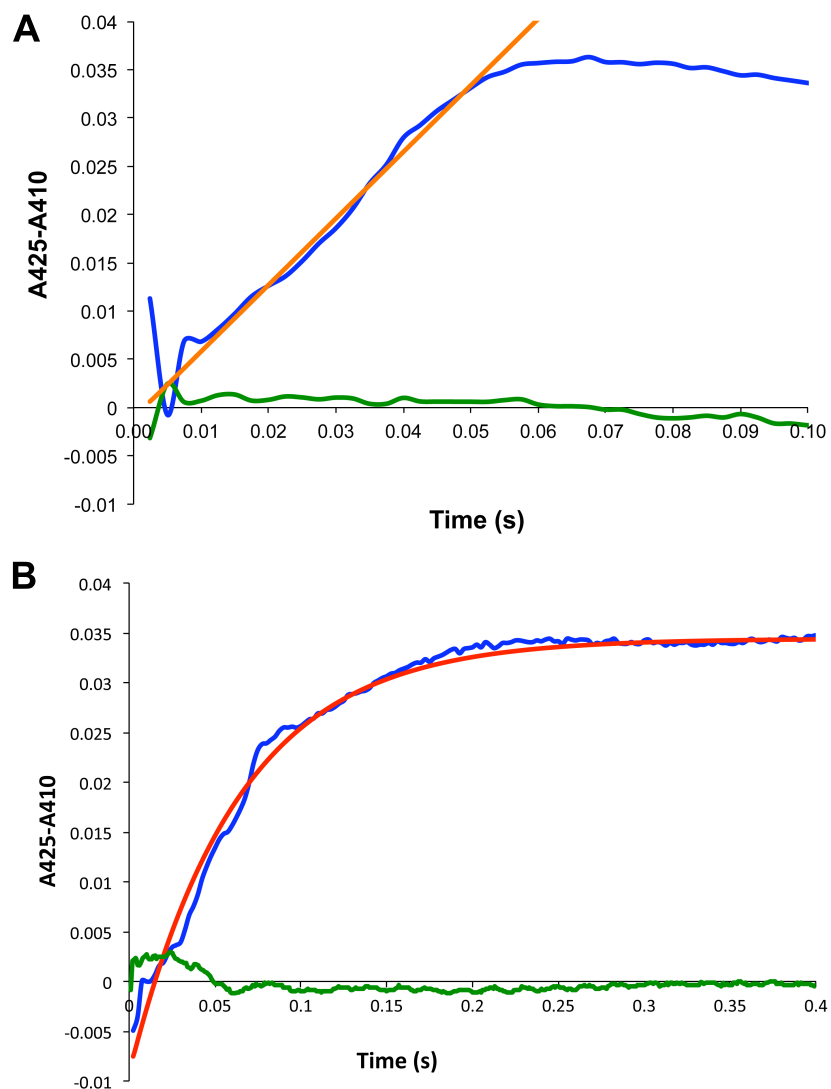
Figure 5.3: Stopped-flow kinetics of *b* heme reduction. Traces are indicated for *A*) wild-type SQR *B*) SdhB[I150H] mutant. In blue, Sdh-enriched membranes were reacted with 200 mM succinate. In green, membranes reacted with buffer. Kinetic traces at 410 nm were subtracted from traces obtained at 425 nm. Each trace represents the average of three separate replicates. Best fit lines used to estimate the rate of reduction are indicated in red.

5.6 References

1. Marcus, R. A. (1956) On the Theory of Oxidation-Reduction Reactions Involving Electron Transfer.1, *J Chem Phys 24(5)*, 966-978.

2. DeVault, D., and Chance, B. (1966) Studies of photosynthesis using a pulsed laser. I. Temperature dependence of cytochrome oxidation rate in chromatium. Evidence for tunneling, *Biophys J 6*, 825-847.

3. Jortner, J. (1976) Temperature dependent activation energy for electron transfer between biological molecules, *The Journal of Chemical Physics 64*, 4860.

4. Hopfield, J. J. (1974) Electron transfer between biological molecules by thermally activated tunneling, *Proceedings of the National Academy of Sciences of the United States of America 71*, 3640.

5. Marcus, R. A., and Sutin, N. (1985) Electron transfers in chemistry and biology, *Biochim. Biophys. Acta 811*, 265-322.

6. Moser, C. C., Keske, J. M., Warncke, K., Farid, R. S., and Dutton, P. L. (1992) Nature of biological electron transfer, *Nature 355*, 796-802.

7. Moser, C. C., Chobot, S. E., Page, C. C., and Dutton, P. L. (2008) Distance metrics for heme protein electron tunneling, *Biochim Biophys Acta 1777*, 1032-1037.

8. Moser, C. C., Anderson, J. L., and Dutton, P. L. (2010) Guidelines for tunneling in enzymes, *Biochim Biophys Acta 1797*, 1573-1586.

9. Cheng, V. W., Ma, E., Zhao, Z., Rothery, R. A., and Weiner, J. H. (2006) The iron-sulfur clusters in *Escherichia coli* succinate dehydrogenase direct electron flow, *J Biol Chem 281*, 27662-27668.

10. Maklashina, E., Berthold, D. A., and Cecchini, G. (1998) Anaerobic expression of *Escherichia coli* succinate dehydrogenase: functional replacement of fumarate reductase in the respiratory chain during anaerobic growth, *J Bacteriol 180*, 5989-5996.

11. Page, C. C., Moser, C. C., Chen, X., and Dutton, P. L. (1999) Natural engineering principles of electron tunnelling in biological oxidation-reduction, *Nature 402*, 47-52.

12. Messner, K. R., and Imlay, J. A. (2002) Mechanism of superoxide and hydrogen peroxide formation by fumarate reductase, succinate dehydrogenase, and aspartate oxidase, *J Biol Chem 277*, 42563-42571.

13. Cherepanov, A. V., and De Vries, S. (2004) Microsecond freeze-hyperquenching: development of a new ultrafast micro-mixing and sampling technology and application to enzyme catalysis, *Biochim Biophys Acta 1656*, 1-31.

14. Tran, Q. M., Rothery, R. A., Maklashina, E., Cecchini, G., and Weiner, J. H. (2006) The quinone binding site in *Escherichia coli* succinate dehydrogenase is required for electron transfer to the heme *b*, *J Biol Chem 281*, 32310-32317.

15. Wiertz, F. G., and de Vries, S. (2006) Low-temperature kinetic measurements of microsecond freeze-hyperquench (MHQ) cytochrome oxidase monitored by UV-visible spectroscopy with a newly designed cuvette, *Biochem Soc Trans 34*, 136-138.

16. Yankovskaya, V., Horsefield, R., Tornroth, S., Luna-Chavez, C., Miyoshi, H., Leger, C., Byrne, B., Cecchini, G., and Iwata, S. (2003) Architecture of succinate dehydrogenase and reactive oxygen species generation, *Science 299*, 700-704.

17. Gutman, M. (1978) Modulation of mitochondrial succinate dehydrogenase activity, mechanism and function, *Mol Cell Biochem 20*, 41-60.

18. Maklashina, E., and Cecchini, G. (1999) Comparison of catalytic activity and inhibitors of quinone reactions of succinate dehydrogenase (Succinate-ubiquinone oxidoreductase) and fumarate reductase (Menaquinol-fumarate oxidoreductase) from *Escherichia coli*, *Arch Biochem Biophys 369*, 223-232.

19. Tomasiak, T. M., Maklashina, E., Cecchini, G., and Iverson, T. M. (2008) A threonine on the active site loop controls transition state formation in *Escherichia coli* respiratory complex II, *J Biol Chem 283*, 15460-15468.

20. Lancaster, C. R., Gross, R., and Simon, J. (2001) A third crystal form of *Wolinella succinogenes* quinol:fumarate reductase reveals domain closure at the site of fumarate reduction, *Eur J Biochem 268*, 1820-1827.

Chapter 6: Concluding Remarks

6.1 General Conclusions and Discussion

When studying enzyme mechanisms, the value of high-resolution structural data cannot be overstated. Although not essential, having a structure to reference when designing experiments and interpreting data simplifies the process infinitely. Thus, it is truly fortunate to be an enzymologist in the 21st century, an age of exponentially increasing amounts of crystallographic data. I was lucky that at the time I began my thesis research, the crystal structure of *E. coli* SQR had been recently elucidated (*1*), which supplemented the structure of *E. coli* QFR that had been solved a few years earlier (*2*). I have no doubt that these seminal developments were crucial for much of the work presented in this thesis.

The x-ray structure of *E. coli* SQR revealed potential interactions between several conserved residues within the Q-site and the bound ubiquinone. In Chapter 2, I probed the role of these residues using site-directed mutagenesis, in collaboration with the laboratory of Dr. Gary Cecchini from UCSF. These studies highlighted the critical nature of SdhC^{S27}, SdhC^{R31}, and SdhD^{D82} in the reduction of UQ. The role of SdhD^{Y83} was also examined and I found that the tyrosyl side chain was important, but not essential, despite the observation that the phenolic hydroxyl group was the nearest protein contact to the O1 carbonyl of UQ according to the x-ray structure of *E. coli* SQR (PDB entry: 1NEK (*1*)). However, this is in contrast with later experiments in *S. cerevisiae* SQR, which showed that the yeast enzyme was much less tolerant to mutations at the equivalent Tyr residue

(*3*). These findings support the theory that in *E. coli* SQR, the UQ can bind at two positions at the Q-site (*4*). The UQ is bound to the outer site in the 1NEK x-ray structure (*1*) but it is only at the inner site where the UQ is brought in close proximity to SdhC[S27], SdhC[R31], and SdhD[D82], which function either as direct proton donors or by coordinating catalytic water molecules.

Unexpectedly, impairment of the Q-site had effects on the succinate-dependent reduction of the heme. With a non-functional Q-site, one might expect that the heme should reach its equilibrium reduction level faster, since electrons cannot leave the system. This suggested that some mechanism was in place to limit electron tunneling from FS3 to the heme, and complete and rapid heme reduction by succinate requires a functional Q-site.

The work presented in Chapter 3 represented the most important scientific contribution of this thesis. The instability of wild-type SQR in the absence of heme had been noted a decade earlier (*5, 6*), and previous efforts at removing the heme via mutation of the axial ligands were unsuccessful (*7, 8*). Fortuitously, I discovered that mutation of either of the heme axial ligands to a Tyr was sufficient to prevent the incorporation of heme into the enzyme. Although there was some evidence that the heme mutants were not as stable as the wild-type enzyme, the mutants retained significant catalytic activity. Overall, these studies presented the most compelling evidence to date that the heme is not essential for the known physiological function of *E. coli* SQR. Moreover, the heme-free SQRs produce statistically identical amounts of ROS

per enzyme turnover, suggesting that the heme does not have a role in the suppression of superoxide production.

At this point, the only function we could assign to the heme was a structural one. However, even the structural stability that the heme provided could be substituted for via mutation, although the mutants were less stable when removed from the native membrane; additionally, the lack of heme in *E. coli* QFR does not affect its robustness. Without a clear function, why would an organism devote so much energy into the incorporation of heme into SQR and why would the heme be so well conserved amongst all the different SQR homologs? The answer that the heme did not serve a function other than a structural one was unacceptable to me, and led to the work presented in Chapter 4.

The working hypothesis was that the heme might have a regulatory role in the enzyme; perhaps the heme acts as a redox sensor, to gauge the redox state of the Q-pool. If the redox state of the heme could manipulate enzyme function, then modulating its midpoint potential should have a measurable effect. The plan was to find mutations that could both increase and decrease the midpoint potential of the heme, but in the end, only decreases in heme potential could be identified. When the effects of these mutations were quantified, the evidence was unconvincing. Whatever trend may have existed was not solid enough to make any conclusions. Again, I was stuck at an impasse. Modulating the redox state of the heme did not appear to have any consequences.

Nevertheless, the serendipitous nature of scientific discovery revealed itself again when I re-examined the data and noticed an unexpected biophysical trend. The EPR spectrum of the *b* heme in *E. coli* SQR is not a homogenous signal, but the source of the heterogeneity had never been identified until I proposed that the root of it might be out of plane distortion of the porphyrin ring, which is heavily influenced by the surrounding protein scaffold. The significance of these multiple conformations has not yet been determined, but it might provide a physical mechanism by which the heme could use redox-linked conformational changes to communicate the status of the Q-pool to other parts of the enzyme.

The data presented in Chapter 5 originated from some of the most privileged and satisfying research I have done, in part due to the opportunity to perform research abroad, and especially because it took so much technical problem-solving to get to the point where we could acquire useful data. In this work, empirical electron tunneling rates were determined through wild-type SQR and an SdhB[I150H] mutant, which drops the potential of the lowest-potential [4Fe-FS] cluster, FS2, by 125 mV (*9*). The high resolution of crystallographic structures enables an accurate estimation of distances between redox cofactors; this, in combination with the midpoint potentials determined by redox potentiometry allowed us to generate a reasonable approximation of the electron tunneling rates through the enzyme. The simplicity of the *E. coli* SQR electron transfer relay and the ability to unambiguously determine the redox state of each prosthetic group made it

ideal for the study of electron transfer. This was a unique opportunity to collaborate with Dr. Simon de Vries at TU Delft and use his homemade MHQ machine to compare theoretical Duttonian electron transfer rates with experimental data.

As is common in science, things never go as smoothly in practice as one would like to imagine, but once we overcame the major hurdle of activating the enzyme properly, the rest was relatively simple. Most importantly, we were able to successfully demonstrate a lag in electron transfer downstream of FS2 as a result of the SdhB^{I150H} mutant. Furthermore, heme reduction is observable on a much slower timescale than reduction of the [Fe-S] clusters. It was assumed that once FS3 was reduced, a number of electrons would tunnel to the Q-site while another population would tunnel to the heme. However, we did not see any evidence of heme reduction in the period before the first turnover of UQ. The MHQ data suggested that as long as oxidized quinone was available to the enzyme, electrons would preferentially tunnel to the Q-site rather than the heme.

6.2 Future Directions

The big question remains: what is the role of the heme in mitochondrial Complex II? Why has the mitochondrial homolog evolved a heme that is 200 mV lower in potential than the one in the *E. coli* enzyme? I think these questions can only be solved once we are able to elucidate the function of the heme *b* in *E. coli* SQR, which was the central goal of my

research. In a sense, it was a partial success; I was able to provide evidence against conventional theories on the role of the heme. We now know that the heme is not essential for both the succinate dehydrogenase and fumarate reductase activities of *E. coli* SQR and we know that it is not involved in the suppression of ROS. Surely, these are important findings, but I can't help but feel somewhat unsatisfied. We know what the heme *doesn't* do, but we still have very little idea what it *does* do.

I showed there is a complex electronic relationship between the heme, the [3Fe-4S] cluster, and the Q-site. We still don't have a clear explanation for some of the more peculiar observations. Why does the loss of Q-site functionality affect heme reduction rates *and* the extent of heme reduction? Why do we see zero heme reduction in our MHQ experiments until after the turnover of quinone?

The simple Duttonian view of electron transfer assumes very little influence from the protein matrix, and assigns it a generic packing density variable; the main evolutionary force allowing competent tunneling appears to be the minimization of distances between redox cofactors (*10*). The alternative model of electron tunneling postulates that electron tunneling between cofactors is more efficient through specific pathways (*11, 12*). The pathway model distinguishes between covalent bonds, hydrogen bonds, Van der Waals interactions, and empty space to calculate the different pathways that electrons can take through the protein; some pathways are more optimal than others and those dominate. While the two models tend to agree with

each other, in some cases the results diverge (*13*). In SQR, the binding of UQ involves numerous hydrogen-bonding interactions; these interactions should enhance electron transfer rates, according to the tunneling pathway model (*14*). As well, two conserved tryptophan residues are found in a chain between FS3 and the Q-site, SdhB[W163] and SdhB[W164]; tryptophan residues have been shown to facilitate increased electron transfer rates (*15*) and our lab is currently doing structure-function studies on these two tryptophan residues. Thus, a gating mechanism could explain why electron tunneling from FS3 to the quinone, and quinone to heme, could be faster than from FS3 to the heme. To determine if this is possible would require an in-depth theoretical analysis on the optimal electron transfer pathways within the membrane domain – a difficult, but not impossible task (*12, 16*).

While a gating mechanism may explain why rates of electron transfer may be affected, it fails to address why Q-site mutants decrease the final reduction level of the heme. The theory that UQ binding may cause a negative shift in the midpoint potential of the heme, proposed in Chapter 2.7, could be a plausible explanation. Some evidence suggests that this might be the case. The binding of PCP induces a ~30 mV decrease in the potential of the heme in *E. coli* SQR (our work, unpublished). The phenomenon of redox potential shifts of nearby hemes, sometimes by up to 100 mV, upon binding of Q-site inhibitors has been demonstrated in other systems such as *E. coli* nitrate reductase (*17*), the succinate:menaquinone oxidoreductase in *B. subtilis* (*18*), and mitochondrial complex III (*19*). However, any effect caused by oxidized

UQ is not likely to alter the apparent redox potential of the heme, as determined by redox potentiometry, since any endogenous UQ in the reaction is reduced to UQH_2 before the heme can be titrated. Thus, we are limited to using UQ analogs to study effects on heme potential from Q-binding. It would be useful to screen other Q-site inhibitors to see if more substantial effects on heme midpoint potential can be observed. Although in Chapter 4 I tried to generate SQR mutants that had increased heme potential, I did not find any. It is almost certainly possible, since some protein-bound *b*-type hemes can be found with midpoint potentials as high as +400 mV (*20*). If a suitable mutant were found that increased the potential of the heme closer to that of UQ, then a cooperativity effect on heme reduction would indicate that UQ might be influencing heme potential. An SQR mutant with a very high heme midpoint potential would also enable us to study the consequences when the heme is *always* reduced since we have already examined instances where the heme is almost *never* reduced.

Regardless of the mechanism, it appears that the heme is designed to respond to the availability of UQ or, in other words, the redox state of the Q-pool. Since all these curious results might be dependent on the presence of UQ, these experiments should be repeated in a UQ-deficient strain of *E. coli*.

The MHQ experiments presented in Chapter 5 provide interesting commentary on the effect that the low-potential cluster has on electron tunneling rates and the ability to use *E. coli* SQR as a model system. Although we were able to glean some interesting kinetic trends, the procedure must be

optimized in order to gather accurate and reliable numbers. Once we have solved all the issues, we may be able to use the technology to examine the kinetics of electron transfer through the membrane domain of SQR. It would be interesting to see if the kinetics of FS3 and heme reduction would be more similar if the Q-site were empty, by using a ubiquinone deficient strain, for example. Also, we could measure electron transfer rates between the Q-site and FS3; and between the Q-site and the heme by adding reduced plumbagin to the enzyme and running in reverse.

It's possible that the function of the heme is very specific and only manifests under specific conditions that we have not yet tested. For example, when substrate levels are limiting, or when membrane potential is very high. It may be involved in signaling. Protein supercomplexes have been identified in both mitochondria and bacterial respiratory chains, although SQR has only been shown to interact with itself and has not yet been identified as a component of any supercomplex (*21*). The association of various components of the respiratory chain is believed to increase electron flux, or reduce ROS production. If SQR does participate in protein-protein interactions, conformational changes in the heme may regulate the activity of *other* proteins; or promote or antagonize the cooperative associations with other proteins.

Whatever the function of the heme is, future scientists are now armed with heme-free SQR mutants and the library of SQRs with different heme potentials. These are valuable additions to the toolkit that must be used to

investigate under what conditions the heme may be useful. The greatest of Complex II mysteries, the role of the heme, still lingers and clearly, much work is still required if we are to ever solve it.

6.3. References

1. Yankovskaya, V., Horsefield, R., Tornroth, S., Luna-Chavez, C., Miyoshi, H., Leger, C., Byrne, B., Cecchini, G., and Iwata, S. (2003) Architecture of succinate dehydrogenase and reactive oxygen species generation, *Science 299*, 700-704.

2. Iverson, T. M., Luna-Chavez, C., Cecchini, G., and Rees, D. C. (1999) Structure of the *Escherichia coli* fumarate reductase respiratory complex, *Science 284*, 1961-1966.

3. Silkin, Y., Oyedotun, K. S., and Lemire, B. D. (2007) The role of Sdh4p Tyr-89 in ubiquinone reduction by the *Saccharomyces cerevisiae* succinate dehydrogenase, *Biochim Biophys Acta 1767*, 143-150.

4. Horsefield, R., Yankovskaya, V., Sexton, G., Whittingham, W., Shiomi, K., Omura, S., Byrne, B., Cecchini, G., and Iwata, S. (2006) Structural and computational analysis of the quinone-binding site of complex II (succinate-ubiquinone oxidoreductase): a mechanism of electron transfer and proton conduction during ubiquinone reduction, *J Biol Chem 281*, 7309-7316.

5. Nakamura, K., Yamaki, M., Sarada, M., Nakayama, S., Vibat, C. R., Gennis, R. B., Nakayashiki, T., Inokuchi, H., Kojima, S., and Kita, K. (1996) Two hydrophobic subunits are essential for the heme *b* ligation and functional assembly of complex II (succinate-ubiquinone oxidoreductase) from Escherichia coli, *J Biol Chem 271*, 521-527.

6. Nihei, C., Nakayashiki, T., Nakamura, K., Inokuchi, H., Gennis, R. B., Kojima, S., and Kita, K. (2001) Abortive assembly of succinate-ubiquinone reductase (complex II) in a ferrochelatase-deficient mutant of *Escherichia coli*, *Mol Genet Genomics 265*, 394-404.

7. Maklashina, E., Rothery, R. A., Weiner, J. H., and Cecchini, G. (2001) Retention of heme in axial ligand mutants of succinate-ubiquinone xxidoreductase (complex II) from *Escherichia coli*, *J Biol Chem 276*, 18968-18976.

8. Vibat, C. R., Cecchini, G., Nakamura, K., Kita, K., and Gennis, R. B. (1998) Localization of histidine residues responsible for heme axial ligation in cytochrome b_{556} of complex II (succinate:ubiquinone oxidoreductase) in Escherichia coli, *Biochemistry 37*, 4148-4159.

9. Cheng, V. W., Ma, E., Zhao, Z., Rothery, R. A., and Weiner, J. H. (2006) The iron-sulfur clusters in *Escherichia coli* succinate dehydrogenase direct electron flow, *J Biol Chem 281*, 27662-27668.

10. Page, C. C., Moser, C. C., Chen, X., and Dutton, P. L. (1999) Natural engineering principles of electron tunnelling in biological oxidation-reduction, *Nature 402*, 47-52.

11. Onuchic, J. N., Beratan, D. N., Winkler, J. R., and Gray, H. B. (1992) Pathway analysis of protein electron-transfer reactions, *Annu Rev Biophys Biomol Struct 21*, 349-377.

12. Beratan, D., and Skourtis, S. (1998) Electron transfer mechanisms, *Curr Opin Chem Biol 2*, 235-243.

13. Jasaitis, A., Johansson, M. P., Wikstrom, M., Vos, M. H., and Verkhovsky, M. I. (2007) Nanosecond electron tunneling between the hemes in cytochrome bo_3, *Proc Natl Acad Sci U S A 104*, 20811-20814.

14. Gray, H. B., and Winkler, J. R. (1996) Electron transfer in proteins, *Annu Rev Biochem 65*, 537-561.

15. Shih, C., Museth, A. K., Abrahamsson, M., Blanco-Rodriguez, A. M., Di Bilio, A. J., Sudhamsu, J., Crane, B. R., Ronayne, K. L., Towrie, M., Vlcek, A. J., Richards, J. H., Winkler, J. R., and Gray, H. B. (2008) Tryptophan-accelerated electron flow through proteins, *Science 320*, 1760-1762.

16. Prytkova, T. R., Kurnikov, I. V., and Beratan, D. N. (2005) *Ab initio* based calculations of electron-transfer rates in metalloproteins, *J Phys Chem B 109*, 1618-1625.

17. Rothery, R. A., Blasco, F., Magalon, A., Asso, M., and Weiner, J. H. (1999) The hemes of *Escherichia coli* nitrate reductase A (NarGHI): potentiometric effects of inhibitor binding to NarI, *Biochemistry 38*, 12747-12757.

18. Smirnova, I. A., Hagerhall, C., Konstantinov, A. A., and Hederstedt, L. (1995) HOQNO interaction with cytochrome *b* in succinate:menaquinone oxidoreductase from *Bacillus subtilis*, *FEBS Lett 359*, 23-26.

19. Kunz, W. S., and Konstantinov, A. A. (1983) Effect of b-c_1-site inhibitors on the midpoint potentials of mitochondrial cytochromes *b*, *FEBS Lett 155*, 237-240.

20. Mizusawa, N., Yamashita, T., and Miyao, M. (1999) Restoration of the high-potential form of cytochrome b_{559} of photosystem II occurs via a two-step mechanism under illumination in the presence of manganese ions, *Biochim Biophys Acta 1410*, 273-286.

21. Sousa, P. M., Silva, S. T., Hood, B. L., Charro, N., Carita, J. N., Vaz, F., Penque, D., Conrads, T. P., and Melo, A. M. (2011) Supramolecular organizations in the aerobic respiratory chain of *Escherichia coli*, *Biochimie 93*, 418-425.

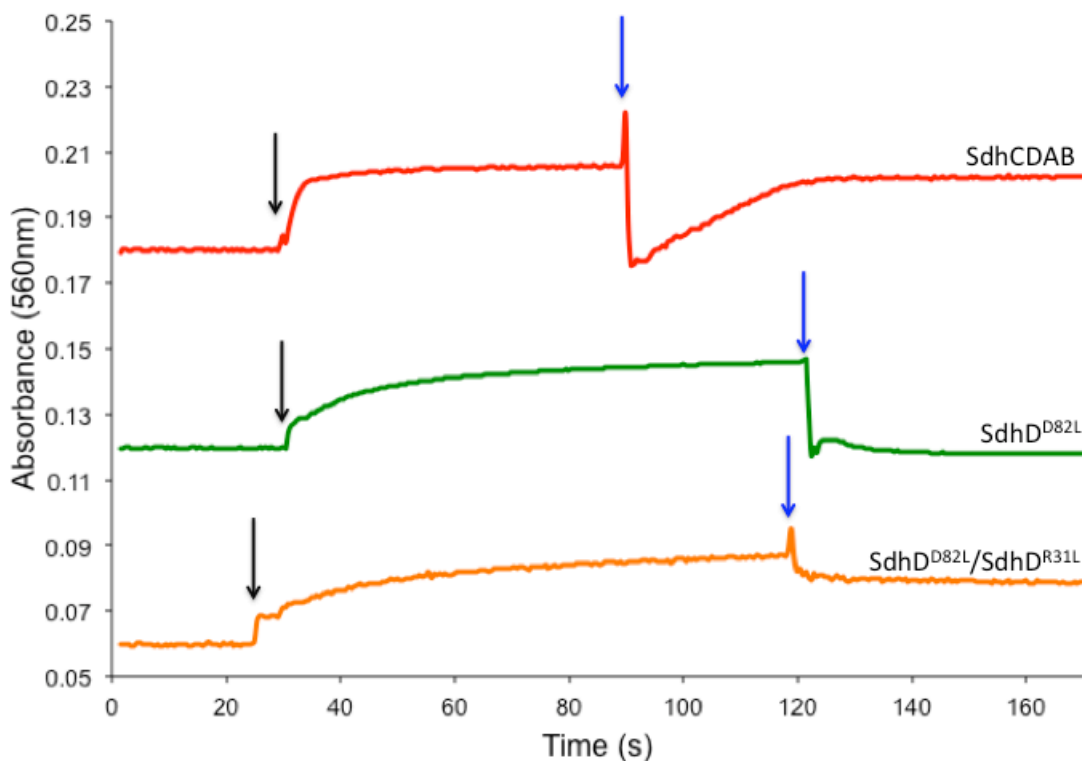**Appendix A – Supplementary Figures for Chapter 2**

Figure A.1: Effects on the redox state of the heme upon the addition of Q_0 to succinate-reduced SQR. Reduction of the heme is followed at 560 nm. At the time points indicated by the black arrows, 8.7 mM succinate is added to air-oxidized SQR-enriched membranes. At times indicated by the blue arrows, 0.35 mM Q0 is added to the cuvette. In wild-type Sdh, the heme is gradually reduced until all the Q_0 is exhausted but in the SdhDD82L mutant, the heme is permanently oxidized. Similar results are observed in the SdhC[R31L] and SdhC[S27A] mutants. Q_0 is unable to oxidize the heme in a double mutant.

Appendix B – Supplementary Figures for Chapter 4

Mutant	Mutagenic Oligonucleotide (5' to 3')
SdhD-V19D	GATTTCATCCTCGATCGCGCTACCGC
SdhD-A23D	CGTTCGCGCTACCGATATCGTCCTGACG
SdhC-F38D	GTGTGATCACCGATGTTGCAGTGGGGATCCTGC
SdhC-V85D	CTGGCGTATCACGACGTCGTAGGTATTCG
SdhC-T37I	CCGGTGTGATCATCTTTGTTGCAGTGGGGATCCTGC
SdhC-F38S	GTGTGATCACCGATGTTGCAGTGGGGATCCTGC
SdhD-A23S	CGTTCGCGCGACGTCTATCGTCCTGACG
SdhC-V87D	GTATCACGTCGTCGACGGTATTCGCCAC
SdhC-V85T	CTGGCGTATCACACCGTCGTAGGAATTCGCCAC
SdhC-H30G	CCGGAAACGCGTCCGAGAATGGACGCTATC
SdhC-H30A	CACACCGGAAACGCGTGCGAGAATGGACGC
SdhC-H30S	CACACCGGAAACGCGTGAGAGAATGGACGC
SdhC-R31L	TCCATTCTCCATCTGGTTTCCGGTGTGATCACC
SdhC-R91L	TATTCGCCTCATGATGAT
SdhD-R20L	GATTTCATCCTCGTTCTGGCTACCGCTATCG

Table B.1: List of mutagenic oligonucleotides. A universal primer (M13 – forward or reverse) was used in combination with the appropriate mutagenic oligonucleotide in each PCR reaction.
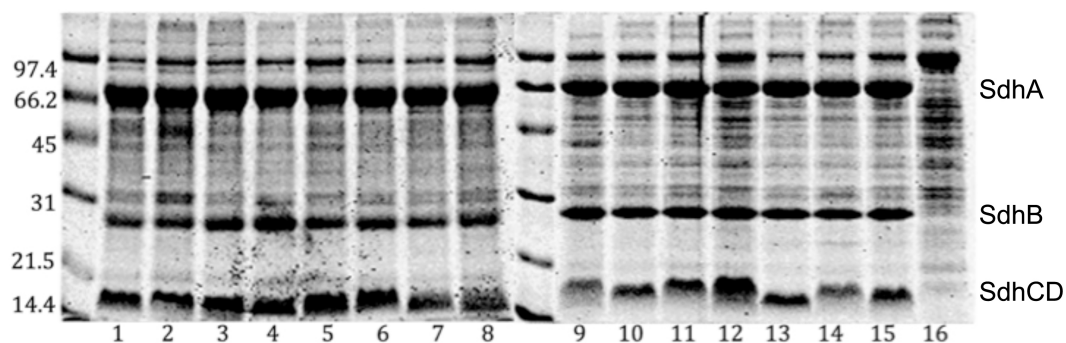
Figure B.1: SDS-PAGE gels of Sdh-enriched membranes. Expression levels of each Sdh subunit are similar in all the mutants. Lane 1, SdhCDAB. Lane 2, SdhD^{V19D}. Lane 3, SdhD^{A23D}. Lane 4, SdhC^{F38D}. Lane 5, SdhC^{V85D}. Lane 6, SdhC^{T37I}. Lane 7, SdhC^{F38S}. Lane 8, SdhC^{H30A}/SdhC^{V87D}. Lane 9, SdhD^{A23S}. Lane 10, SdhC^{V87D}. Lane 11, SdhC^{V85T}. Lane 12, SdhC^{H30G}. Lane 13, SdhC^{H30A}. Lane 14, SdhC^{H30S}. SdhC^{F38D}/SdhC^{V87D}.
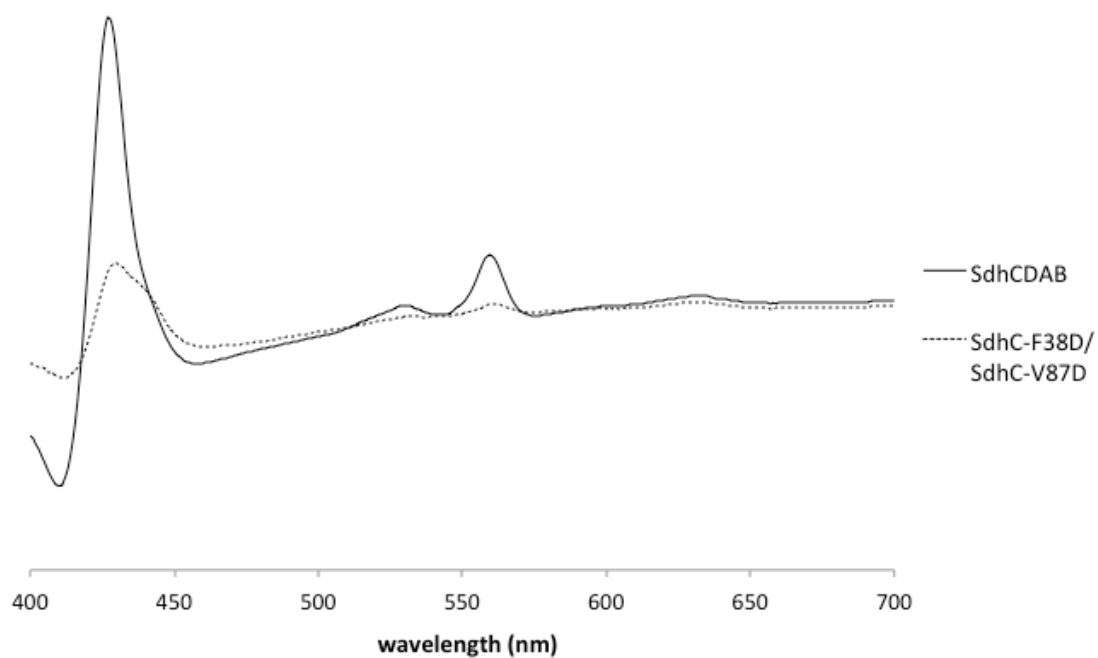
Figure B.2: Succinate-reduced minus air-oxidized absorbance spectrum.

The 100 mV decrease in heme E_m in the SdhC^{F38D}/Sdh^{V87D} mutant significantly diminishes its succinate reduction capacity.